DEVELOPMENT OF FLAME RETARDANT AND ANTIBACTERIAL NANOPARTICLE DOPED POLYPROPYLENE FIBERS

MASTER OF SCIENCE THESIS

Ayfer İrem KOCA

Eskişehir, 2019

DEVELOPMENT OF FLAME RETARDANT AND ANTIBACTERIAL NANOPARTICLE DOPED POLYPROPYLENE FIBERS

Ayfer İrem KOCA

MASTER OF SCIENCE THESIS

Department of Advanced Technologies/Nanotechnology Program

Supervisor: Prof. Dr. Mustafa Erdem ÜREYEN

Co-Supervisor: Assoc. Prof. Dr. Ümit Halis ERDOĞAN

Eskişehir

Eskisehir Technical University

Institute of Graduate Programs

July, 2019

This thesis study was supported by Eskisehir Technical University Scientific Research Projects under the Project Nr. ***BAP-1404E292****.*

FINAL APPROVAL FOR THESIS

This thesis titled "Development of Flame Retardant and Antibacterial Nanoparticle Doped Polypropylene Fibers" has been prepared and submitted by Ayfer İrem KOCA in partial fulfillment of the requirements in "Eskişehir Technical University Directive on Graduate Education and Examination" for the Degree of Master of Science in Department of Advanced Technologies has been examined and approved on 25/07/2019.

Committee Members		**Signature**
Member (Supervisor)	: Professor Mustafa Erdem ÜREYEN	.....
Member	: Assoc. Professor Hande ÇELEBİ	.....
Member	: Asst. Professor Göktuğ GÜNKAYA	.....

.....

Prof. Dr. Murat TANIŞLI

Director of Institute of Graduate Programs

ABSTRACT

DEVELOPMENT OF FLAME RETARDANT AND ANTIBACTERIAL NANOPARTICLE DOPED POLYPROPYLENE FIBERS

Ayfer İrem KOCA

Department of Advanced Technologies-Nanotechnology Program

Eskisehir Technical University, Institute of Graduate Programs, July, 2019

Supervisor: Prof. Dr. Mustafa Erdem ÜREYEN

Co-Supervisor: Assoc. Prof. Dr. Ümit Halis ERDOĞAN

The present study aimed to produce flame retardant (FR) and antibacterial nanoparticle doped polypropylene (PP) fibers containing phosphorus-based flame retardants (PBFRs). The synergistic effect of inorganic FR additives (Aluminum trihydroxide (ATH), zinc borate (ZnB), nano-silica (nano-SiO_2), and carbon nanotube (CNT)) on the flammability of PBFR/PP systems were investigated to reduce the total amount of FRs which is essential for fiber spinning. Two different PBFRs, ammonium polyphosphate-based (APP) and cyclic phosphonate-based (CPP), were studied. In addition to the antibacterial additives (Cupric oxide (Nano-CuO) and zinc oxide (ZnO)), a coupling agent (MPA) and a hindered amine light stabilizer (HAS) were also used in the FR formulations. Thermal properties and flammability of the prepared composites were determined by limiting oxygen index (LOI), thermogravimetric analysis (TG-DTG), cone calorimeter test and micro combustion calorimetry (MCC). All combinations of HAS and CPP showed a synergetic effect by acting with a gas phase mechanism. Only synergistic effect on PP/CPP/HAS system was found with Nano-CuO resulting in an increase in LOI. Antibacterial analysis showed that only Nano-CuO containing fibers had antibacterial activity. Flame retardant and antibacterial nanoparticle doped PP fibers were produced successfully by melt spinning at the loading of additives up to 5.5 wt%.

Keywords: Technical textile, Flame retardant, Halogen-free, Polypropylene, Fiber

ÖZET

NANOBOYUTLU GÜÇ TUTUŞUR VE ANTİBAKTERİYEL KATKILI POLİPROPİLEN LİF GELİŞTİRİLMESİ

Ayfer İrem Koca

İleri Teknolojiler Anabilim Dalı-Nanoteknoloji Programı

Eskişehir Teknik Üniversitesi, Lisansüstü Eğitim Enstitüsü, Temmuz, 2019

Danışman: Prof. Dr. Mustafa Erdem ÜREYEN

İkinci Danışman: Doç. Dr. Ümit Halis Erdoğan

Bu çalışmada fosfor esaslı güç tutuşur malzeme içeren nanoboyutlu güç tutuşur ve antibakteriyel katkılı polipropilen lif geliştirilmesi amaçlanmıştır. Lif çekimi için gerekli olan toplam katkı oranını düşürebilmek amacıyla, inorganik katkıların (Alüminyum trihidroksit (ATH), çinko borat (ZnB), nano silika (nano-SiO_2) ve karbon nanotüp (CNT)) fosfor esaslı güç tutuşur içeren polipropilen sistemin yanıcılığı üzerindeki etkisi incelenmiştir. Amonyum polifosfat (APP) esaslı ve halkalı fosfonat (CPP) esaslı iki farklı fosfor esaslı malzeme çalışmada kullanılmıştır. ZnB ve ATH katkılarının tane boyutu eksenel değirmende öğütülerek düşürülmüş ve tane boyutu ve zeta potansiyeli ile x-ışını difraktometresi (XRD) ile karakterize edilmiştir. İnorganik katkılara ek olarak bağlayıcı bir ajan (MPA) ile engellenmiş amin ışık stabilizatörü (HAS) de güç tutuşur formulasyonlarına katkılandırılmıştır. Çalışmada antibakteriyel etki sağlayabilmek amacıyla nano-bakır oksit (nano-CuO) ve çinko oksit (CuO) katkıları kullanılmıştır. Antibakteriyel katkıların CPP ve HAS içeren sistemin yanmazlığı üzerindeki etkileri de ayrıca incelenmiştir. Hazırlanan kompozisyonların termal özellikleri ve yanmazlıkları limit oksijen indeks testi (LOI), termogravimetrik analiz (TG-DTG), konik kalorimetresi ve mikro yanma kalorimetresi (MCC) ile değerlendirilmiştir.

Öğütme prosesi neticesinde, ZnB ve ATH'in tane boyutları başarıyla mikron seviyesinden nano seviyesine düşürülmüştür. LOI sonuçları incelendiğinde, tek başlarına katkılandırıldıklarında CPP esaslı güç tutuşurun APP esaslı güç tutuşura göre PP'nin LOI değerini daha çok arttırdığı görülmüştür. İnorganik güç tutuşur katkılar ile hem APP hem

de CPP esaslı sistemlerin LOI değerlerinin düştüğü saptanmıştır. Sadece CNT içeren APP esaslı kompozisyonun MPA ile sinerjik etki gösterdiği görülmüş ve bu kompozisyonun hem LOI değerleri hem de termal bozunma sıcaklıkları MPA varlığında artmıştır. CPP ve HAS oranları çeşitlendirilerek hazırlanan kompozisyonlarda bu iki katkı arasında sinerjik etki olduğu ve gaz fazında etkinlik gösterdiği saptanmıştır. En büyük sinerjik etki, % 3,5 oranında CPP ile % 1,5 oranında HAS içeren kompozisyonda bulunmuş, PP'nin LOI değeri % 26.6'ya yükselmiştir. Bütün inorganik katkılar arasından, sadece nano-CuO katkısı, CPP/HAS içeren kompozisyon ile sinerjik etki göstermiş ve % 0,25 oranında katkılandırılması ile bu kompozisyonun LOI değerini % 27'ye yükseltmiştir. Diğer kompozisyonlarla kıyaslandığında, nano-CuO ilavesi maksimum ısıl salınım değerini (PHRR) ve toplam isi salınımı (THR) değerlerinde en yüksek düşüşe sebebiyet verirken, tutuşma süresini geciktirmiştir.

Eriyikten lif çekilmesi öncesinde, nano-CuO ve ZnO içerenlerin kompozisyonların antibakteriyel aktivitesi, tek filamentli PP lifleri üretilerek incelenmiştir. Kompozit numunelerinin yanmazlık testleri ve tek filamentli liflerin antibakteriyel analizleri ışığında, güç tutuşur ve antibakteriyel multifilament liflerin erikten lif çekilmesi yöntemi ile üretimi için nano-CuO varlığında/yokluğunda CPP/HAS içeren kompozisyonların kullanılması kararlaştırılmıştır. Üretilen liflerin karakterizasyonu; çekme testi, antibakteriyel analiz, taramalı elektron mikroskopu (SEM), optik mikroskop ve renk testi ile yapılmıştır. Sadece nano-CuO içeren kompozisyonların antibakteriyel aktivite gösterdiği saptanmıştır (>log2). SEM analizine göre, nano-CuO ilavesi lif boyunca düzgün bir dağılım göstermiştir. En yüksek çekme mukavemeti, % 0,25 nano-CuO içeren lifte bulunmuştur.

Son olarak üretilen nanoboyutlu güç tutuşur ve antibakteriyel katkılı lifler kullanılarak atkı örme yöntemi ile kumaşlar hazırlanmıştır. Kumaşların karakterizasyonu, konik kalorimetresi testi, antibakteriyel test ve optik mikroskop ile gerçekleştirilmiştir. nano-CuO varlığında saf PP kumaşın PHRR and THR değerleri düşmüştür. Ancak tutuşma süresi ve toplam yanma süresi azalmıştır. Lif analizlerine paralel şekilde sadece nano-CuO içeren kumaşlar antibakteriyel aktivite göstermiştir.

Anahtar Kelimeler: Teknik tekstil, Güç tutuşur, Halojen içermeyen, Polipropilen, Lif

Dedicated to my family,

ACKNOWLEDGEMENTS

First of all, I would like to express my gratitude to my supervisor, Prof. Dr. Mustafa Erdem ÜREYEN for sharing his knowledge and experience with me generously, for his guidance, understanding, kind support, encouraging advices and motivation throughout this study. I also would like to thank to my co-supervisor, Assoc. Prof. Dr. Ümit Halis ERDOĞAN for his guidance and invaluable technical support.

I also would like to acknowledge the Textile Engineering Department of Dokuz Eylul University for providing me every opportunity to use the instruments during the characterization of the fibers in their laboratories.

I would like to thank the employees of TEKSMER for sharing their expertise on technical textiles during the production of fibers.

Finally, I would like to thank my father, mother, sister and brother, namely Battal KOCA, Ayşe KOCA, Zeliha Ceren KOCA, and Halil Çağatay KOCA for their great love, patience, invaluable moral support and encouragement during all stages of my life.

Ayfer İrem KOCA

25/07/2019

STATEMENT OF COMPLIANCE WITH ETHICAL PRINCIPLES AND RULES

I hereby truthfully declare that this thesis is an original work prepared by me; that I have behaved in accordance with the scientific ethical principles and rules throughout the stages of preparation, data collection, analysis and presentation of my work; that I have cited the sources of all the data and information that could be obtained within the scope of this study, and included these sources in the references section; and that this study has been scanned for plagiarism with "scientific plagiarism detection program" used by Anadolu University, and that "it does not have any plagiarism" whatsoever. I also declare that, if a case contrary to my declaration is detected in my work at any time, I hereby express my consent to all the ethical and legal consequences that are involved.

.....

Ayfer İrem KOCA

TABLE OF CONTENTS

Page

LIST OF TABLES

Page

LIST OF FIGURES

Page

ABBREVIATIONS

AATCC : American Association of Textile Chemists and Colorists
APP : Ammonium Polyphosphate
ASTM : American Society for Testing and Materials
ASTM : American Society for Testing and Materials
ATH : Aluminum Trihydroxide
ATO : Antimony Trioxide
avCO : Average Carbon Monoxide Yield
avCO2 : Average Carbon Dioxide Yield
avMLR : Average Mass Loss Rate
CNT : Carbon Nanotube
Nano-CuO : Cupric Oxide
dtex : Decitex
FPI : Fire Performance Index
FR : Flame Retardant
HRC : Heat Release Capacity
HRR : Heat Release Rate
ISO : International Organization for Standardization
JIS : Japanese Industrial Standard
K/S : Color Strength
LOI : Limiting Oxygen Index
MCC : Micro Combustion Calorimetry
MPA : Multifunctional Processing Aid
MWCNT : Multi-walled Carbon Nanotube
PCFC : Pyrolysis Combustion Flow Calorimetry
PdI : Polydispersity Index
PHRR : Peak Heat Release Rate
PP : Polypropylene
R % : Reflectance
SEM : Scanning Electron Microscopy
SiO_2 : Silica

TGA : Thermogravimetric Analysis

THR : Total Heat Release

THR/TML : Total Heat Release/Total Mass Loss

TPHRR : Temperature at Peak Heat Release Rate

TTI : Time to Ignition

UL : Underwriters Laboratories

XRD : X-ray Diffraction

Z-average : Particle Size

ZnB : Zinc Borate

ZnO : Zinc Oxide

ΔE* : Color Difference

1. INTRODUCTION

Flame retardant polypropylene (PP) fibers are widely used in the textile industry and related fields such as transportation, electric wire and cable, and decorative materials, due to their good processing performance, excellent chemical and thermal resistance in addition to their low cost [1]. PP burns rapidly without leaving a char residue due to its fully aliphatic carbon structure [2]. Halogenated flame retardants are very effective in polypropylene [3,4]; however, their usage is being banned or restricted because of their hazardous effect on health and environment [5-7]. Halogen-free flame retardants (HFFRs) were proposed as an alternative to halogenated flame retardants. Phosphorous based flame retardant additives represent a broad class of HFFRs and they have become attractive for researchers and industry for more than 30 years [8]. However, high levels of loading of phosphorus-based flame retardant additives are generally needed to achieve a reasonable flame retardancy which limits the applicability of polypropylene in some fields such as fiber spinning [9]. By incorporating synergist additives into the system, the concentration of phosphorous-based flame retardant (PBFR) additives can be reduced. The synergistic effect of PBFRs was examined by different researchers with several inorganic additives such as zinc borate (ZnB) [10-12], aluminium trihydroxide (ATH) [13-15], silica (SiO_2) [16-19], carbon nanotube (CNT) [20-22], zinc oxide (ZnO) [23,24].

The class of phosphorus-based flame retardants includes a broad range of inorganic and organic compounds, including phosphates, phosphonates, phosphinates, phosphine oxides, phosphates and red phosphorus [25]. This study was conducted to produce flame retardant and antibacterial PP fibers containing PBFRs by melt spinning method. For this purpose, two different PBFRs were chosen to investigate their effects on the flammability of polypropylene in the presence/absence inorganic additives; an inorganic PBFR (ammonium polyphosphate, Exolit AP 760) and an organic PBFR (cyclic phosphonate, Aflammit PCO 900). The inorganic additives were utilized to reduce the needed amount of PBFRs which is essential for the melt spinning of PP.

In the first part of this study, the effect of ammonium polyphosphate-based (APP) flame retardant on the flammability of PP was investigated by the incorporation of APP to the polypropylene. Next, inorganic additives; ZnB, ATH, nano-SiO_2, and CNT were incorporated into the PP blend to define their synergistic effect on the flame retardancy of the PP/APP system. The particle size of ZnB and ATH were decreased to submicron

scale by a planetary mill, prior to use. The ground powders were characterized by particle size and zeta potential measurements, and X-ray diffraction (XRD). A coupling agent (MPA) was also used to improve the dispersibility of nano-sized inorganic additives. The same processes were applied in the second part of the study but with cyclic phosphonate-based (CPP) flame retardant. A hindered amine light stabilizer (HAS) is also blended with CPP to investigate the synergetic effect between these flame retardants. Antibacterial additives (cupric oxide (Nano-CuO) and zinc oxide (ZnO)) were also blended in PP to observe their influence on the flammability of PP/CPP/HAS system before melt spinning process of the fibers. All composites were prepared by melt compounding in a twin-screw extruder followed by an injection molding technique. Thermal properties and flammability of the prepared composites were determined by limiting oxygen index (LOI), thermogravimetric analysis (TGA-DTG), cone calorimeter test and micro combustion calorimetry (MCC).

For the production of flame retardant and antibacterial PP fibers, formulations were chosen by considering the flammability test results of prepared composites. Two different types of PP fibers were produced: as-spun monofilament PP fibers and melt-spun multifilament PP fibers. As-spun monofilament PP fibers were first produced to examine the antibacterial activity of each composition prior to the melt spinning process. Final fibers, which were flame retardant and antibacterial, were produced by melt spinning. Characterization of melt-spun fibers was made with tensile test, SEM, optical microscopy inspection, and color test. The melt-spun multifilament fibers were also knitted by a laboratory type single jersey knitting machine to produce flame retardant and antibacterial fabrics. Cone calorimeter test, antibacterial analysis and optical microscope inspection were conducted on the fabrics.

The investigation of the toxicology and environmental impact of the used flame retardant compositions and their combustion products are outside the scope of this study.

2. BACKROUND INFORMATION

2.1. Polypropylene

Polypropylene is a thermoplastic material, of which the chemical formula is $(C_3H_6)_n$ is, produced by the polymerization of propene (or propylene) monomer. Depending on the steric arrangement of methyl groups (CH_3) in the polymer chain, PP can be in three different forms: isotactic, syndiotactic and atactic. Isotactic (crystallizable) PP (i-PP) is in which all the methyl groups are aligned on the same side of its backbone chain. If the alignment of the methyl groups alternates on both sides of the polymer backbone chain, the resulted PP is called syndiotactic PP. A PP structure where methyl groups are positioned without any specific order is called atactic (noncrystallizable) PP (a-PP). The structure of isotactic, syndiotactic and atactic PP molecule is illustrated in Figure 2.1. Commercial polypropylene products contain predominantly isotactic polypropylene (about 95 wt%), the rest is in an atactic or syndiotactic polypropylene. Of all these polypropylenes, only isotactic PP meets the requisites needed to produce a solid plastic material. To polymerise PP in isotactic form, two different catalysts are used: Ziegler-Natta or metallocene. Polypropylene is available in the market as a homopolymer and a copolymer. Homopolymer PP term, which corresponds to i-PP, is used to describe the polypropylene with the content of only propylene monomer in the semicrystalline solid form. Homopolymer PP comes to the forefront by serving more rigidity and better resistance at elevated temperatures than copolymer PP. Copolymerised PP makes enable to produce film and fiber products with a softer feel than those with homopolymers, however, the price of PP copolymer is higher compared to that of PP homopolymer [26,27].

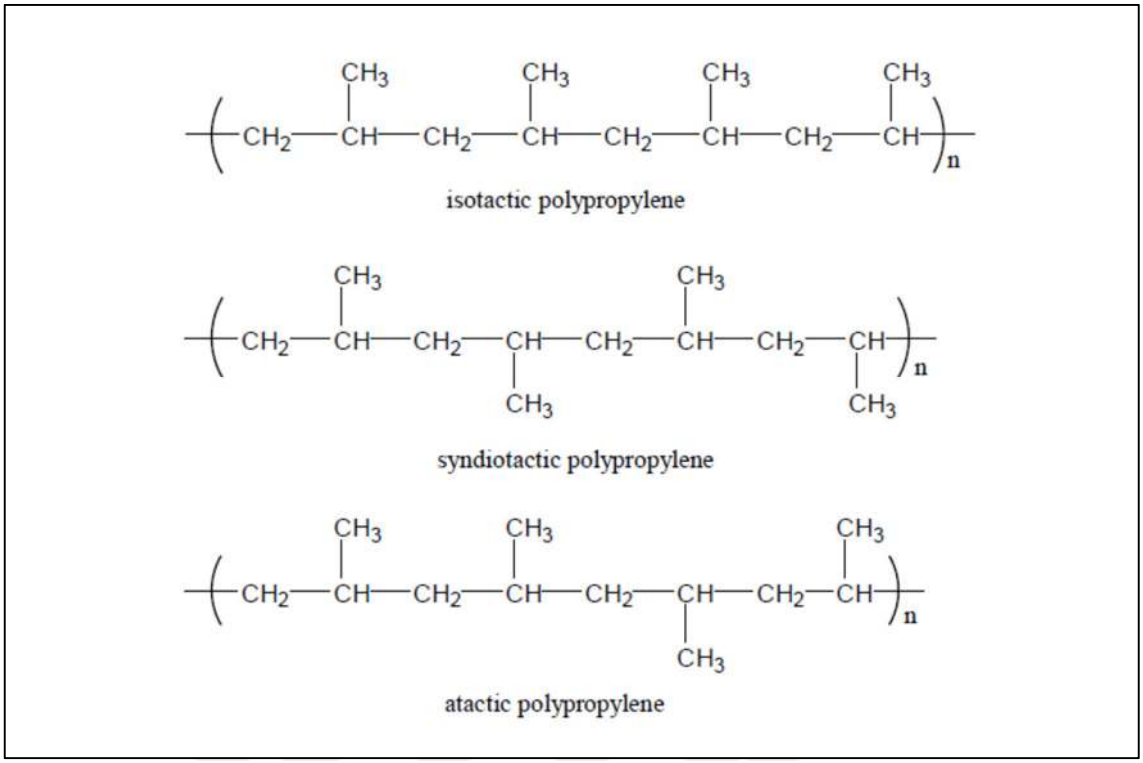

Figure 2.1. *The structure of isotactic, syndiotactic and atactic PP molecule*

Isotactic PP has a crystalline melting point of about 160-175 °C that differs by the grade and the frequency/heating rate. For injection molding of the isotactic propylene, mold temperature that is in the range of 20-60 °C is preferable, allowing the possibility of reduced warpage and increased dimensional stability. Thus, in this study, the temperatures for the melting and molding of polypropylene is chosen as 180 °C and 35 °C, respectively.

Since polypropylene is a low-cost material in addition to its superior properties, it is one of the widely used thermoplastic polymers in the market especially in the applications of plastics and fibers. Typical applications of PP are listed in Table 2.1. [27]

Table 2.1. *Typical applications of PP*

Sector	Typical applications
Household goods	Buckets, bowls, bottle crates, toys, bottle caps, bottles, food processor housing, video cassettes, luggage
Automotive industry	Radiator expansion tanks, brake fluid reservoirs fittings, steering wheel covers, wheel arch liner, bumpers, bumper covers, side strips, spoilers, mudguards, battery cases, tool boxes
Fibers	Artificial sport surfaces, monofilaments for rope and cordage, stretched tapes, woven carpet backing, packaging sacks and tarpaulins, staple fibers, coarse fibers, filament yarns, fine fibers
Domestic appliances	Dishwasher parts such as top frame, basement, tubs, extruded gaskets, water duct, water softener compartment, etc. Washing machine parts such as a detergent dispenser, door frames, inlet and outlet pipes, bellows, feet and wheel, housings and ducts, etc. Refrigerator parts such as boxes, containers, drawers, ducts, inlet and outlet pipes etc. Microwave oven cabinet, irons and coffee maker body parts
Packaging	Margarine and ice-cream tubs, films, compartmentalised meal trays, thin-walled packaging for, e.g., disposable food trays, dessert cups and confectionery boxes, strapping tapes, blister packaging
Pipes and fittings	Solid rods, punching plates, hot wire reservoirs, tower packings for distillation columns, domestic wastewater pipes, pressure pipes, heat exchangers, corrugated pipes, small diameter tubing, e.g., biro cartridges, drinking straws
Furniture	Stackable chairs

Several additives are incorporated into PP addressing different functionalities. Commonly used functional additives for PP are listed in Table 2.2.[27]. This study focuses on mainly the effect of several flame retardants on the flammability of polypropylene; however, a light stabilizer is also added to PP to check its synergic effects with FRs in addition to providing stability against visible light. Moreover, antibacterial additives and multifunctional processing aid are also used in different FR formulations.

Table 2.2. *Commonly used functional additives for PP*

Additive	Functionality
Antistatic agents	To reduce the accumulation of dust and associated possible fire hazard
Slipping agents	To decrease the friction between the film and the machinery during processing
Anti-blocking agents	To avoid films sticking together
Metal deactivators	To reduce degradation due to the presence of metals
Blowing agents	To reduce density
Nucleating agents	To improve transparency and clarity
Antifogging agents	To prevent condensation forming
Biocides	To control the growth of micro-organisms and bacteria
Flame retardants	To reduce the flammability of the material or to suppress smoke
Antioxidants	To prevent thermal-oxidative degradation during processing and service
Lubricants	To lower melt viscosity and prevent sticking to the metal surface
UV stabilizers	To protect against harmful UV radiation
Light stabilizer	To provide stability against visible light

2.2. The Definition of Flame Retardancy

Flame retardancy term refers to the ability of a material that suppress or slow down the combustion process under the specific fire scenario. Some materials have this ability inherently (e.g. aramid fibers), thanks to their chemical structure that makes them resist to break down into flammable molecular fragments. However, some other materials (e.g. polyolefins) need to be made flame retardant by intervention. The flame retardancy ability can be brought into these materials by using some chemical compounds called flame retardants [28,29].

A flame-retardant material can also be called fire retardant. These terms correspond to the similar meaning and can be substituted for each other. An ideal flame retardant material should meet some special requirements; high resistance to ignition and flame propagation, a low rate of combustion and smoke generation, low combustibility and toxicity of combustion gases, maintenance of the original base material's performance, no change in appearance, sustentation of flammability during use and compliance to flame retardant regulations [30,31].

2.3. The Need for Non-Halogenated Flame Retardants

Flame retardants are generally classified into halogenated and non-halogenated flame retardants. Until recently, the majority of the flame retardants were halogen based and mostly used in electronics, building insulation, transportation, and home furnishings. These flame retardants work in the gas phase and act directly on the flame by quenching of reactive radical species. Chlorine (chlorinated) and bromine (brominated) FRs are mainly used halogenated flame retardants. Brominated retardants are more effective than chlorinated ones however they associated with more concerns about human health.

Halogenated flame retardants are very effective in a wide range of polymers; however, they are reported to be toxic, persistent and bioaccumulative. Under thermal stress, they produce halogenated dioxins and furans during combustion which are extremely toxic. They are semi-volatile and can migrate from products into dust that leads to human exposure by inhalation. Furthermore, they can be absorbed into human bodies by dermal contact with treated products. Moreover, they can adsorb on walls and windows by forming thin films. In the case of landfilling, they can leach into water and soil and therefore transfer into plants and animals through the food chain.

Many halogenated flame retardants have been pointed out the reason for many health problems in animals such as cancer, immune and endocrine disruption, and adverse reproductive and neurodevelopmental effects [32]. In humans; reproductive abnormalities, diabetes, thyroid dysregulation, cognitive changes and cryptorchidism have been linked to these chemicals [33-37].

Due to growing concerns over the harmful nature of halogen-based flame retardants, some of their usage was banned or restricted under some environmental regulatory restrictions such as REACH, WEEE and RoHS. According to REACH (Registration, Evaluation and Authorization of Chemicals), flame retardants manufactured and marketed in the EU are supposed to be registered with their hazard data [38]. Tris-(1-aziridinyl)-phosphine oxide (TEPA), tris-(2,3-dibromo-propyl)-phosphate (TRIS) and polybrominated biphenyls (PBB) are not allowed in the articles that contact the skin (e.g. textiles) under REACH regulation [39]. Recycling of electronic waste and the separation of plastics containing brominated compounds were subjected under the EU directive of WEEE (Waste Electrical and Electronic Equipment) [40]. The use of brominated compounds in electric and electronic (E&E) equipment was restricted by the release of

another EU directive, RoHS (Restriction of the use of certain Hazardous Substances) [41].

Industry and academia are now focused toward halogen-free flame retardants (HFFRs) as an alternative to halogenated flame retardants. PINFA (the Phosphorus, Inorganic and Nitrogen Flame Retardants Association) was established in EU and North America to make continuous improvement on environmental and health impact of their flame retardant products and supply information to their customers [42]. The ENFIRO project was conducted to compare the fire performance of halogen-free flame retardants with halogenated flame retardants and it is revealed that HFFRs not only showed similar fire performance but also improved smoke suppression and produced less toxic components [43].

2.4. Modes of Action of Flame Retardants

Flame retardants are chemical compounds that affect the combustion process by inhibiting or even suppressing. There are several ways that they function chemically and/or physically in the solid, liquid, or gas phase. With the addition of flame retardants, it is a complex process dominated by one of these ways; however, they occur concurrently during the combustion [44]. Physically active flame retardants act before entering the combustion cycle while chemically active ones unfold their effect during the combustion cycle in the gas phase and solid phase states. The mode of action of chemically active flame retardants is more efficient than that of physically active flame retardant [45]. A schematic illustration of the mode of action for flame retardants is given Figure 2.2. [46].

2.4.1. Physical action

- **By formation of a protective layer**

Under an external heat flux, some flame retardants form a protective layer with a low thermal conductivity between the condensed (solid) polymer and the pyrolysis gases that leads to a limitation of the heat transfer to the solid polymer. It then diminishes the degradation rate of the polymer and reduces the transfer of as combustible volatile gases and oxygen that feed the flame. This physical action is the principle of intumescence systems [47]. Phosphorus additives, boric acid-based additives, inorganic borates, and low melting glasses are examples of this kind of flame retardants.

- **By cooling**

Some flame retardants degrade endothermically. The endothermic reactions take in heat and cool the polymer to a temperature below that is needed for sustaining the combustion process. Aluminum trihydrate (ATH), magnesium hydroxide (MDH) and zinc borate (ZnB) act in this manner. This action is also known as heat sink mechanism.

- **By dilution**

The addition of some flame retardants (e.g. fillers such as talc or chalk) results in the formation of non-flammable gases. It then leads to dilution of pyrolysis gases to an amount that the ignition limit of the gas mixture is not reached.

2.4.2. Chemical Action

- **Condensed-phase activity**

Two different reactions can occur. Flame retardants can break the polymer chains so that the polymer drips and breaks off the sphere of influence of the flame. Or, the flame retardants can cause the formation of a carbonized layer (charring) at the surface of the polymer by chemical transformation of the degrading polymer chains that acts as a physical barrier between the gas and the condensed phases protecting the underlying material from the flame.

- **Gas-phase activity**

The gas-phase activity is based on the interruption of the radical mechanism of the combustion by the flame retardant or the products generated during the degradation of that. This interruption can be caused in the presence of such flame retardants releasing specific radicals (e.g., $Cl^{\bullet}$ and $Br^{\bullet}$) in the gas phase that quench highly reactive species (such as $H^{\bullet}$ and $OH^{\bullet}$) so that less reactive or even inert molecules is formed. Once the radical mechanism is interrupted, it leads to the reduction of fuel arisen from the exothermic reactions during the combustion. Then the system starts to cool down decreasing the supply of flammable gases until a complete suppression of those occurs. Halogen-containing additives are the most widely used flame retardants acting in this manner.

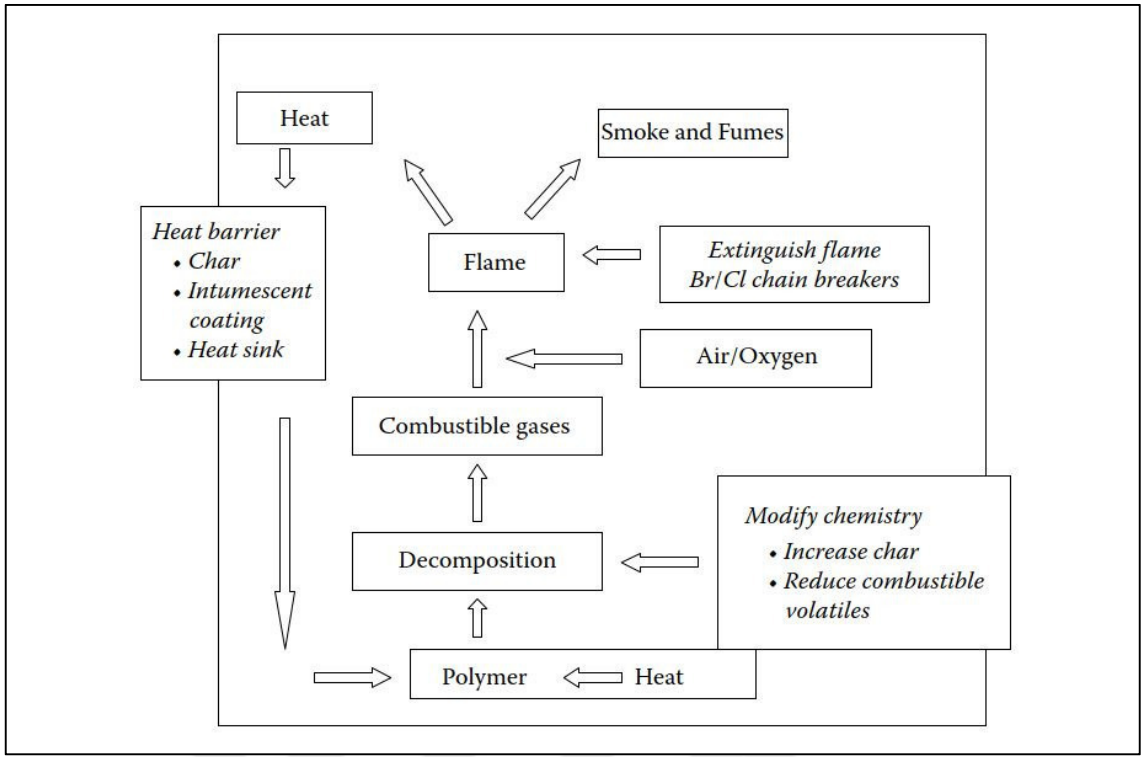

Figure 2.2. *The modes of action of flame retardants*

2.5. Flame Retardancy of Textiles

2.5.1. Flame-retardant strategies in textiles

Flame retardants affect the combustion process by inhibiting or even suppressing. There are several ways that they function chemically and/or physically in the solid, liquid, or gas phase. In the presence of flame retardants, the combustion of the textiles can be interrupted by different strategies. These strategies are classified into five different categories; removal of heat (a), enhancement of decomposition temperature (b), lowered formation of flammable volatiles and increased char formation (c), suppression of the access to oxygen or dilution of flame (d) and interference with flame chemistry and/or increase fuel ignition temperature (e).

The strategies are introduced in Figure 2.3. with their involvement in the relevant stages of the combustion cycle of the textiles [48].

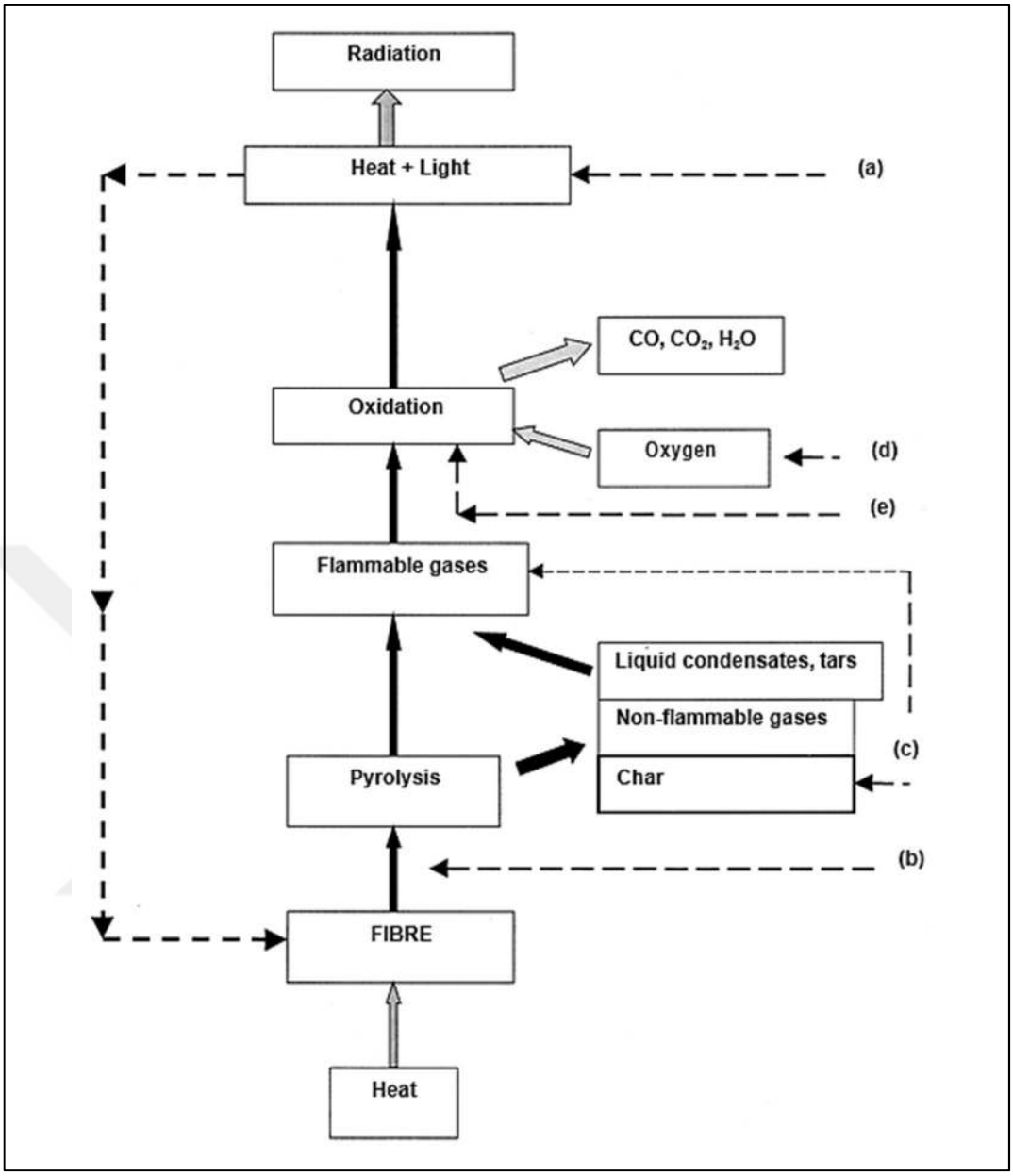

Figure 2.3. *Combustion cycle of the textiles*

The heat arisen from ignition and combustion can be removed through the degradation, dehydration and high heat of fusion. Inorganic and organic phosphorus-containing agents and aluminium hydroxide can be utilized in back coatings of the textiles for the removal of heat (a).

The combustion of the textiles can be suspended by the enhancement of decomposition temperature; however, this enhancement generally is not achieved by using flame retardant additives but reinforcing inherently flame-and heat-resistant fibers

(e.g. aramids, modacrylic, polybenzimidazole fibers, semi carbon and phenolic fibers) in textile composites (b).

The addition of some flame retardants may lead to a decrease in the formation of the flammable volatiles as well as an increase in char formation during combustion. Phosphorus and nitrogen-containing additives, for example, provide this kind of effect in cellulose and wool. In wool, the same effect can also be provided with heavy metal complexes (c).

The access of oxygen to the oxidation stage of the combustion can be hindered or flame dilution can be realized in the presence of flame retardants. These effects can be obtained by using some hydrated and char-promoting flame retardants that release water during combustion. The utilization of halogen-containing flame retardants releasing hydrogen halide results in the same effect as well (d).

Some flame retardants can interfere with flame chemistry and/or increase fuel ignition temperature during combustion. Halogen-containing flame retardants act in this way mostly when they used with antimony oxides (e).

2.5.2. Approaches to obtain flame retardancy in textiles

Flame retardant articles can be obtained by four approaches; reactive approach, additive approach, surface approach and flame retardant finishing. When flame retardants are introduced as co-monomers to react during polymerization, it is called a reactive approach. The additive approach indicates the addition of flame retardant additives to the polymer either before, during or following polymerization. The surface modification of fibers by grafting flame retardant chemicals, and flame retardant finishing that used to transfer FR chemicals to fabrics by impregnation, spraying, foaming and coating are both called surface approach [49].

The schematic representation of these approaches is illustrated in Figure 2.4. [50].

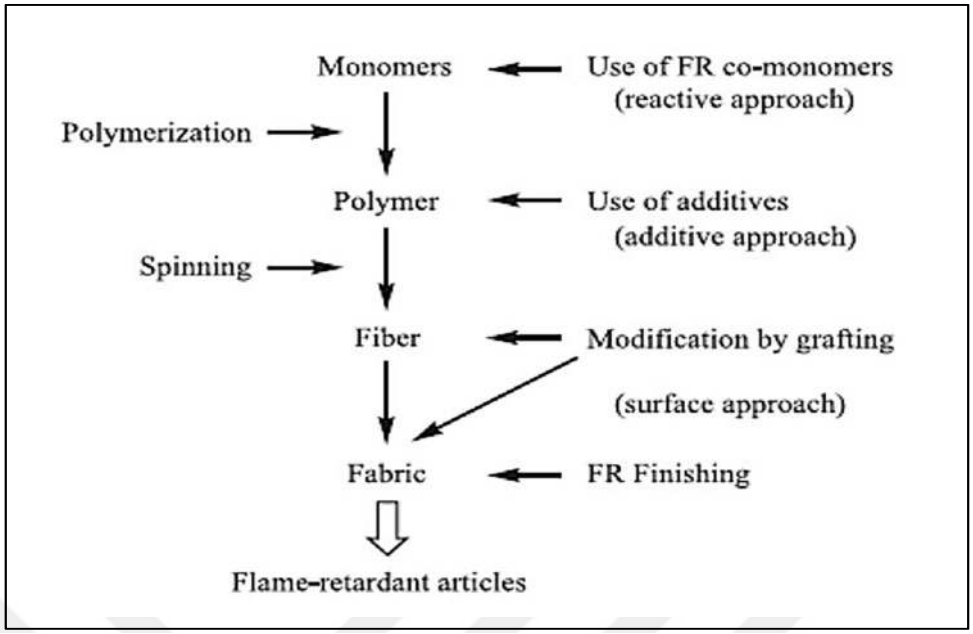

Figure 2.4. *Schematic representation of flame retardancy approaches for polymers and textiles*

For the production of flame retardant composites, the additive approach is extensively used due to enabling high loadings of flame retardants to the polymer. However, it is not favored for the textile fiber production as the additives can clog spinnerets during spinning and weaken the fiber as well. By the additive approach, flame retardants are generally blended in the polymer by compounding, especially in thermoplastics. Regarding their acting mechanism, flame retardant additives could be employed as plasticizers or fillers. If there is compatibility between FR additive and chemical structure of the plastic, the additive called plasticizer, otherwise, it is considered as a filler.

Despite the drawbacks of the additive approach in fiber spinning, it promises the longer durability against washing compared to conventionally produced flame retarded textiles. It is economical to blend the flame retardants in melt polymer before fiber spinning as well. From this point of view, the additive approach is applied to produce both flame retardant polymer composites and textile fibers in this study.

2.6. Flame Retardant Polypropylene

2.6.1. Flame retardant additives for polypropylene fibers

The additive formulations to produce flame retardant polypropylene fibers were first examined with the use of bromo-organic species in the presence of a synergist. Despite their hazardous effect on health and environments, halogen-antimony and phosphorus-bromine combinations were reported as the preliminary most effective combinations. A detailed review of flame retardants with their potential use in polypropylene fibers was presented in 2003 by Zhang and Horrocks [2].

For the melt spinning of polypropylene fibers, several flame retardants (such as FR-370®, SaFRon® 5371) were developed by Dead Sea Bromine (ICL) researchers. Pentabromobenzyl acrylate was first introduced to be grafted during melt processing of polypropylene that yields good launderability and color stability [51]. Afterwards, SaFRon® 5371 was formulated as a proprietary FR blend for polypropylene carpet fibers. This blend has a content of 63 % bromine and 2.6 % phosphorus and provides the flame retardancy without the utilization of antimony trioxide synergist.

The most promising flame retardant additive for the production of flame retardant PP fibers was offered by ICL with a brand name of FR-370®. It has a chemical formula of tris(tribromoneopentyl) phosphate containing 70 % bromine and 3 % phosphorus in its composition. FR-370® shows an excellent flame retardant efficiency and thermal stability in polypropylene for fiber spinning. Compared to aromatic bromine compounds, it results in relatively improved UV and light stability as well. Furthermore, it does not require to be compounded in collaboration with antimony oxide which may clog spinneret holes during spinning and decrease the fiber strength due to its coarse grain size. The synergetic effect of free radical generators such as 2,3-dimethyl-2,3-diphenylbutane (Perkadox® 30, Akzo Nobel or CCDFB-90, Peroxid-Chemie) with FR-370 was invented in Bromine Compounds Ltd. FR-1025 is another attractive flame retardant additive developed by ICL for PP fiber spinning. It includes pentabromoacrylate and can be used without antimony oxide as well.

A hindered amine, Flamestab® NOR116 (Basf), was proposed to replace antimony trioxide as a synergist for halogen and non-halogen-containing flame retardants. In the presence of this additive, the required level of decabromodiphenyl oxide (DBDPO) in PP blend was lowered compared with when antimony trioxide is present [52]. Flamestab®

NOR 116 is a hindered amine radical stabilizer (an oligomer-linked N-alkoxy-2,2,6,6-tetramethyl-4-substituted-piperidine) and only a small amount of it (0.5-1.5 %) was reported to be enough to pass NFPA 701, MVSS 302, or DIN 4102/B-2 standards. However, it is not declared, halogen-free flame retardant PP fibers developed by Asota GmbH (Linz, Austria) could contain Flamestab NOR 116 as they get the highest S1 classification in European Radiant Panel Test EN ISO 9239-1. Not only NOR 116 improves the flame retardancy and thermal stability of the PP fibers but also provides an improved UV stability. Compared with FR-370, it gives better outdoor stability in PP textiles [53,54]. Similar to NOR 116, Hostavin® NOW XP (Clariant) can be employed as a synergetic for melt spinning of PP fiber. It is a hindered amine light stabilizer as well but of the aminoether class. Incorporation of Hostavin® NOW XP can increase the oxygen index of PP fibers while avoiding yellowing.

SiO_2 nanoparticles are another flame retardant additives examined in PP fibers. Erdem, Cireli and Erdogan (2009) showed that the LOI of PP filaments have increased gradually in the presence of SiO_2 nanoparticles [55].

2.7. Flammability Test Methods

Flammability tests have been developed to examine the performance of associated material in an actual fire. During these tests, different burning parameters of the material such as burning time, dripping, smoke emission, flame spread, and heat release are measured under specific conditions depending on the chosen test method.

Flammability test methods classified into two types depending on the exposure conditions. The first type of flammability tests (also called small-flame exposure ignition tests) is utilized to assess the ignitability of a material when subjected to a small heat source for a short time. The Underwriters Laboratories (UL) 94 and Limiting Oxygen Index (LOI) tests are two commonly used small-flame exposure ignition tests. The second type of flammability tests (also called reaction-to-fire tests) uses thermal exposure to determine the response of a material to the temperatures and heat fluxes in a growing fire. This type of tests can be performed as a bench-scale test and large-scale test. Cone Calorimeter and Micro Combustion Calorimetry (MCC or PCFC (Pyrolysis Combustion Flow Calorimeter)) are two commonly used examples of such bench-scale tests [56]. Flammability test methods used in this study are described in the following sections.

2.7.1. Limiting oxygen index (LOI)

Limiting Oxygen Index term, simply refer to the minimum oxygen concentration (expressed as volume percent) in the oxygen/nitrogen mixture that is necessary for the ignition of specimen with the application of candle-like flame. This test was first proposed in 1966 [57], standardized as NF T 51-071 (in France) [58], ASTM D 2863 (in the United States) [59] and ISO 4589 (international standard) [60].

The schematic illustration of LOI test apparatus is given in Figure 2.5. [61].

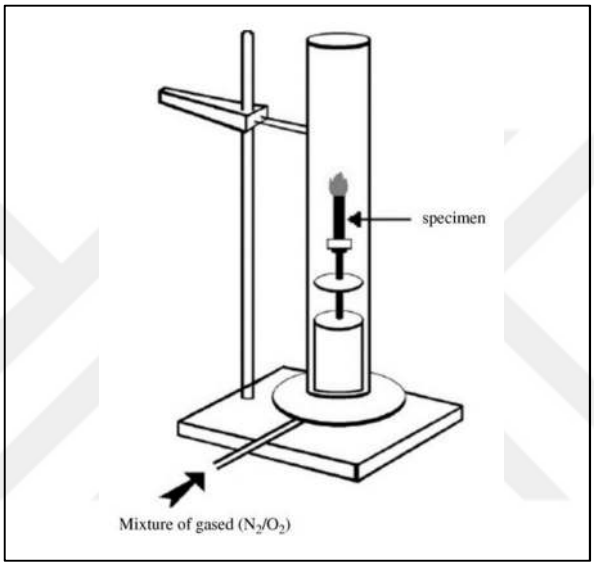

Figure 2.5. *The LOI test apparatus*

During the test, the mixture of these gases depending on the desired oxygen concentration for the test is supplied from the bottom of the vertical glass chimney. When the mixture is got to be stable, the specimen is ignited at its upper end with a burner and it is observed whether the ignition is started or not. The criteria specified at ASTM D2863 to determine the specimen's response for Oxygen Index Measurements is given in Table 3 [59]. If the limit for either "period of burning after ignition(s)" or "extend of burning" is exceeded during the combustion, the specimen is assigned with "X" response; otherwise, it is assigned with "O" response. Later, the following oxygen concentration is adjusted depending on the response that is given by the previous specimen:

i. the oxygen concentration is increased if the specimen gave "O" response; otherwise
ii. the oxygen concentration is decreased if the specimen gave "X" response.

Table 2.3. *The criteria specified at ASTM D2863 for Oxygen Index Measurements*

Test Specimen Type	Ignition Procedure	Alternative Criteria	
		Period of Burning After Ignition(s)	Extent of Burning
I, II, III, IV, and VI	A (top surface ignition)	180	50 mm below the top of the specimen
I, II, III, IV, and VI	B (propagating ignition)	180	50 mm below the upper reference mark
V	propagating ignition	180	80 mm below the upper reference mark (on the frame)

I: for molding materials
II: for cellular materials
III: for sheet materials
IV: alternative size for self-supporting molding or sheet materials
V: for flexible film or sheet
VI: for thin film; limited to film that can be rolled by the wire specified in 6.7

By examining a series of specimens in different oxygen concentrations, the limiting oxygen index (LOI) is determined. According to the ASTM D2863, the successive steps for the calculation of the LOI value is summarized below:

Step 1: Considering the criteria in Table 3, a series of specimens are tested and assigned with "X" or "O" response until two oxygen concentrations are found that differ by ≤1.0 % in percent volume. For those oxygen concentrations, one specimen must give an "O" response and the other specimen must give an "X" response. The oxygen concentration at which the specimen gives "O" response is defined as the preliminary oxygen concentration for Step 2.

Step 2: Starting from the preliminary oxygen concentration found in Step 1, the oxygen concentration is changed by 0.2 % of the total gas mixture (d) until a different response is obtained by means of "X" or "O".

Step 3: Starting from the oxygen concentration at which the specimen gives a different response at Step 2, the oxygen concentration is differed by maintaining d=0.2 % again. Considering the responses of the specimen, five specimens are tested in this step and the last oxygen concentration is designated as C_F.

Step 4: The limiting oxygen index (LOI) is calculated by using the formula [59]:

$$LOI = C_F + kd \tag{2.1}$$

where C_F is the last oxygen concentration found in Step 3, k is a factor specified in ASTM D2863 and read from the relevant table depending on the order of the five responses at Step 3 (such as XOOOO, XOXOX, and OOOOX), d is step size for the concentration changes (d=0.2 %, unless otherwise instructed).

Considering the proportion of oxygen in the air which is 21%, materials are classified as combustible or self-extinguishing depending on their LOI values. If the LOI value is lower than 21%, materials are categorized as combustible while those with an LOI above 21% are called as self-extinguishing. Any polymeric material (such as fibers, textiles and plastics) with at least 25 % LOI may be considered to be flame retardant. In other words, 25 % or higher oxygen concentration must be present for the burning of such material [48,62]. The higher LOI means that the material shows better flame retardant property [25,61].

2.7.2. Cone calorimeter

The Cone Calorimeter is the most effective bench scale instrument to define the fire behavior of materials [63]. The name of cone calorimeter stems from the conical shape heater that is used to irradiate the specimen during the test. Cone calorimeter test is standardized as ASTM E 1354 and ISO 5660 [64].

The principle of the cone calorimeter is based on the measurement of the oxygen consumption in the combustion gases of a sample while the sample is exposed to an external heat flux by a heater. The schematic view of cone calorimeter is shown in Figure 2.6. [25]. Due to the irradiance delivered by a conical radiant heater, the material starts to decompose, and flammable gases emerge from the sample. The combustion is prompted by an electric spark. The gases evolved from combustion pass through the heating cone and are caught by an exhaust duct system with a centrifugal fan and a hood.

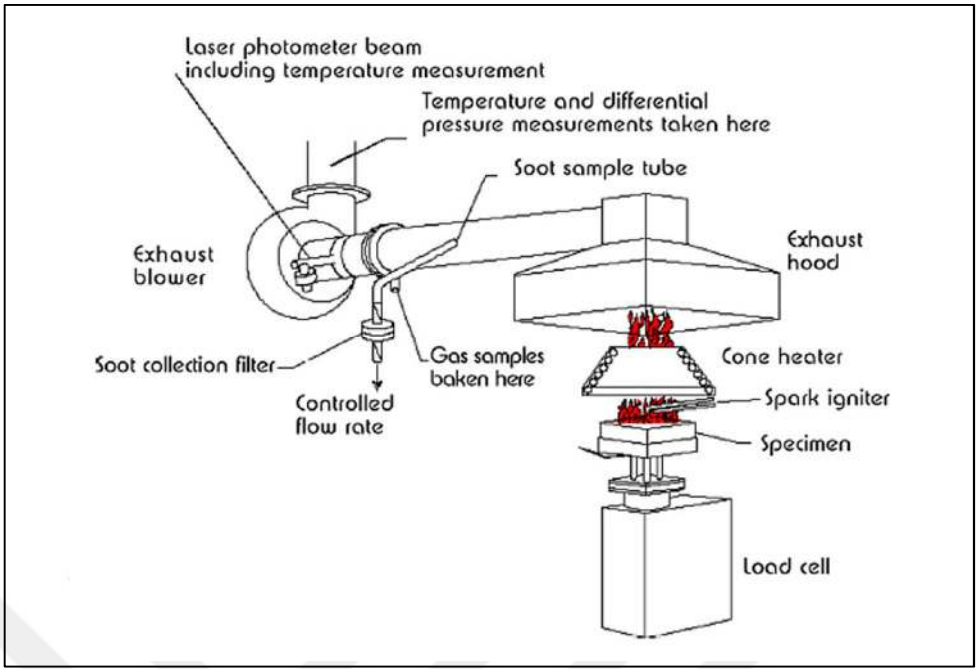

Figure 2.6. *The schematic view of cone calorimeter*

External heat flux used in cone calorimeter test can differ from 10 kW/m^2 to 100 kW/m^2; the irradiances of 35 kW m^2 and 50 kW m^2 are most widely used irradiances to get reproducible results for the test. The horizontal direction between the sample surface and heater is typically 2.5 cm. The horizontally located sample is generally preferred. The dimensions of the sample used in the test are 100 mm x 100 mm with a maximum thickness of 50 mm. In a cone calorimeter, large amounts of data can be obtained, such as heat release rate (HRR), peak of heat release rate (pHRR), time to ignition (TTI), time of combustion (TOF), total heat released (THR), mass loss rate (MLR), total smoke released (TSR) and specific extinction area (SEA) [25,61,63-65].

2.7.3. MCC

Microscale combustion calorimeter (MCC) is a non-flaming combustion test which measures the heat release rate of milligram-sized materials. MCC also called pyrolysis-combustion flow calorimeter (PCFC), reproduces the flaming combustion by separating the pyrolysis and oxidation processes in a controlled manner. MCC instrument is described under ASTM D7309. According to the ASTM D7309, MCC test can be operated for anaerobic pyrolysis and oxidative (aerobic) pyrolysis, which are classified in Method A and B respectively. Most generally, it is used according to the method A for

complete combustion. Since the pyrolysis process is anaerobic in flaming combustion due to the consumption of the available oxygen by the flame itself, pyrolysis (condensed phase) and combustion (gas phase) processes are decoupled and designed to completion in MCC. A schematic representation of the combustion processes in flame and MCC is illustrated in Figure 2.7. [66].

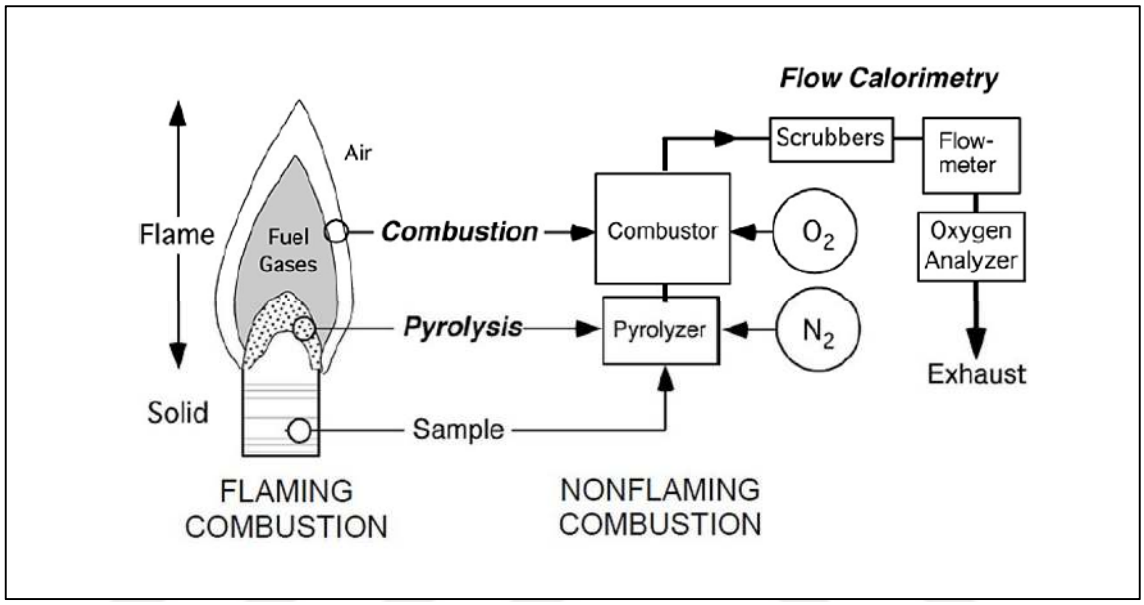

Figure 2.7. *A schematic representation of the combustion processes in flame and MCC*

During the test under anaerobic conditions, a 1–10 mg sample is heated up to 750 °C max, at a heating rate of 0.5-4 K/s (typically 1 K/s) in the pyrolizer where thermally decomposed to gaseous fuel. The volatile thermal decomposition products generated from the pyrolyzed sample are migrated by an inert gas stream (typically nitrogen) into the combustor chamber. Prior to entering the combustor, pyrolysis products are mixed with excess oxygen (80/20 nitrogen/oxygen flow) and temperature of combustor is fixed typically at 900 °C to ensure complete combustion. In the combustor, pyrolysis products are oxidized to carbon dioxide, water, and acid gases. As pyrolysis products consumes oxygen during oxidization, the amount of oxygen consumed is detected by an oxygen analyzer and the heat release rate of the samples is calculated according to the Thornton's rule (extended by Huggetts for solids afterwards). In case of oxidative pyrolysis, 80/20 nitrogen/oxygen flow is used in the prolyzer and the test conducted in the same way as described. The resistance of a material or a char to thermo-oxidation can be evaluated by

utilizing the aerobic pyrolysis (method B). In MCC, the data of peak of heat release rate (PHRR), heat release capacity (HRC), total heat release (THR) and temperature at pHRR (Tmax) are obtained.

Due to its separated design for pyrolysis and combustion, combustion (oxygen rate and temperature) is monitored by a controlled heating rate in MCC. However, in cone calorimeter and other tests, heating rate is not controlled or distributed homogeneously. Compared to other tests (e.g. cone calorimeter) in which larger amounts of material must be introduced, MCC requires only a small amount of material. Thus, MCC enables the evaluation of flammability of the new formulations without the need of sample preparation processes such as extrusion and injection molding. On the other hand, thermal barrier effect driven especially by intumescent phenomena may not be determined in MCC because of the too small sample size that vanishes the effect. Nevertheless, the difference between the results of MCC and cone calorimeter can be utilized to identify the mode-of-action of flame retardants such as charring.

2.8. Antibacterial Applications in Textiles

An antimicrobial is a substance which has the abilitiy to kill or inhibit microbial growth. Antimicrobial term covers a broad range of substances which are classified according to target microorganism: Substances that are effective against bacteria, viruses and fungi are called antibacterials, antivirals and antifungals (antimycotics), respectively.

During production, usage or storage, textile materials (woven, nonwoven, knitted, and composites) can host the growth of micro-organisms which cause detrimental effects on both customer and textiles itself (see Figure 2.8 [67]. Especially in hospital and healthcare institutions, the possibility for the exposure of microorganism becomes higher since these places are ideal environments for the proliferation and spread of micro-organisms. Because of their hydrophobic properties, synthetic fibers are more resistant to microorganisms than natural fibers. Carbohydrates in cellulosic fibers and protein in animal fibers can be a nutrient and energy source for microorganisms under suitable conditions such as temperature and humidity [68]. Thus, several antimicrobial agents varying in chemical composition, efficacy, application method, impact on individuals and the environment, and cost were developed to impart antimicrobial functionality to textiles. These antimicrobial agents include Quaternary Ammonium Compounds (QAC),

N-halamines, Chitosan, Polybiguanides, Bioactive Plant-based Antimicrobial Agents, Halogenated Phenols and Nanoparticles of Noble Metals and Metal Oxides [69]. In terms of their chemical structure, antimicrobial agents are classified into organic and inorganic structures. Chitosan, N-halamines and quaternary ammonium salts are the most commonly used organic agents. Inorganic microbial agents are mainly metals and metal oxides (such as silver, titanium dioxide, zinc oxide and copper oxide) and their nano-sized derivatives [69]. Heavy metals (such as Ag, Zn and Cu) are very favorable due to their broad spectrum biocidal activity at very low loadings either in the free state or in compounds. Since the silver (Ag) is effective against a broad range of microorganisms, being active for a long time, thermally stable, little toxic to mammalian cells and easy to use, it is the most used antibacterial among those metals [70]; however, it is an expensive material. Zn and Cu are cost effective alternatives of silver although they have relatively less antibacterial capacity than that of it. Studies that were conducted to improve the activity of metal and metal oxide antimicrobials has led to the development of a new generation of biocides: their nano-sized derivatives; such as nano silver (Ag), nano zinc oxide (ZnO) and nano copper II oxide (Nano-CuO). Due to the high specific surface area of nanosized metal and metal oxides arising from their small particle size, more interaction is expected between the nanoparticles and microorganisms in addition to the more release of metal cations from the particle surface, and hence, an increased biocidal activity. Oxidative stress is suggested as the main mechanism of nanoparticles that causes damages in the lipids, proteins, and DNA of microorganisms. A classification of antimicrobial agents depending on their efficiency, mechanism of antimicrobial activity and washing resistance is diagrammed in Figure 2.9 [69].

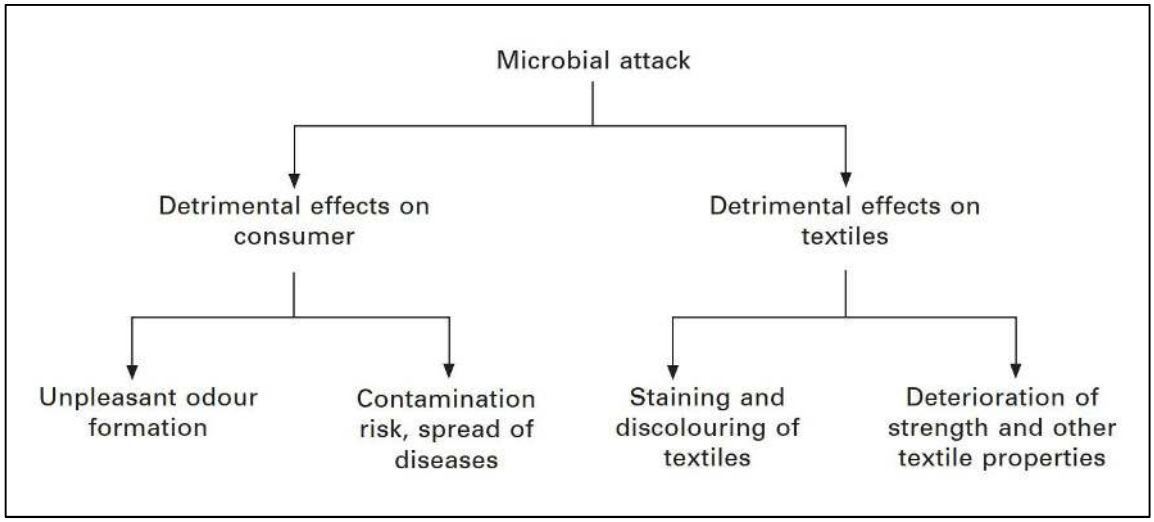

Figure 2.8. *Effects of microbes on consumers and textiles*

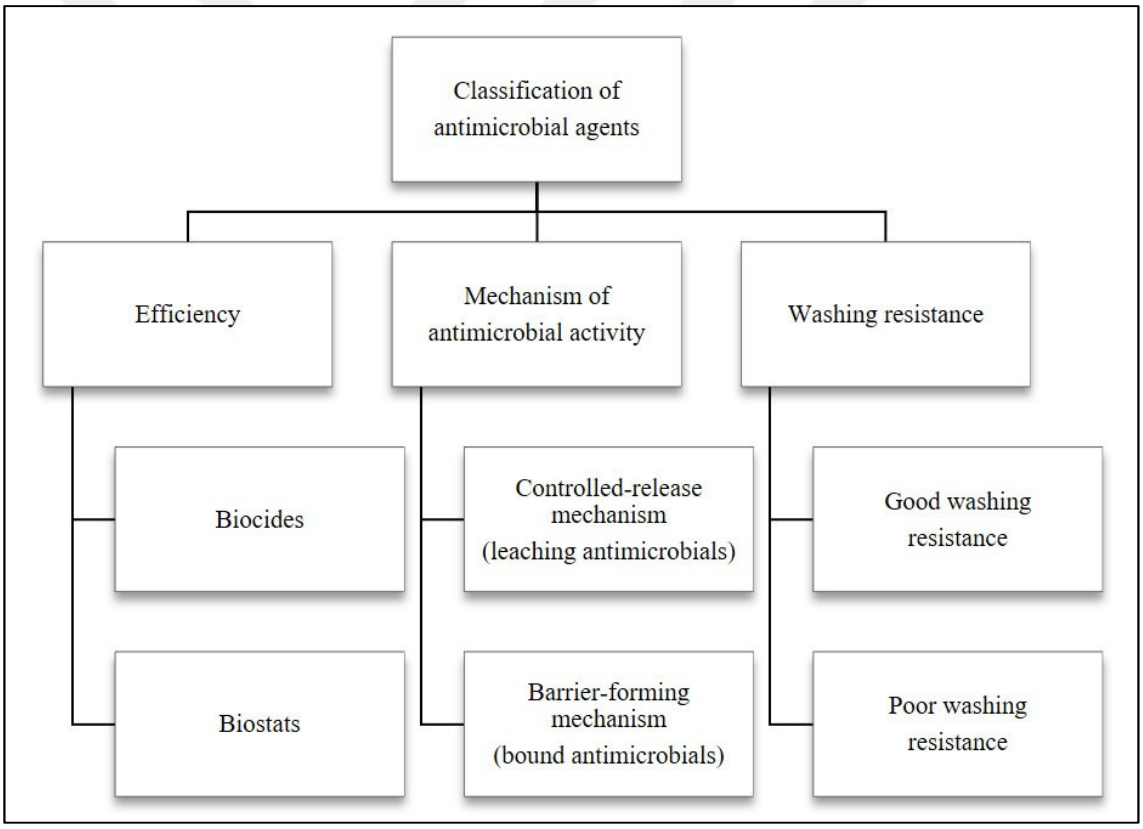

Figure 2.9. *Classification of antimicrobial agents*

Antimicrobial textiles can be produced by either the incorporation of an antimicrobial agent into the polymer melt before extrusion or into the spinning bath (Figure 2.10.a) or after-treatment of the fiber, yarn or the fabric with antimicrobial agents during finishing processes by different techniques such as coating, exhaust, spray, pad–dry–cure and foam

(Figure 2.10.b). In the case of the production of antimicrobial fibers/yarns, chemical bonding of antimicrobials onto the fibers (Figure 2.10.c) is another method in addition to those mentioned above. Incorporation of antimicrobial agents to the fiber matrix is suitable only for synthetic fibers. Since the active agents are physically embedded within the fiber structure and need to migrate to the surface, a slow-release rate of those agents is expected. To achieve a reasonable antibacterial activity in melt-spun fibers, an antimicrobial agent that was incorporated into polymer melt must be diffusible and distributed homogeneously within the fiber [71] . After-treatment methods can be applied both natural and synthetic fibers, however, the possibility of interference with textile handling properties should be considered. Regarding the efficacy of an antimicrobial finish, one must take into consideration the mechanism of antimicrobial activity, method of application, and efficiency and durability of the antimicrobial agent. Among these methods, the best durability is provided by chemical bonding [67].

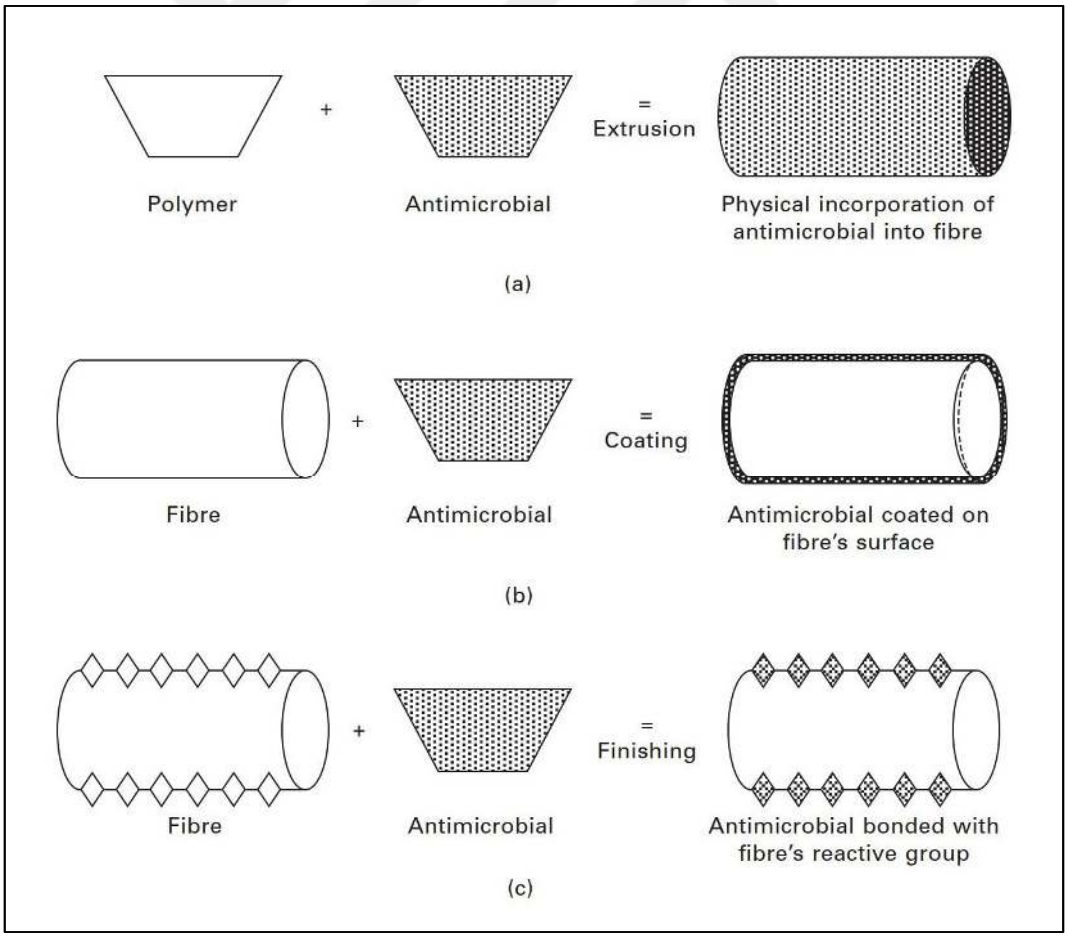

Figure 2.10. *Illustration of antimicrobial fibre production*

.

Antimicrobial agents can be classified into two groups depending on their effects on the growth of antimicrobials: biocidal and biostatic. The biocides (bactericides and fungicides) are capable of killing microorganisms (bacteria and fungi) while the biostats (bacteriostats and fungistats) are effective to inhibit the growth of microorganisms (see Figure 2.11) [71]. The concentration of the active agent in the textile affects the mechanism of antimicrobial activity greatly. Biostatic activity is assessed regarding the minimum inhibitory concentration (MIC). The minimum biocidal concentration (MBC) is utilized for the assessment of biocidal activity, however, MBC value is needed to be excessed [69].

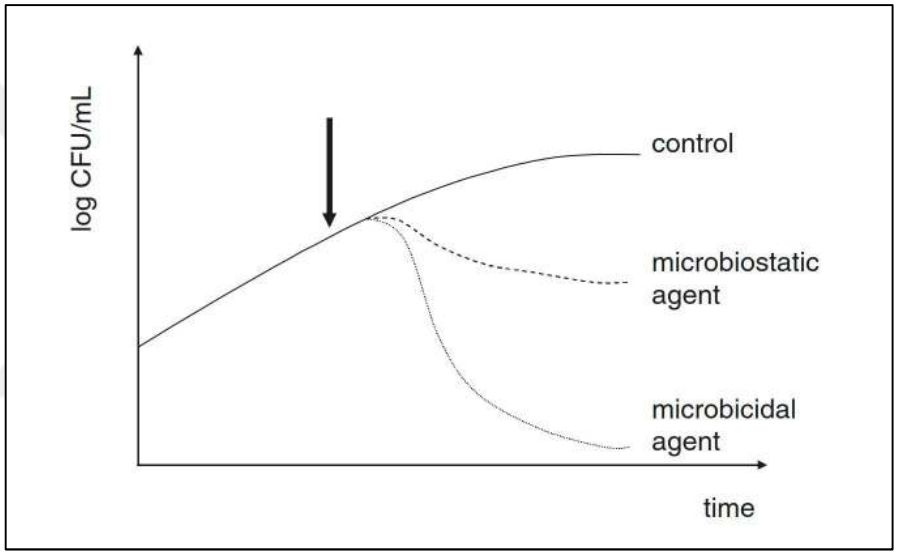

Figure 2.11. *Changes in microbial growth after addition of an antimicrobial agent (arrow represents the addition an antimicrobial agent; CFU colony forming unit)*

Some selected studies that were conducted to determine antibacterial activity of ZnO and Nano-CuO in the polypropylene textiles are summarized below:

Kara, Ureyen, and Erdogan [72] studied the antibacterial activity of cupric oxide (Nano-CuO) powders in PP fibers. PP/Nano-CuO composite fibers were produced by the melt spinning of the compositions prepared by the physical incorporation of Nano-CuO (0.3 wt% and 1 wt%) into the PP matrix. For each Nano-CuO content Cross-sectional shape of the filaments within each fiber was varied by using the three different shapes: circular, trilobal and triangular. The antibacterial efficiency of the produced fibers was tested according to the JIS L 1902 by utilizing quantitative test method against *Escherichia coli*

(*E. coli*, gram-negative bacteria). Regardless of the cross-sectional shape, all fibers showed strong antibacterial activity against E. coli with an antibacterial reduction of >log3.

Fiedot, Karbownik, Maliszewska, Rac, Wozniak, and Teterycz [73] examined the deposition of hexagonal ZnO rods onto the surface PP fabrics to increase its antibacterial efficiency. 1/1 plain weave PP fabric with a thickness of 0.20 mm was used. Deposition of one-dimensional structures of zinc oxide on PP fabrics was performed with chemical bath deposition (CBD) at 75 °C and 90 °C. To change the property of the surface of PP fabrics from hydrophobic to hydrophilic, some PP fabrics were treated with Remote-Oxygen-Plasma technique prior to deposition. Antibacterial activity of the fabrics against *Staphylococcus aureus* (Gram-positive bacteria) and *Escherichia coli* (Gram-negative bacteria) were assessed according to the ISO 20645 with inhibition zone test. The weight of the fabrics was recorded before and after the ZnO deposition. It is found that the number of ZnO rods on the surface of the fabrics was three times higher in the presence of oxygen treatment, especially those formed at 90 °C. Moreover, the adhesion of ZnO rods was also much better for the fabrics subjected to plasma.

E. coli is found to be much more susceptible to ZnO deposited PP fabrics than S. Aureus; for the fabric treated by plasma at 90 °C, the survival rate of *E. Coli* was even below the detection limit while it was about 27±1% for S. Aureus after 24-hour incubation. According to the authors, these results can be associated with the differences in cell wall thickness, the morphology of the outer cell membrane and the mobility of those bacteria. Moreover, the authors supposed that the size, shape, and orientation of ZnO rods on the fabric surface are the key parameters affecting the antibacterial properties of ZnO rods.

For *E. Coli*, a correlation was found between antibacterial activity and the aspect ratio of ZnO rods: the greater aspect ratio was present, higher antibacterial activity was observed. The reason for this could be enhanced efficiency of the photocatalytic process that leads to the generation of more reactive oxygen species (ROS). The formation of ROS ($^{\bullet}O_2^-$, H_2O_2, $^{\bullet}OH$ for ZnO) is proposed to be the most important mechanism of ZnO toxicity to E. coli. SEM images of the interaction between *E. coli* and ZnO particles is given in Figure 2.12.

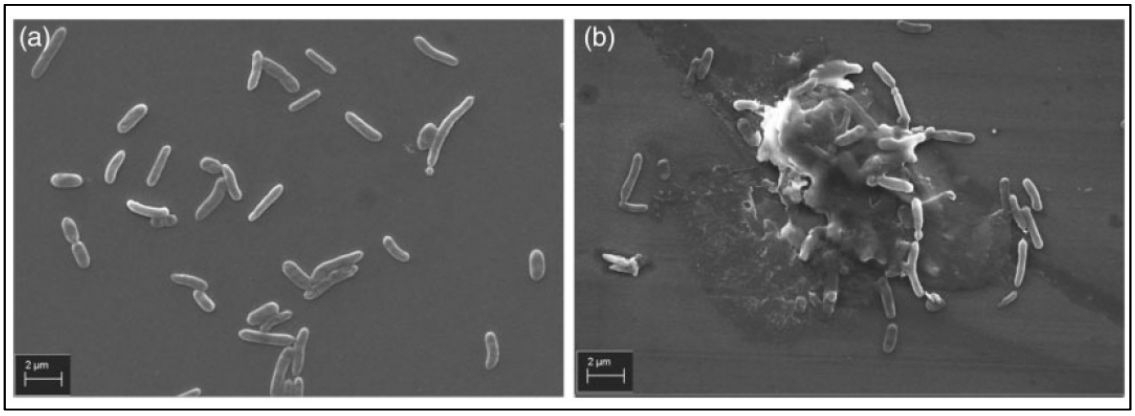

Figure 2.12. *The interaction of between E. coli and ZnO particles: (a) E. coli alone (control); (b) E. coli treated ZnO*

The antibacterial efficiency of *S. aureus* was higher on the PP fabrics which were not subject to plasma. The increased efficiency of *S. aureus* on those fabrics was related to the mobility of target bacteria and the distance between ZnO rods, since S. aureus is a non-motile bacterium and ZnO rods did not form a compact structure on the surfaces of the fabrics in the absence of oxygen plasma. Fabrics were also washed (according to PN-EN ISO 6330) after the grown of ZnO rods to evaluate the effect of washing on the antibacterial activity of the fabrics. Results showed that the washing process resulted in a decrease of about 10 % on the antibacterial activity of the fabrics subjected to plasma. İn case of the untreated fabrics, decrease in antibacterial activity was even higher, of about 45 %. However, it must be noted that ZnO layer was more stable at the fabrics subjected to plasma against washing that it caused damage of ZnO rods on the fabrics of about 15% while this value was about 65 % for those on the untreated fabrics.

Erem, Ozcan and Skrifvars [74] studied the antimicrobial activity of cupric oxide (Nano-CuO) nanoparticles (NPs) in PP fibers. Prior to melt spinning, compositions containing Nano-CuO NPs were prepared by the incorporation of Nano-CuO NPs into PP matrix at four different concentrations (0.5 %, 1 %, 3% and 5%). Those compositions were, then, melt-spun into nanocomposite fibers having round cross sectional shape. To improve the absorptivity of the surfaces of nanocomposite PP fibers, either cold plasma or chemical finishing was applied. Cold plasma treatment was performed on the nanocomposite fibers for 15 min by using dielectric barrier discharge plasma. Chemical finishing is done with the application a silicone softener to the nanocompostite fibers. Antibacterial activity of the produced fibers against Staphylococcus aureus (Gram-positive bacteria) and Klebsiella pneumoniae (Gram-negative bacteria) were tested

according to the ASTM E2149–01 by utilising the quantitative method. comparing the number of CFUs between the treated and untrreat fibers. They found that Staphylococcus aureus was more susceptible to ZnO–NPs than Klebsiella pneumoniae. The differences between the antibacterial activity of two bacteria is accociated with to the different external structures of those that Staphylococcus aureus has thicker peptidoglycan structure than Klebsiella pneumoniae. They also found that chemical finishing had a greater impact on the antibacterial efficiency of ZnO–NPs than plasma threatment resulting in more bacterial reduction. This reduction was correlated with the water absorption of the fibers that chemical finishing resulted in more water absorpion than the plasma treatment. The graphs of the antimicrobial activity of ZnO–NPs in PP nanocomposite fibers versus ZnO–NPs contents were given in Figure 2.13.

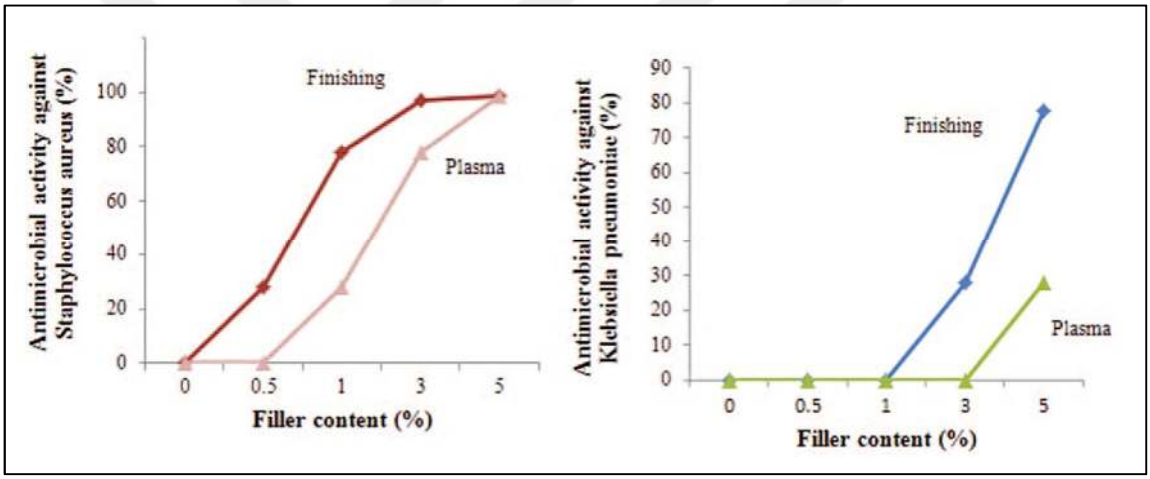

Figure 2.13. *Antimicrobial activity of ZnO–NPs in PP nanocomposite fibers*

2.9. Antibacterial Test Methods

Several test systems have been established to asses the antibacterial activity of the textiles. A list of standards to test the performance of textiles/fabrics are tabulated in Table 2.4. [75]. These systems can be classifieds into two major methods: agar diffusion test and suspension test [76].

Table 2.4. *Industrial standard evaluation tests for the assesment of antibacterial activity of the textiles/fabrics*

Standart	Title
AATCC 30	Antifungal Activity, Assessment on Textile Materials
AATCC 90	Antibacterial Activity, Assessment of Textile Materials
AATCC 100	Assessment of Antibacterial Finishes on Textile Materials
AATCC 147	Antibacterial Activity Assessment of Textile Materials
ASTM E2149	Standard Test Method for Determining the Antimicrobial Activity of Antimicrobial Agents Under Dynamic Contact Conditions
ASTM E2722	Standard Test Method for Using Seeded-Agar for the Screening Assessment of Antimicrobial Activity in Fabric and Air Filter Media
ISO 20645	Textile fabrics - Determination of Antibacterial Activity
ISO 20743	Textiles-Determination of Antibacterial Activity of Antibacterial Finished Products
JIS L 1902	Testing for Antibacterial Activity and Efficacy on Textile Products
SN 195920	Textile Fabrics - Determination of the Antibacterial Activity
SN 195924	Textile Fabrics; Determination of the Antibacterial Activity

Agar diffusion test is quick and easy to perform methods which use the zone of inhibition around the sample to determine the antibacterial activity. Textile articles are placed on the surface of agar plates filled with bacteria culture to detect if bacterial growth around articles is hindered. If a textile article shows a clear zone of inhibition, it is evident that bacteria are susceptible to an antibacterial agent. the diameter of zone of inhibition provides ınformation about the antimicrobial activity potency or the release-rate of the diffusive agent. In case that the bacteria are resistant to antibacterial agent, no zone of inhibition appears around the textile article. The presence of the zone of inhibition is not fully evident that bacteria are killed, however, it might only be an indication of the prevented growing of those. Since the efficiency of the agar diffusion tests is based on the diffusion of the antibacterial agent from textile into agar, covalently attached antimicrobial agents are not expected to show a zone of inhibition. It must be noted that the agar diffusion test is an effective method on the fabrics, however, for other textile articles, it can yield very poor or imprecise results. An example of the zone of inhibition obtained by testing of wound dressing is shown in Figure 2.14. [77].

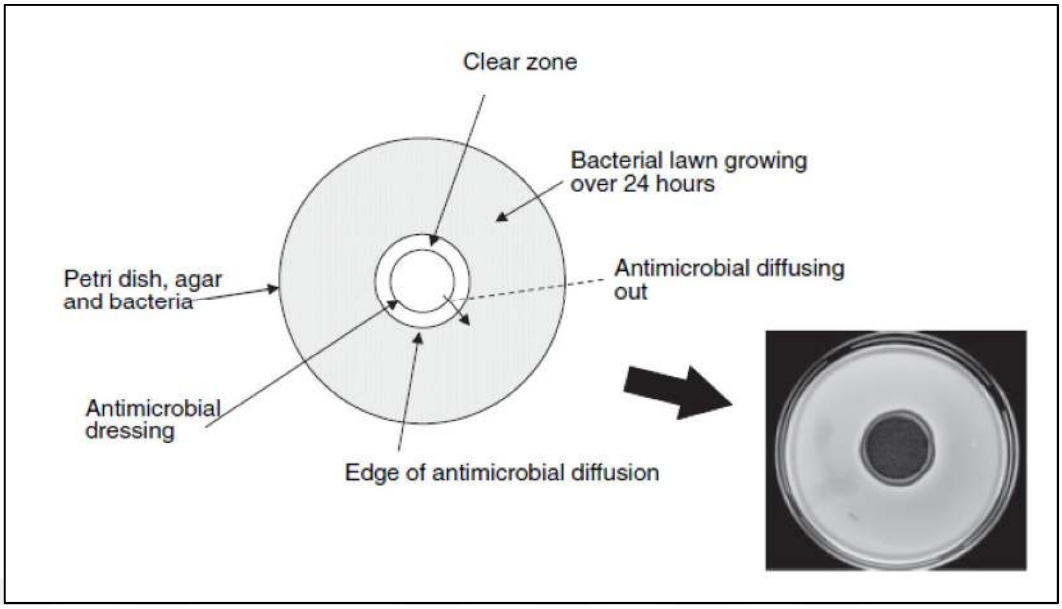

Figure 2.14. *Illustration of the zone of inhibition*

Suspension test uses a suspension medium in which the bacteria were exposed with textiles articles containing antibacterial agents. It is a quantitative method that the number of bacterias was counted before and after the exposure for the control sample and treated sample and the difference between those are expressed in log reduction. This method enables the antimicrobial agent to affect the growth of bacteria even the antibacterial agent cannot diffuse out the textile. Therefore, unlike the agar diffusion test, it is possible to assess the antibacterial activity of textile containing non-diffusible agents. Among these test, JIS L 1902 and ISO 20743 stepped forward by serving realistic, flexible, sensitive and reproducible results, even though they are time consuming and expensive methods at the same time. A summary of the textile methods with the respective standards is given in Table 2.5. [75].

Table 2.5. *A summary of the textile methods with the respective standards*

Classification	Main Steps			Standards
Agar zone of inhibition methods	 Samples on bacteria inoculated nutrient agar		 Measure zones of inhibition after incubation	AATCC 147 ISO 20645 SN 195920
	 Bacteria inoculated nutrient agar on top of the sample	 Measure zone of inhibition after incubation	 Determine number of CFUs in suspension after dissolving agar	AATCC 30 AATCC 90 ASTM E2722
Suspension methods	 Submerge sample in bacterial suspension in medium	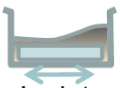 Incubate under shaking	 Determine number of CFUs in suspension	ASTM E2149
	 Submerge porous sample in bacterial suspension	 Remove liquid, incubate, detach bacteria by vortexing or sonication	 Determine number of CFUs in suspension	JIS L 1902 SN 195924 AATCC 100 ISO 20743

2.10. Production Methods of Polymer Composites and Fibers

In this study, polymer composites were produced by the incorporation of flame retardant additives to polypropylene by extrusion and following injection molding. Considering thermal properties and flammability of the polymer composites, the blends that resulted in better flame retardancy were determined to be used for the melt spinning of FR fibers. These processes are described in this section.

2.10.1. Extrusion

Extrusion is used mostly for processing thermoplastics (e.g. PVC, polyethylene, polypropylene), however, thermosets can also be extruded by adding catalysts (especially rubber).

During extrusion process, raw plastic materials like granules, pellets, or powder -in the presence/absence of additives- are supplied to the extruder barrel through the hopper which feeds the extruder with the material. The hopper is mounted on the barrel of the extruder and transfer the material through a hole into the heated barrel while the extruder screw is rotating. The extruder screw is employed material intake, conveying and

homogenizing the material as well as building up the necessary pressure to flow through the nozzle. During compounding, the material is melted by the combination of external heating and heat from the internal friction arose from moving against the barrel walls and the screw surface. Molten materials push in the grooves of the screw flank in the direction of the screw tip while screw is rotating. Some extruders can have either one or two screws and screws can be positioned in the horizontal or vertical direction. When the molten material is homogenized, it is forced through a small opening called nozzle to be transferred for molding into the desired shape. Extrusion process of the polymers is given in Figure 2.15.

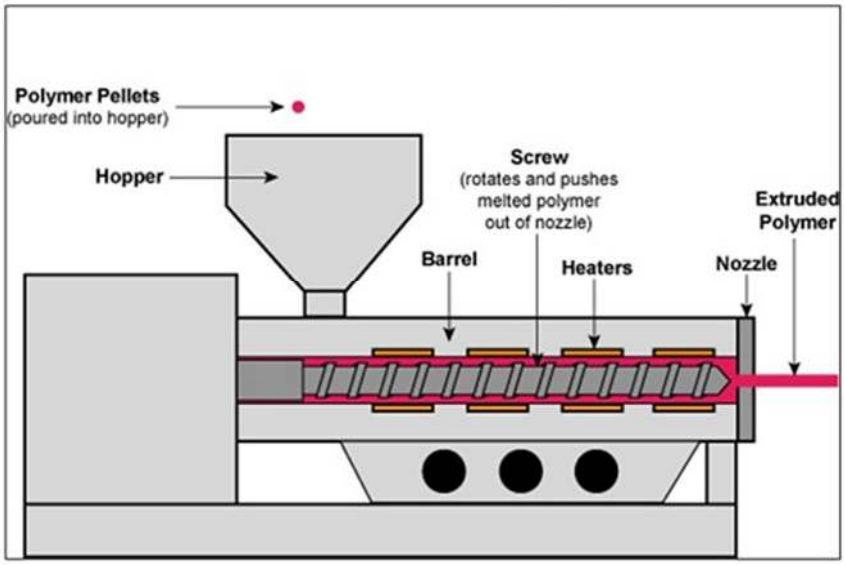

Figure 2.15. *Extrusion process of the polymers*

2.10.2. Injection molding

Injection molding is a manufacturing process for plastic articles in which molten material is injected into the cavity of a tool under high pressure.

Following the extrusion process, the desired volume of the molten material is delivered into a cold mold directly from the nozzle of the injection molding machine as illustrated in Figure 2.16. The needed pressure is supplied by an axial stroke of a rotating screw or a piston (also called plunger or ram). In case of micro injection molding machines, molten material is transferred from extruder to the mold via filling into the separate barrel of injection unit and then it is placed to the sprue bush of the mold. By

applying high pressure with a piston, molten polymer is injected into the cavity of the mold. In both machines, the injection process is completed, when the cavity is almost completely filled with. During the cooling time, the plastic melt solidifies in the cavity in most plastics by solidification and takes on the shape of the mold. When the molded part gets cold and sufficiently stable, the tool can be opened and the molded part in the desired shape can be ejected from the mold.

In an injection molding system, the pressure has the importance to compensate for the material shrinkage of the molding. The cycles of the injection molding process must be repeatable for a reliable quality of the injection molding articles.

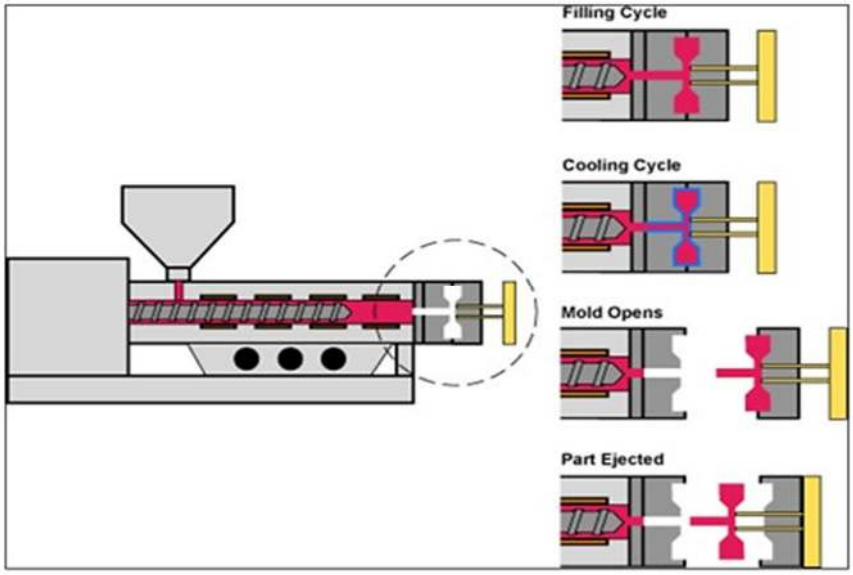

Figure 2.16. *Injection molding process of the polymers*

2.10.3. Fiber melt spinning process

Melt spinning is a manufacturing process used to produce synthetic (polymeric) fibers. Although it requires a polymer that is not decomposed by the temperatures needed for extrusion, it is the most cost-effective method due to the absence of solvents, high production rate and the simplicity of the process among other methods for fiber production [78,79].

A typical melt spinning process includes an extruder with a spinning attachment. In the extruder part, the polymer is melted and mixed with additives. When the molten material is homogenized, it is transferred to the top of the spinning tower by the rotating

screws of the extruder. A metering pump is positioned at the spinning tower to ensure the flow the molten polymer to the spin pack. A spin pack contains a filter, a breaker plate, and a spinneret where molten polymer passes through them respectively. The filter is used to remove the foreign or agglomerated particles that might clog spinneret holes. A spinneret is a metallic die which contains many microscopic orifices in different shapes. When the molten polymer exits the spinneret, it is immediately subjected to a cold blown air which solidifies it into filaments. Finally, the filaments (or filament bundles) wound up on a bobbin after passing a serious of rollers (godets). Along their path to the bobbin, a drawing process is applied, usually with the introduction of heat, which increases the molecular orientation of the resulted filaments. The schematic representation of a typical melt spinning process is given in Figure 2.17 [80].

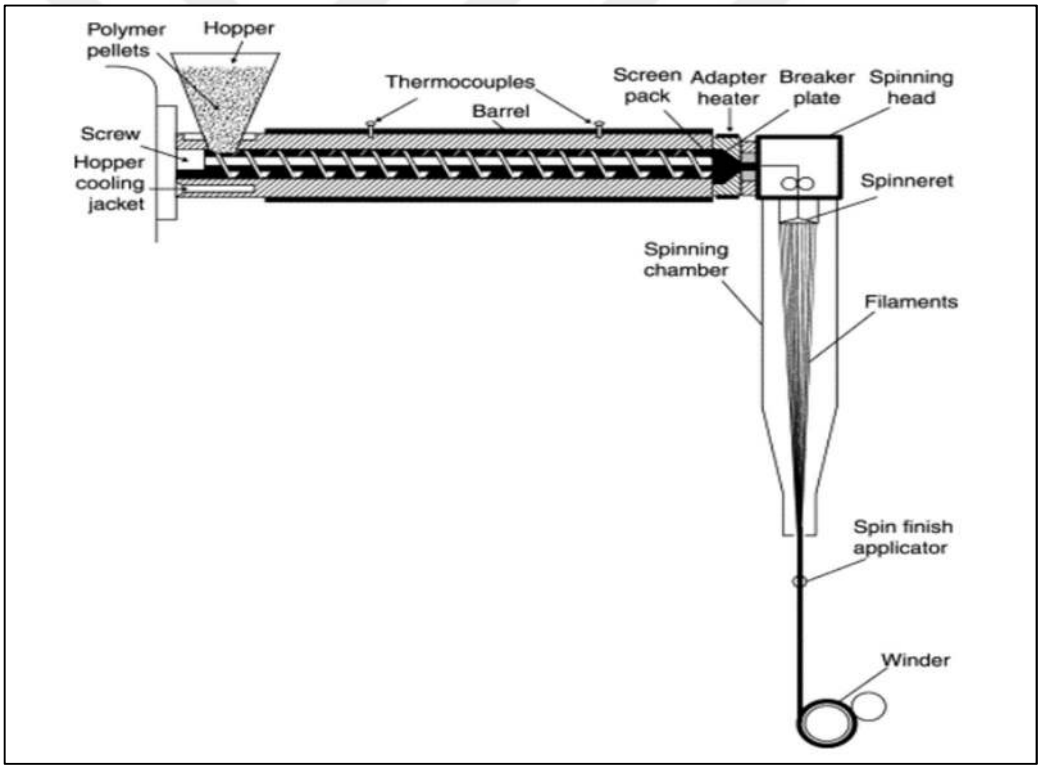

Figure 2.17. *The schematic representation of a typical melt spinning process*

Melt spinning can be used to produce monofilament and multifilament fibers. Depending on the shape of the spinneret orifices, the cross-sectional shape of the filament can be round, triangular, trilobal, octalobal, etc. By adding a separate extruder and metering pump to the melt spinning setup, bicomponent fibers can also be extruded with

different cross-sections such as core/sheath, segmented pie, islands in the sea, etc. During the melt spinning, fiber properties are affected by many parameters depending on each other: extrusion temperature, mass flow rate of polymer (or melted mixture), the shape of spinneret orifices, spinning speed, cooling conditions along the spinline and the spinline design [81,82].

3. MATERIALS AND METHODS

3.1. Particle Size Reduction of Flame Retardant Powders

Zinc Borate (ZnB) with a chemical formula of $2ZnO.3B_2O_3.3.5H_2O$ was obtained from Üçgen Kimya, Turkey. Average particle size of ZnB is 9.6 μm. Aluminium trihydroxide (ATH) with an average particle size of 7 μm was supplied by Merck, Germany.

Flame retardant powders (ZnB and ATH) were wet milled by planetary mill (Pulverisette 5, Fritsch GmbH, Germany) under ambient conditions to reduce the particle size of the powders to submicron scale. Ethanol (Merck, Germany, %96) was utilized as the dispersing medium. Grinding bowl and grinding balls both made of zirconium oxide were used. Milling parameters were given in Table 3.1. Size reduction of FR powders was performed without using stabilizers.

Table 3.1. *Milling parameters of flame retardant powders*

Material (g)			Time (min)	Rate (rpm)
FR powder	**Ethanol**	**Zirconium oxide balls**	60	500
90	10	120		

3.1.1. Characterization methods of the ground FR powders

3.1.1.1. Particle size and zeta potential measurements

Particle size and zeta potential of the samples were measured using a zetasizer (Nano ZS 3600, Malvern, UK). Before measurement, samples were diluted in ethanol. Measurements were repeated three times for each sample and average values were recorded. After milling, ethanol was removed by a rotary evaporator (Hei-VAP, Heidolph GmbH, Germany).

3.1.1.2. XRD

XRD (Miniflex 600, Rigaku, Japan) analysis was performed to define the crystal structure of the ground FR powders. X-ray diffraction patterns were obtained at a scan rate of 4°/min with a step size of 0.05° under CuKα radiation. The X-ray intensities of the samples were recorded in the 2theta (2θ) range of 10-70° and 5-50° for ZnB and ATH, respectively.

3.2. Production of Flame Retardant PP Composites

For the production of flame retardant PP composites, two different type phosphorus-based flame retardants; ammonium polyphosphate-based and cyclic phosphonate (organic phosphorus)-based powders were used. All flame retardants were commercially available and detailed in the following sections. In the first part of the study, the effect of ammonium polyphosphate-based flame retardant on the flammability of polypropylene was investigated by the incorporation of APP-based FR to the polypropylene. Next, inorganic FR additives; zinc borate (ZnB), aluminium trihydroxide (ATH), nano-silica (SiO_2), and carbon nanotube (CNT) were incorporated into the PP blend to define their synergistic effect on the flame retardancy of the PP/ APP-based FR system. The same processes were applied in the second part of the study but with cyclic phosphonate-based flame retardant. A hindered amine light stabilizer (HAS) was also blended with cyclic phosphonate-based FR to investigate the synergetic effect between these flame retardants. In addition to FR additives, antibacterial additives (nano-CuO and ZnO) were also blended in PP to examine their antibacterial activity on PP/cyclic phosphonate-based FR/HAS system. The influence of both nano-CuO and ZnO on the flammability of PP/cyclic phosphonate-based FR/HAS system was also observed before melt spinning process of the fibers.

3.2.1. Production of ammonium polyphosphate-based flame retardant PP composites

3.2.1.1. Materials

Isotactic polypropylene with a melt flow index (MFI) of 35 g/10 min (230 °C, 2.16 kg) was used. Ammonium polyphosphate-based flame retardant (Exolit AP 760, industrial) was obtained from Clariant Plastics and Coatings AG, Germany. The properties of commercially available ammonium polyphosphate-based flame retardant used in these studies are given in Table 3.2. A multifunctional processing aid (Plastaid T) was obtained from Fine Organics, India as well. Exolit AP 760 and Plastaid T were represented by APP and MPA, respectively, within the entire text. The ground ZnB and ATH which were produced in this study (see section 3.1.) were used. Multi-walled carbon nanotubes ((MWNTs), represented by CNT within the entire text) (Purity: >95%, specific surface area: > 200 m^2/g, average diameter of 10 - 20 nm, and length of 0.5 - 2 μm) were

purchased from Grafen Co., Turkey. Nano silica powder (particle size 60 nm) was supplied by Evonik.

Table 3.2. *The properties of ammonium polyphosphate-based flame retardant*

Trade Name	Supplier	Chemical Composition	P_2O_5 %	N %
Exolit AP 760	Clariant	Ammonium polyphosphate	19 - 21	14

3.2.1.2. Preparation of PP composites

Reference PP and flame retardants were dried in a vacuum oven at 65 °C for 3 h before use and were mixed by using a mechanical mixer before processing. Samples were compounded by a twin-screw micro compounder operated at 180°C and molded by injection (DSM Xplore, The Netherlands) as illustrated in Figure 3.1.

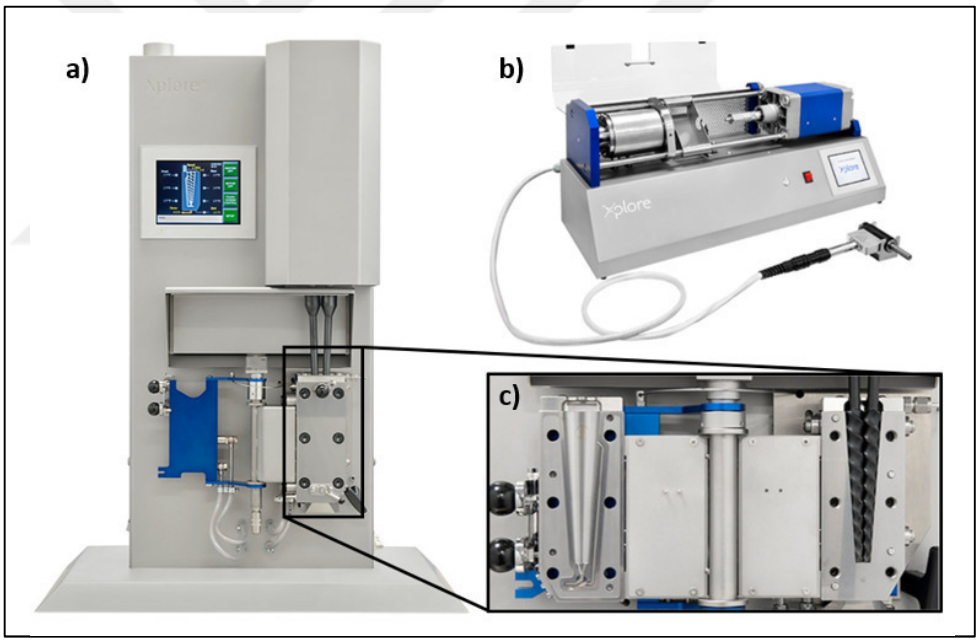

Figure 3.1. *a) Twin screw micro compounder, b) injection molder, c) barrel of the compounder with twin screws*

Table 3.3. shows the compounding and injection molding parameters of the composites.

Table 3.3. *Compounding and injection molding parameters*

Parameters	Values
Compounder barrel temperature (°C)	180
Screw speed (rpm)	120
Force (N)	120
Injection pressure (bar)	5
Injection mold temperature (°C)	35
Injection barrel temperature (°C)	185

5 wt% and 10 wt% of the APP were blended in PP as a preliminary study. Sample compositions are given in Table 3.4. The maximum loading of FRs were held constant at 10 wt%. This maximum value was presumed to be an upper limit to consider their potential use for polypropylene fiber spinning [9].

Table 3.4. *Sample compositions of PP/APP composites*

Sample ID	Composition (%)	
	PP	APP
A1	95	5
A2	90	10

The effects of inorganic additives on the flammability of polypropylene/APP composites were studied afterwards. As it is difficult to disperse nanosized inorganic additives (especially multi-walled carbon nanotubes) into polymer matrix homogeneously, they were incorporated in the presence of a coupling agent (MPA) to have more homogeneous dispersion that could improve their effects. Table 3.5 shows the composition of PP/APP composites blended with inorganic additives with and without MPA. The content of the inorganic additives was kept at 2 wt % for a fair comparison of their effects.

Table 3.5. *Sample compositions of PP/APP composites blended with inorganic additives*

Sample ID	Composition (%)						
	PP	APP	ZnB	ATH	nano-SiO_2	CNT	MPA
AI1	82	8	-	-	-	-	-
AI2	91	8	-	-	-	-	1
AI3	90	8	2	-	-	-	-
AI4	89	8	2	-	-	-	1
AI5	90	8	-	2	-	-	-
AI6	89	8	-	2		-	1
AI7	90	8	-	-	2	-	-
AI8	89	8	-	-	2	-	1
AI9	90	8	-	-	-	2	-
AI10	89	8	-	-	-	2	1
AI11	89	8	1	1	-	-	1
AI12	89	8	1	-	1	-	1
AI13	89	8	1	-	-	1	1

LOI, TGA, Cone Calorimetry and SEM were done for the characterization of samples.

3.2.2. Production of cyclic phosphonate-based flame retardant PP composites

3.2.2.1. Materials

Isotactic polypropylene with a melt flow index (MFI) of 35 g/10 min (230 °C, 2.16 kg) was also used in this part of the work. Cyclic phosphonate (Aflammit PCO 900, industrial) was supplied by Thor GmbH, Germany. Monomeric N-alkoxy hindered amine (Flamestab NOR116, analytical, as shown in Figure 3.2) was obtained from BASF Schweiz AG, Switzerland. Aflammit PCO 900 and Flamestab NOR116 were represented by CPP and HAS, respectively, within the entire text. The same FR additives (ZnB, ATH, nano-SiO_2, and CNT) used for the production of APP-based composites (see section 3.2.1.1.) were used. Nano cupric oxide (nano-CuO) (Purity: >99%, the average diameter of 30-50 nm) was purchased from ChemPur GmbH, Germany. Zinc oxide (ZnO) was supplied by Merck, Germany.

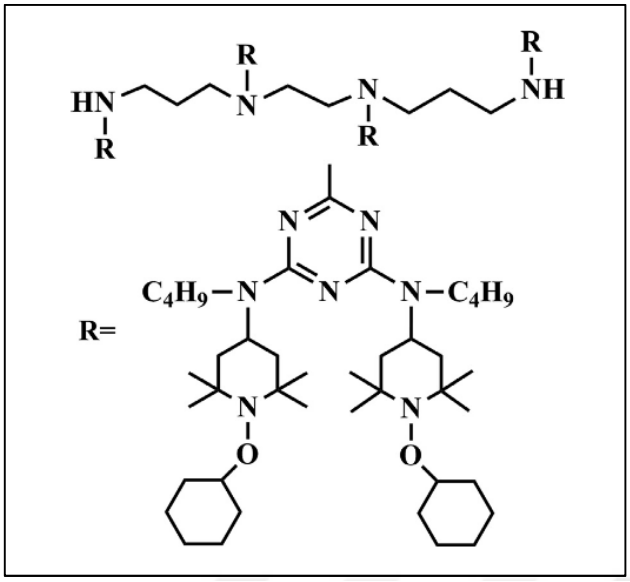

Figure 3.2. *Chemical structure of Flamestab NOR116*

The properties of commercially available of cyclic phosphonate-based flame retardant used in these studies are given in Table 3.6.

Table 3.6. *The properties of cyclic phosphonate-based flame retardant*

Trade Name	Supplier	Chemical Composition	P %	N %
Aflammit PCO 900	Thor	Cyclic phosphonate	approx. 24%	N/A

3.2.2.2. Preparation of PP composites

Cyclic phosphonate-based flame retardant composites were produced by the incorporation of 3.5 wt%, 5 wt% and 10 wt% to compare its effect with APP-based flame retardant. The same compounding and injection molding parameters given in Table 5.4 were used. Similar to the production of APP-based FR composites, 10 wt% was determined as a maximum loading of CPP. Table 3.7 shows the composition of PP/CPP composites.

Table 3.7. *Sample compositions of PP/CPP composites*

Sample ID	Composition (%)	
	PP	CPP
P1	96.5	3.5
P2	95	5
P3	90	10

HAS was also blended in PP individually to check its flame retardancy effect. However, the content of HAS that is higher than 1.5 wt% is not recommended by the supplier for fiber spinning, 5 wt% of it was incorporated as well for a fair comparison with CPP. Compositions of PP/HAS composites are given in Table 3.8.

Table 3.8. *Sample compositions of PP/HAS composites*

Sample ID	Composition (%)	
	PP	HAS
N1	99	1
N2	98.5	1.5
N3	95	5

Later on, the effect of an N-alkoxy hindered amine (HAS) on PP was examined in the presence of CPP system. Loading of CPP was varied in proportion to the loading of HAS to define the composition that yields a better flame retardancy. The total loading of additives was kept at 5 wt%. Prepared compositions in different ratios were listed in Table 3.9.

Table 3.9. *Sample compositions of PP/CPP/HAS composites*

Sample ID	Composition (%)		
	PP	CPP	HAS
PN1	95	4.5	0.5
PN2	95	4.0	1.0
PN3	95	3.5	1.5
PN4	95	3.0	2.0
PN5	95	2.5	2.5
PN6	95	2.0	3.0
PN7	95	1.5	3.5
PN8	95	1.0	4.0
PN9	95	0.5	4.5

After defining the desired composition, inorganic additives; zinc borate, aluminium trihydroxide, silica, and carbon nanotubes, as well as antibacterial additives; zinc oxide and cupric oxide were incorporated to PP/CPP/HAS composites to define their effects (synergetic or antagonistic) on the flammability and thermal degradation of the defined flame retardant composite. Blended inorganic additives in PP/CPP/HAS composites were given in Table 3.10.

Table 3.10. *Sample compositions of PP/CPP/HAS composites blended with inorganic additives*

Sample ID	Composition (%)								
	PP	**CPP**	**HAS**	**ZnB**	**ATH**	**nano-SiO_2**	**CNT**	**nano-CuO**	**ZnO**
PNI1	94.5	3.5	1.5	0.5					
PNI2	94.5	3.5	1.5		0.5				
PNI3	94.5	3.5	1.5			0.5			
PNI4	94.5	3.5	1.5				0.5		
PNI5	94.75	3.5	1.5					0.25	
PNI6	94.5	3.5	1.5					0.50	
PNI7	94.75	3.5	1.5						0.25
PNI8	94.5	3.5	1.5						0.50

LOI, TGA, Cone Calorimetry, MCC and SEM were done for the characterization of these flame retardant composites.

3.2.3. Characterization of the flame retardant composites

3.2.3.1. LOI

The limiting oxygen index (LOI) values were measured by LOI test device (Concept Equipment, United Kingdom) according to ASTM D 2863. The dimensions of the specimens were 80 mm×10 mm×4 mm. The photograph of LOI device used in this study is shown in Figure 3.3.

Figure 3.3. *The photograph of limiting oxygen index test device*

3.2.3.2. TGA

Thermal analyses were carried out on a thermal analyzer (Q600 SDT, TA Instruments, USA). Samples of 10±0.1 mg were heated in alumina pans from room temperature to 800 °C at a heating rate of 10 °C/min under nitrogen flow.

3.2.3.3. Cone calorimeter

The cone calorimetric test (CCT) was carried out by using a cone calorimeter (Fire Testing Technology Co., UK) according to ISO 5660. Each specimen, with the dimensions of 100mm x 100mm x 3 mm, was wrapped in aluminium foil and exposed horizontally to an external heat flux of 35 kW/m^2. The residues of the samples after the cone calorimetric test were photographed by a digital camera (Canon Mark 3D, Japan).

3.2.3.4. MCC

The micro-combustion calorimeter (MCC) tests were conducted according to ASTM D7309-2007 (Method A) using a micro calorimeter (FAA Micro Calorimeter, Fire Testing Technology, UK). About 3 mg sample was heated from 150 °C to 750 °C using a heating rate of 1 °C/s in a continuous stream of nitrogen flow (80 cm^3/min). The thermal decomposition products (also called “fuel gases”) were mixed with the stream of oxygen (20 cm^3/min) before entering a 900 °C combustion furnace to calculate the data which were determined by oxygen consumption.

3.2.3.5. SEM

Scanning electron microscopy (SEM) measurements were carried out to examine the surface topography of the samples. A scanning electron microscope (TM3030Plus, Hitachi, Japan) were used.

3.3. Production of Flame Retardant and Antibacterial Polypropylene Fibers

Two different type of PP fibers were produced: as-spun monofilament PP fibers and melt-spun multifilament PP fibers. As-spun monofilament PP fibers were first produced to examine the antibacterial activity of each composition blended with antibacterial additives before the melt spinning process. Antibacterial analysis was done for this type of PP fibers. After determining the appropriate compositions which show antibacterial activity, these compositions were spun into multifilament PP fibers by melt spinning for the production of final flame retardant and antibacterial fibers. Tensile test, SEM and optical microscopy inspection, and color test were done for the characterization of melt-spun fibers.

3.3.1. Materials

Compositions blended with CPP/HAS (3.5:1.5) in the presence/absence of nano-CuO and ZnO (0.25 wt% and 0.50wt%, individually) were used for the production of as-spun monofilament PP fibers (see section 3.2.2.2). The same compositions were used for melt spinning of multifilament PP fibers but only containing nano-CuO as the antibacterial additive. Neat PP was used directly without further compounding for both types of fibers.

3.3.2. Preparation of PP fibers

As-spun monofilament PP fibers were spun directly from the die of the twin-screw extruder (DSM Xplore, The Netherlands) after melt compounding and cooled at ambient temperature (at about 25 °C). No drawing process was applied to these fibers.

Multifilament PP fibers were produced by the melt spinning process. Schematic overview of the production of final flame retardant and antibacterial multifilament PP fibers is given in Figure 3.4.

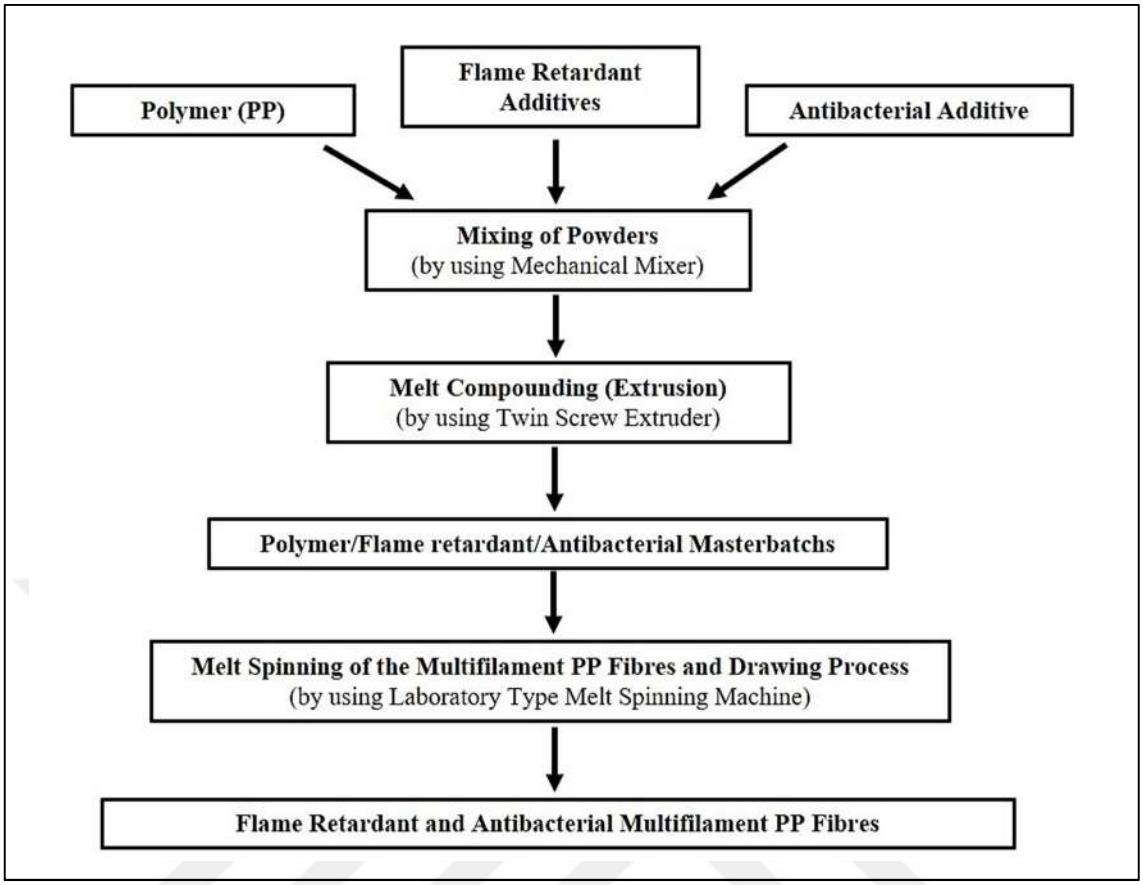

Figure 3.4. *Schematic overview of the production of flame retardant and antibacterial multifilament PP fibres*

Three different FR masterbatches were melt-spun into multifilament fibers in addition to neat PP. FR masterbatches were prepared by melt extrusion using a twin-screw micro compounder (Thermo Fisher Scientific, USA). Prior to compounding, PP and FR additives as well as nano-CuO were dried in a vacuum oven at 65 °C for 3 h before use and were mixed by using a mechanical mixer. After compounding, the blend obtained were cut into a pellet form to be processed afterwards for fiber spinning. The parameters of melt extrusion are given in Table 3.11.

Table 3.11. *Parameters of melt extrusion*

Ekstruder zones	Z1	Z2	Z3	Z4	Z5	Z6	Z7
Zone temperatures (°C)	160	160	170	170	180	180	180
Screw speed (rpm)				120			
Pressure (bar)				50			

Continuous virgin or FR and antibacterial-loaded PP multifilament fibers were made via a spinning process using a melt spinning machine (Fiber Extrusion Technology, Leeds, UK). All compounded blends were fed into the single-screw extrusion and spinning apparatus without any further treatment. In case of the spinning of PP multifilament fibers, neat PP was fed into directly as well. Melt spinning conditions of the spun multifilament fibers is listed in Table 3.12.

Table 3.12. *Spinning parameters of the melt-spun multifilament fibers*

PP	Extrusion speed (rpm)	12.0	Quench air temp. (°C)		21.5
	Pump speed (rpm)	8.0	Draw ratio		1.9
	Extruder zones	T1	T2	T3	T4
	Temperatures (°C)	225.0	235.0	240.0	240.0
	Godets	G1	G2	G3	G4
	Speed (rpm)	400.0	750.0	775.0	775.0
	Temperature (°C)	0.0	65.0	100.0	120.0
PN3	Extrusion speed (rpm)	11.0	Quench air temp. (°C)		18.1
	Pump speed (rpm)	8.0	Draw ratio		2.3
	Extruder zones	T1	T2	T3	T4
	Temperatures (°C)	190.0	220.0	230.0	230.0
	Godets	G1	G2	G3	G4
	Speed (rpm)	200.0	400.0	450.0	455.0
	Temperature (°C)	0.0	60.0	100.0	120.0
PNI5	Extrusion speed (rpm)	45.0	Quench air temp. (°C)		17.9
	Pump speed (rpm)	7.0	Draw ratio		2.3
	Extruder zones	T1	T2	T3	T4
	Temperature (°C)	190.0	210.0	220.0	230.0
	Godets	G1	G2	G3	G4
	Speed (rpm)	200.0	400.0	450.0	455.0
	Temperature (°C)	0.0	60.0	100.0	120.0
PNI6	Extrusion speed (rpm)	45.0	Quench air temp. (°C)		19.4
	Pump speed (rpm)	6.0	Draw ratio		2.8
	Extruder zones	T1	T2	T3	T4
	Temperature (°C)	228.0	238.0	248.0	258.0
	Godets	G1	G2	G3	G4
	Speed (rpm)	200.0	500.0	550.0	555.0
	Temperature (°C)	0.0	60.0	100.0	120.0

Properties of melt-spun multifilament fibers with % nano-CuO content are listed in Table 3.13. Linear density (yarn count) of the PP fibers were calculated by using the direct

system in the unit of decitex (dtex) which equals the total weight in grams of 10,000 meters of the respective fiber [83]. The order of the calculated yarn counts was found to be PP > PN3 > PNI5 > PNI6. The differences in yarn counts could be arisen from not only the different amount of additives loaded but also the parameters of melt spinning process such as temperature profile and draw ratio.

Table 3.13. *Properties of the melt-spun multifilament fibers*

Fiber ID	Cross sectional shape of the fibers	Number of filaments per yarn	Yarn count (dtex)	nano-CuO content (%)
PP	Round	36	170	-
PN3	Round	36	164	-
PNI5	Round	36	102	0.25
PNI6	Round	36	50	0.50

3.3.3. Characterization methods

3.3.3.1. Tensile test

Tensile measurements of multifilament fibers were carried out on a universal testing system (Instron 5969, Instron Co., USA) according to the ASTM D-2256 standard. All the tests were performed using a gauge length of 50 mm and a test speed of 100 mm/min at 21±1 °C. The tests were repeated 15 times for each sample. Average values of the test results were calculated and reported with standard deviations.

3.3.3.2. Antibacterial analysis

Antibacterial activity of the fibers was determined according to the JIS L 1902 by utilizing the absorption method (quantitative test method) against *Escherichia coli (E. coli)* bacteria. To prepare the fiber samples for the test, of about 0.4 g fibers were weighted out and bunched together by positioning parallel to each other with a length of 6 cm. After this, fibers were bound with the same fibers at about 5 mm apart from both ends to give a bale shape as indicated in Figure 3.5 [72].

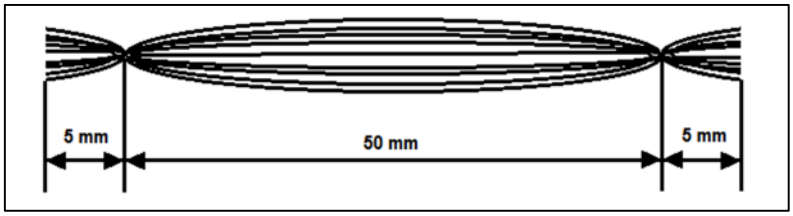

Figure 3.5. *Fibre bale prepared for the actibacterial test*

Six test pieces of neat PP and three test pieces of blended PP fibers were subjected to the test. At the beginning of the test, all test fibers were sterilized by autoclave. A suspension containing $1 \pm 0.3 \times 10^5$ CFU (colony-forming units)/ml is prepared to be used for the inoculation of control and test fibers. *E. coli* culture (200 ml) is diluted in a nutritive broth to prepare the related suspension. The suspension was then inoculated to six test pieces of neat PP (control fiber) and three test pieces of blended PP fibers. Immediately after inoculation, the three test pieces of control fiber was shaken out in the presence of 20 ml of physiological saline and an initial number of bacteria was determined at "zero hour". Other PP fibers were incubated for 24 h at 37 °C to assess antibacterial activity. After 24 h, these fibers were also shaken out with the addition of ice-cooling physiological saline (20 ml).

Comparing the number of bacteria on the surface of neat polypropylene fibers before incubation and blended fibers after the incubation, bactericidal activity value is calculated from the formula:

$$(L) = (M_a) - (M_c) \tag{4.1}$$

where M_a is the common logarithm of the number of bacteria on the neat PP fibers straight after inoculation, M_c is the common logarithm of the number of bacteria on the fibers blended with antibacterial additives after 24 hours of incubation.

3.3.3.3. SEM

A scanning electron microscope (TM3030Plus, Hitachi, Japan) were used to examine the surface topography of the fibers.

3.3.3.4. Optical Microscopy

An optical microscope (Olympus BX43, Tokyo, Japan) was used to examine the morphological properties of the melt-spun fibers along the fiber length and fiber cross section.

The fluorescence micrographs of the melt spun PP filaments were also taken using the same microscope to track the distribution and homogeneity of FR and antibacterial additives.

3.3.3.5. Color test

The color measurements of the melt-spun multifilament PP fibers were performed on a spectrophotometer (CM 3600D, Konica Minolta, Japan) from 400 nm to 700 nm under D65 illuminant with a 10-degree observer angle. Color parameters (CIE-L*, a*, b*, C* and h°) were obtained using the software of the spectrophotometer. Color strength (K/S) values were calculated from the reflectance values (at λ_{max}=400 nm) for each multifilament fibers using the software as well.

3.4. Production of Flame Retardant and Antibacterial Fabrics

Four different flame retardant and antibacterial fabrics were produced. Cone calorimeter test, antibacterial test and optical microscopy inspection were done for the characterization of fabrics.

3.4.1. Materials

The multifilament fibers spun in Section 3.3. were utilized for knitting.

3.4.2. Preparation of flame retardant and antibacterial fabrics

The flame retardant and antibacterial fabrics were produced by weft knitting of melt-spun multifilament fibers in single jersey structure. The knitting process is performed on a laboratory type circular knitting machine (İpekçioğlu, Turkey). The single jersey structure is illustrated in Figure 3.6.

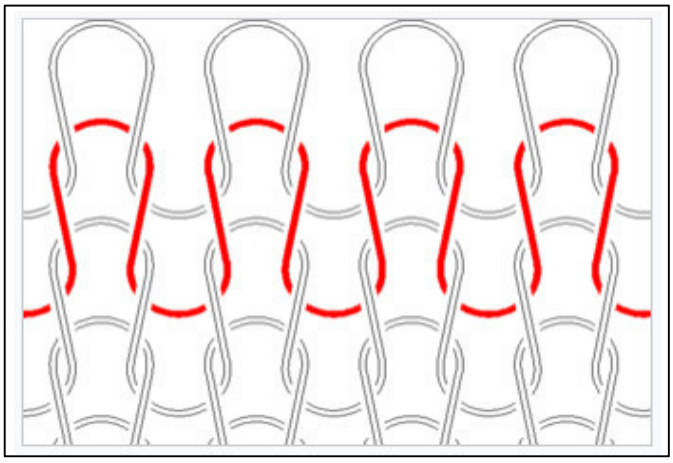

Figure 3.6. *The single jersey structure*

The images of the flame retardant and antibacterial fabrics, photographed by a digital camera (Canon Mark 3D, Japan), are presented in Figure 3.7.

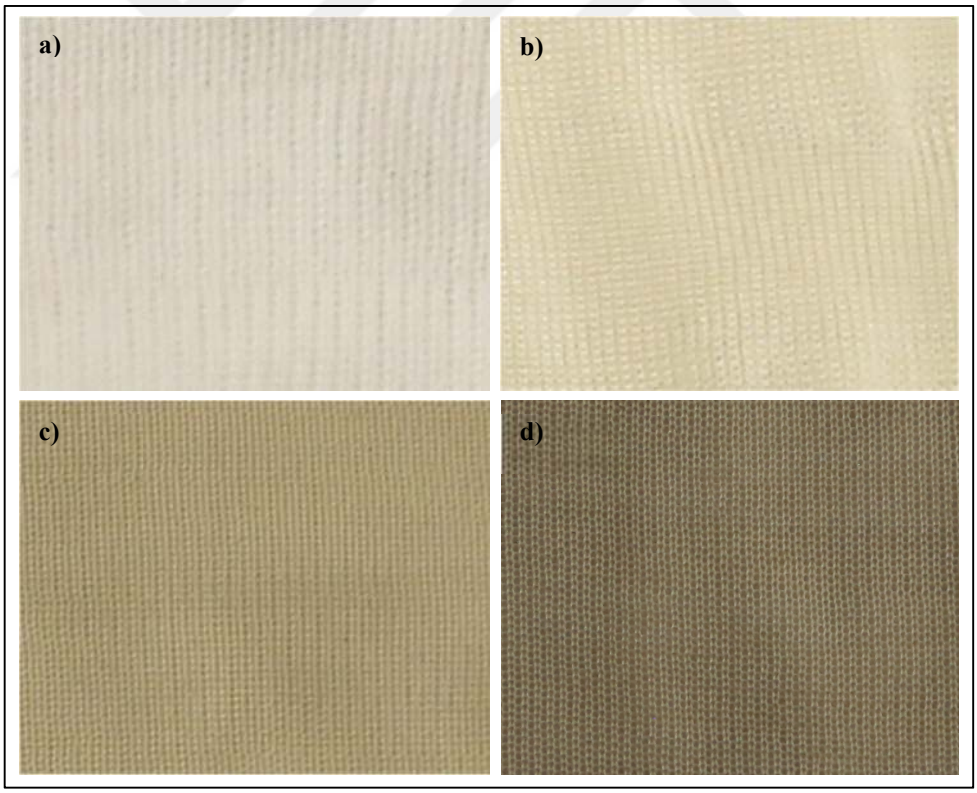

Figure 3.7. *Weft knitted fabrics produced by using flame retardant and antibacterial multifilament fibres*

3.4.3. Characterization methods

3.4.3.1. Cone calorimeter test

The cone calorimeter test used were mentioned previously in Section 3.2.3.3.

3.4.3.2. Antibacterial analysis

The same antibacterial analysis which was mentioned previously in Section 3.3.3.2 were used. Unlike to that section, knitted fabrics of about 0.4 g were cut in a square shape and subjected to the test.

3.4.3.3. Optical microscope

The knitted fabrics were examined by using an optical microscope (SteREO Discovery V20, Zeiss, Germany).

4. RESULTS AND DISCUSSION

4.1. Characterization of the Ground FR Powders

4.1.1. Particle size and zeta potential measurements

Size distribution and zeta potential results of ZnB and ATH powders after grinding are listed in Table 4.1. The particle size of ZnB and ATH were reduced from 9.6 μm to 286,6 nm and from 7 μm to 853.8 nm, respectively. Ground ATH showed a large shift from the isoelectric point with a zeta potential of 27,6 which indicates a less tendency of agglomerate formation and therefore an enhanced dispersion in PP. Despite the tendency of agglomeration of ZnB particles due to its low zeta potential which approaches 0, the grinding process is favourable as the particle size of both powders were successfully decreased from micron to the submicron scale.

Table 4.1. *Size distribution and zeta potential results of ZnB and ATH (Z-average: particle size; PdI, polydispersity index)*

Material	Z-Average (d.nm)	Pdl	Zeta Potential (mV)	Conductivity (mS/cm)
ZnB	286.6	0.251	1.76	0.0137
ATH	853.8	0.263	27.6	0.0022

4.1.2. XRD analysis

The crystal structure of the ground FR powders was defined by XRD analysis. Figure 4.1. shows the X-ray diffraction pattern of ZnB powders before and after the grinding process. The diffraction curves of the ground ZnB powders presented the same diffraction peak positions with those of ungrounded ZnB; however, the intensity of the peaks decreased with grinding which indicates an increase in crystallite size of ZnB.

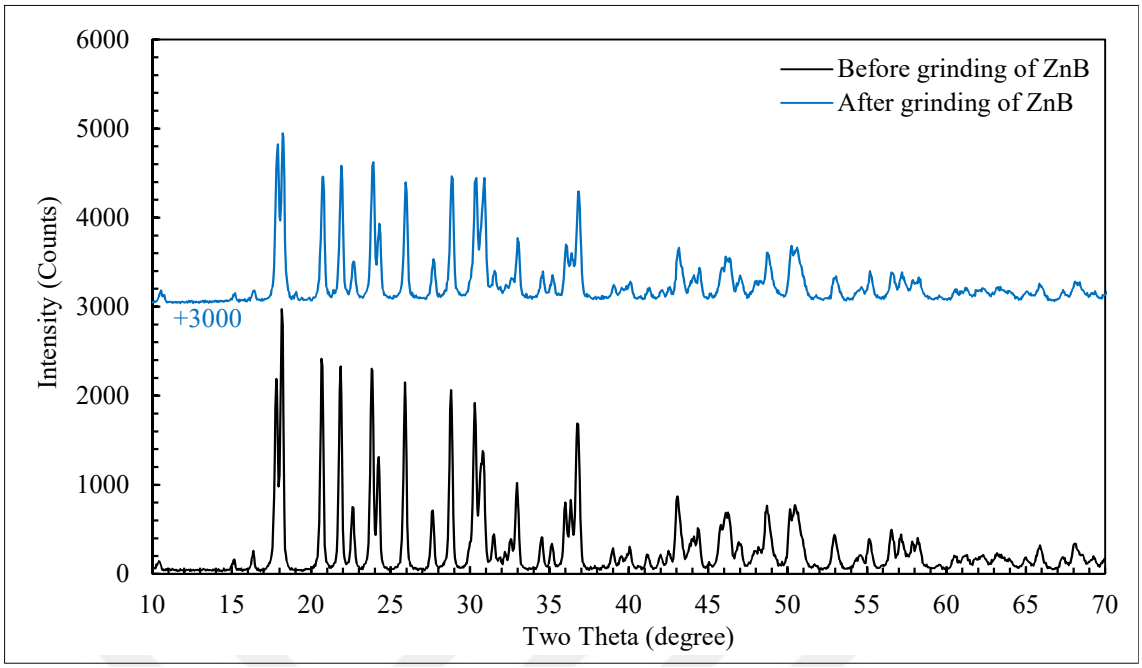

Figure 4.1. *XRD pattern of ZnB before and after grinding*

XRD pattern of ATH is represented in Figure 4.2. Peak positions of ATH did not change with grinding; however, the grinding process caused a reduction in the intensity of the peaks. This means that the crystallite size of ATH was increased with the grinding.

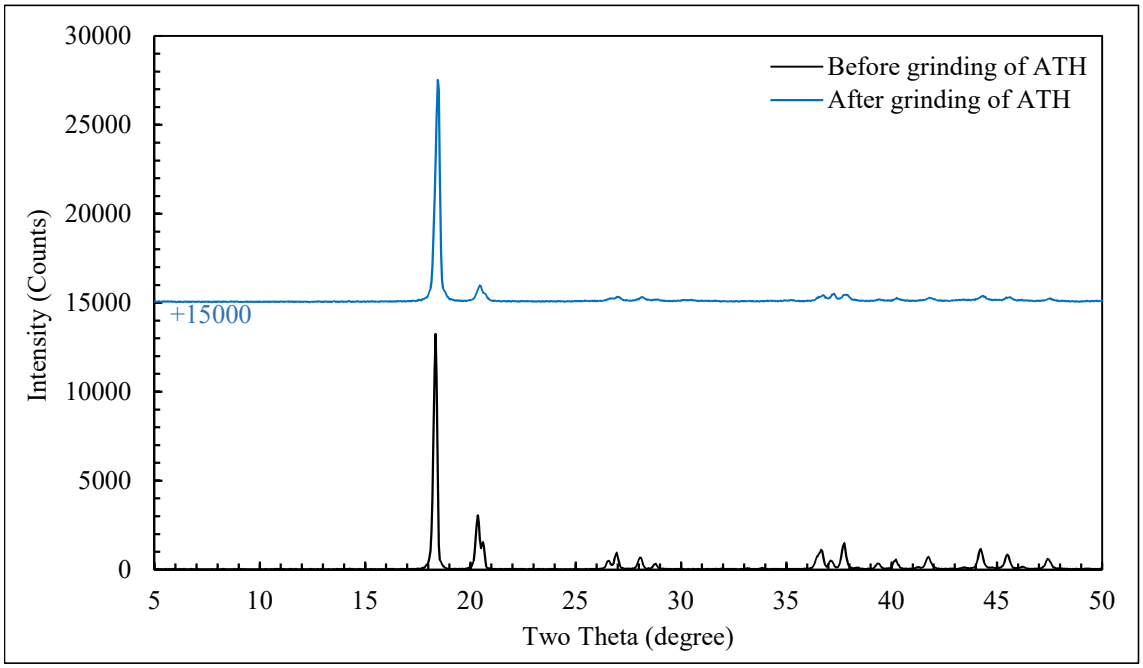

Figure 4.2. *XRD pattern of ATH before and after grinding*

4.2. Characterization of Ammonium Polyphosphate-Based Flame Retardant PP Composites

4.2.1. LOI

The LOI value of reference PP (19 %) increased to 21.5 % and 22.6 % by the addition of 5 wt% and 10 wt% APP, respectively. The LOI values of the PP composites blended with only APP are listed in Table 4.2.

Table 4.2. *LOI values of the PP composites blended with only APP*

Sample ID	LOI (%)
PP	19
A1	21.5
A2	22.6

Several inorganic additives were introduced into PP/APP system individually: zinc borate, aluminium trihydroxide, silica, carbon nanotubes. To examine the effect of several inorganic additives on the flammability of PP/APP system, 2.0 wt% inorganic additives were added to the system and the total content of APP was kept constant (8.0 wt%). This addition of inorganic additives decreased the LOI values of PP/APP blend for all compositions. Incorporating of ZnB, ATH and nano-SiO_2 reduced the LOI value down to around 21.5 %. The most reduction in LOI was found for the composite blended with 2 wt% CNT by 1.4 %. Following these examinations, MPA was also incorporated into the former composites to improve the dispersion of these additives in PP matrix which may lead to a better flame retardancy. The LOI values versus composites containing APP and inorganic additives in the presence/absence of MPA are shown in Figure 4.3.

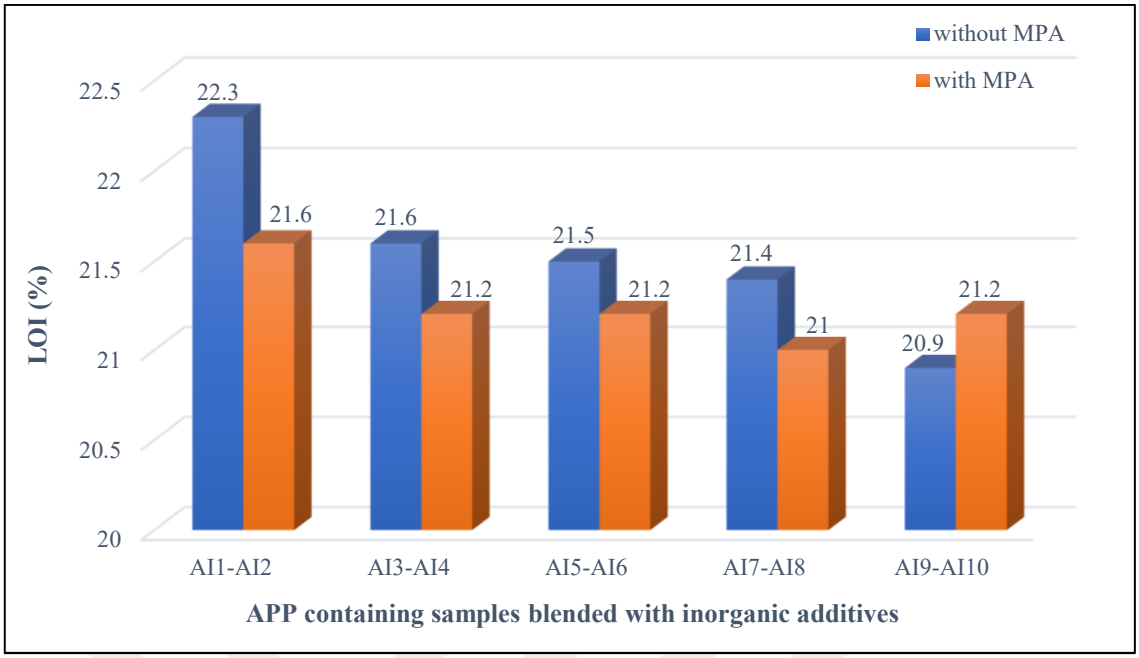

Figure 4.3. *LOI values of PP/APP composites blended with inorganic FR additives (in the absence and presence of MPA, respectively)*

The LOI value of the composite containing only APP (8 wt%) reduced from 22.3 to 21.6 in the presence of 1 wt% MPA. When the same amount of MPA introduced to PP/APP system blended with inorganic FR additives, it resulted in a further decrease of respective LOI values. Only the composite containing CNT showed a synergetic effect with MPA and increased the LOI to 21.2 %. This effect could be associated with the more homogeneous dispersion of CNT in the PP/APP matrix thanks to MPA. However, MPA/CNT combination still yielded a lower LOI than only APP containing composition.

The effect of the combination of inorganic FR additives (1:1) on the flame retardancy of PP/APP system was also examined in the presence of MPA. Total loading of inorganic FR additives was kept at 2 wt% again for a better comparison with their individual effects. ZnB/CNT combination improved the LOI value to 21.4 % which is higher than the LOI values they blended individually. The lowest LOI (21.0 %) was obtained with the ZnB/nano-SiO_2 combination. The LOI values versus composites containing the combinations of inorganic FR additives are presented in Figure 4.4.

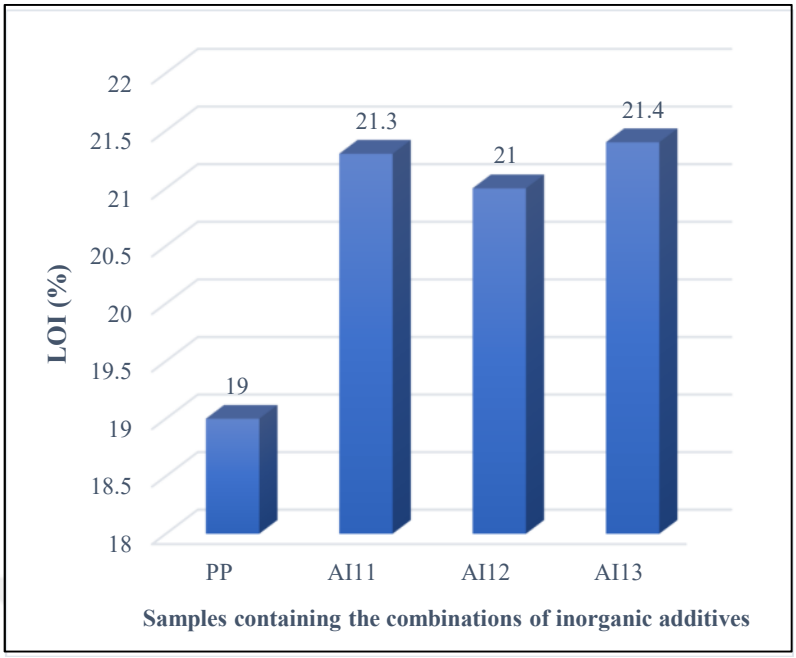

Figure 4.4. *LOI values of the samples containing the combinations of inorganic FR additives in the presence of MPA*

According to these results, inorganic FR additives were found not to be replaceable with APP in the PP matrix as they caused lower LOI values compared to the composites blended with only the same amount of APP. Nonetheless, they still increased the LOI value of neat PP.

4.2.2. TGA

Thermal decomposition behaviour of the composites is characterized by TGA. TG and DTG curves of all investigated systems are shown in Figure 4.5. The detailed thermal decomposition temperatures are shown in Table 4.3. The temperature at 10% weight loss and 50% weight loss is represented by $T_{10\%}$ and $T_{50\%}$, respectively. T_{max} is defined as the temperature of the maximum weight loss rate. TGA curves revealed that a single stage decomposition had occurred both for PP and the composites blended with APP. Reference PP decomposed with a maximum weight loss rate at 454.4 °C without any char residue at 700 °C. The addition of 5 wt% APP into PP matrix shifted the onset temperature of PP from 425.75 °C to 433.20 °C. Further addition of APP (10 wt%) resulted in a slight reduction of onset temperature by 2 °C which indicates a relatively earlier initiation of the decomposition. With the incorporation 5 wt% APP, $T_{50\%}$ and T_{max} values were both

increased by 7 °C. When the amount of APP in the PP matrix was 10 wt%, $T_{50\%}$ and T_{max} were further increased by 8.5 °C and 11.5 °C, respectively. This result refers to a delayed decomposition which is in conformity with the intumescent function of APP.

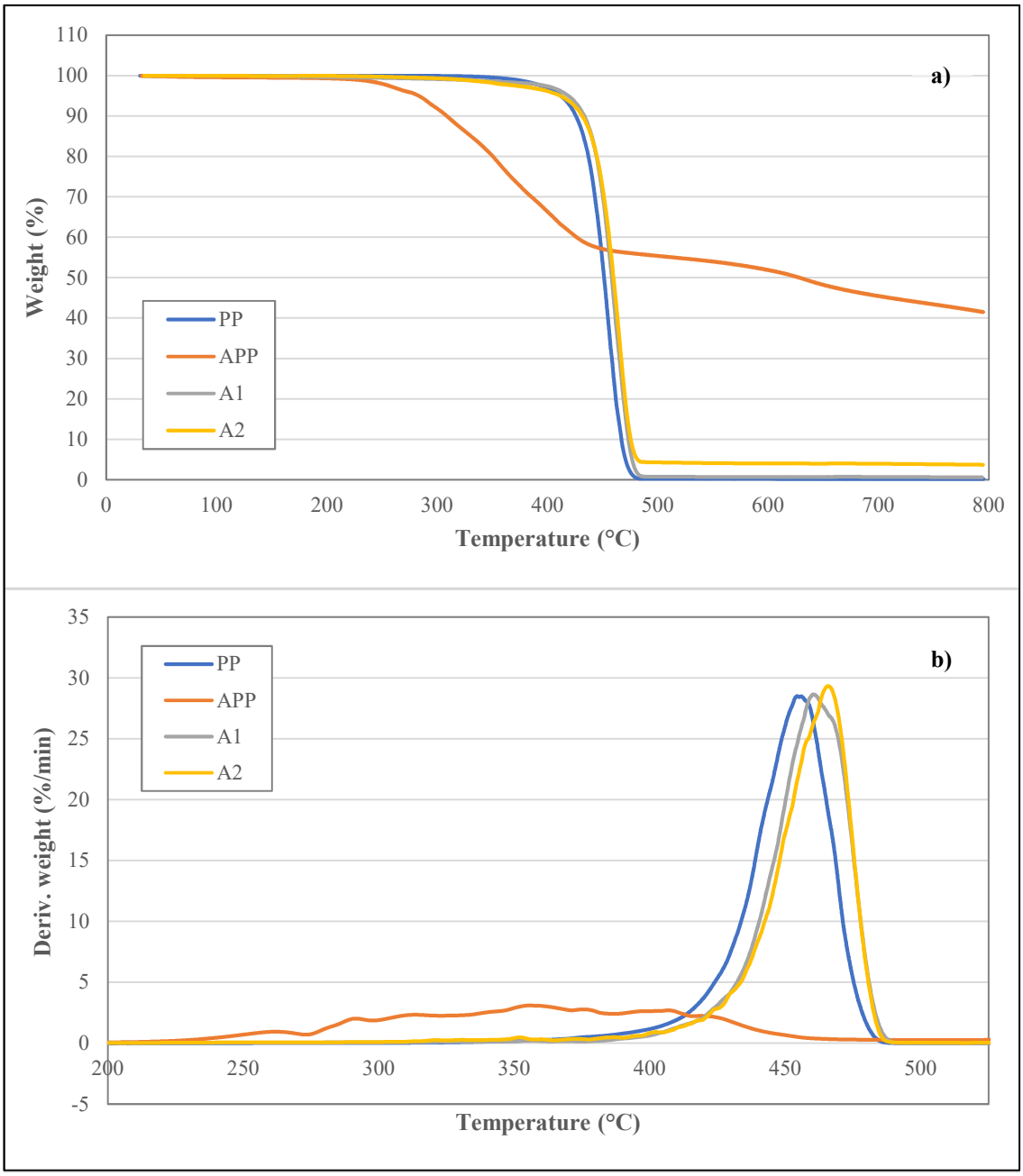

Figure 4.5. *a) TGA and b) DTG curves of PP composites blended with APP*

The residual masses at 500 °C and 700 °C were also increased with the addition of APP. 5 wt% containing composite gave 0.7719 % and 0.7268 % char residue at 500 °C

and 700 °C, respectively. The more APP was added to PP, the more residue yielded. This increase results from the thermal resistance of APP which is able to keep its weight up to 45 wt% at 700 °C.

Table 4.3. *TGA data of PP composites blended with APP*

Sample ID	$T_{10\%}$ (°C)	$T_{50\%}$ (°C)	T_{max} (°C)	Residue at 500 °C (%)	Residue at 700 °C (%)
PP	425.75	451.24	454.40	0.2632	0.2234
APP	308.59	629.81	-	55.42	45.48
A1	433.20	458.27	461.31	0.7719	0.7268
A2	431.15	459.77	465.89	4.3240	3.9800

TG and DTG curves of the composites containing APP and inorganic FR additives in the presence/absence of MPA are shown in Figure 4.6.a and Figure 4.6.b, respectively. The detailed thermal decomposition temperatures are shown in Table 4.4.

The addition of 8 wt% APP (AI1) did not alter the onset temperature of reference PP, however, $T_{50\%}$ and T_{max} temperatures were considerably increased to 458.28 °C and 464.27 °C, respectively. When MPA is added to PP/APP matrix (AI2), it resulted in an increase of onset temperature by 3.55 C; however, decreased T_{max} slightly. When ZnB is added to PP/APP matrix (AI3), $T_{10\%}$, $T_{50\%}$, and T_{max} temperatures were slightly increased; however, all these temperatures were decreased in the presence of MPA (AI4). The highest reduction was in onset temperature by 13 °C. By the inclusion of ATH (AI5), both $T_{10\%}$ and $T_{50\%}$ temperatures were increased; however, T_{max} was slightly decreased. When MPA was present (AI6), it did not result in a considerable change in those temperatures. In the case of the addition of nano-SiO_2 (AI7), $T_{50\%}$ and T_{max} were not differ noticeably; however, onset temperature was increased by 3.25 °C. In the presence of MPA (AI8), onset temperature was further increased while $T_{50\%}$ and T_{max} temperatures remained almost intact. By the addition of MPA, T_{max} of all combinations shifted slightly to lower temperatures, however, only in the presence of CNT, T_{max} was increased to 466.19 °C. Regardless of the presence of MPA, the highest $T_{10\%}$, $T_{50\%}$ and T_{max} temperatures were obtained by the addition of CNT (AI9 and AI10), which indicates a synergic effect between CNT, and both PP/APP and PP/APP/MPA matrix.

All inorganic FR additives resulted in an increase in the residue formation of the composite containing 8 wt%. By the inclusion of MPA, residues of the composites

containing ZnB, ATH, and CNT were increased while the opposite effect was seen for the composite containing any inorganic additive as well as the composite containing nano-SiO_2. Of all inorganic FR additives, the highest residue was obtained by the addition of ATH in both cases; in the presence/absence of MPA.

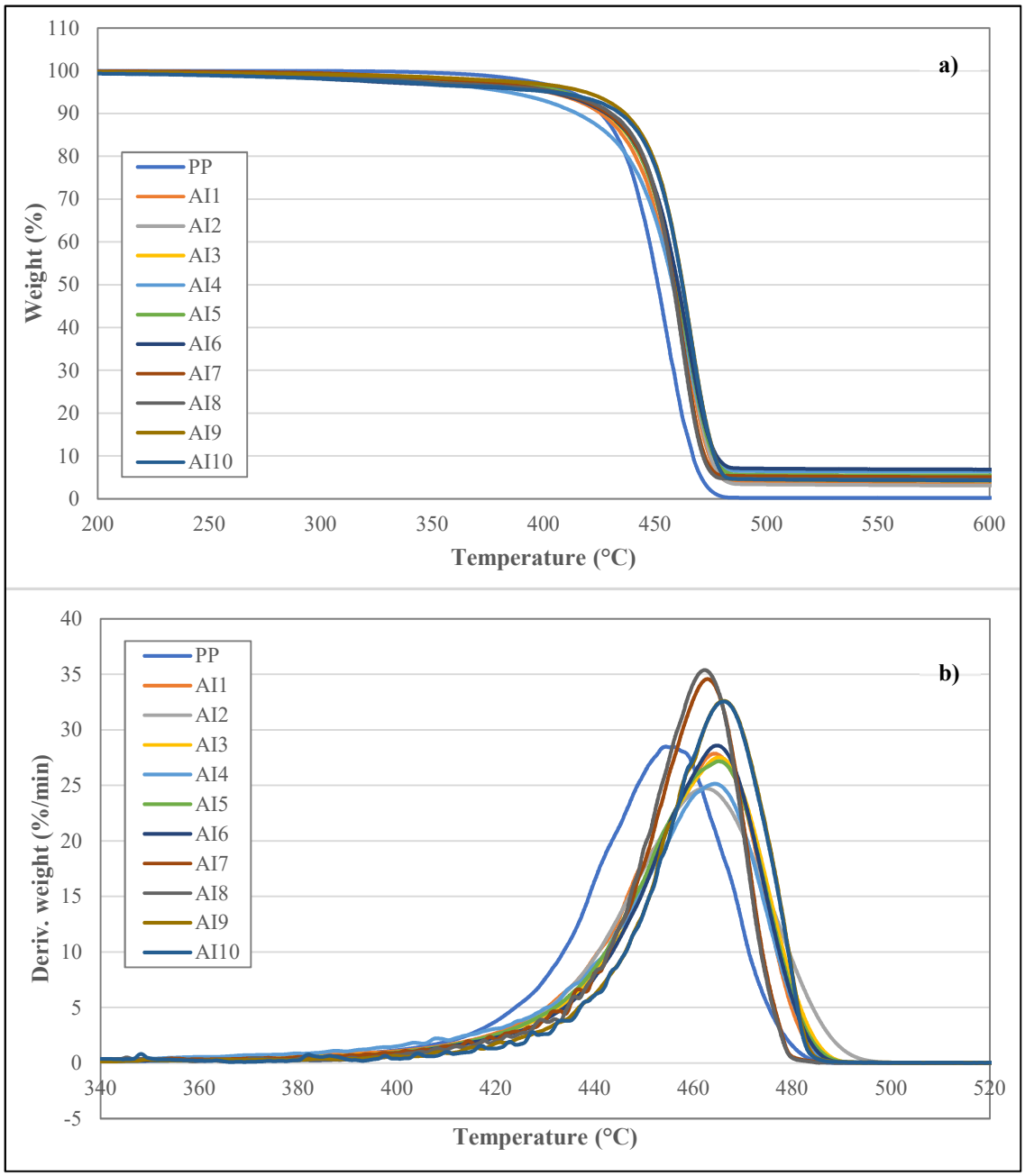

Figure 4.6. *a) TGA and b) DTG curves of PP/APP composites blended with inorganic FR additives*

Table 4.4. *TGA data of PP/APP composites blended with inorganic FR additives*

Sample ID	$T_{10\%}$ (°C)	$T_{50\%}$ (°C)	T_{max} (°C)	Residue at 500 °C (%)	Residue at 700 °C (%)
PP	425.75	451.24	454.40	0.2632	0.2234
AI1	425.47	458.28	464.27	3.708	3.102
AI2	429.02	459.00	462.36	3.371	3.000
AI3	427.74	460.00	465.20	5.351	5.278
AI4	414.73	457.93	464.34	6.460	6.345
AI5	428.44	459.55	462.90	5.590	5.446
AI6	427.80	460.23	462.23	7.071	6.816
AI7	428.72	458.51	465.00	5.288	4.880
AI8	430.09	458.19	464.75	4.637	4.291
AI9	436.38	462.41	466.07	4.511	4.085
AI10	434.10	462.19	466.19	4.552	4.231
AI11	427.39	460.54	465.13	7.223	7.153
AI12	428.29	459.66	464.11	5.370	5.290
AI13	426.79	459.64	465.12	5.476	5.351

All binary combinations of inorganic FR additives (ZnB/ATH, ZnB/nano-SiO_2, ZnB/CNT) were blended into PP/APP matrix in the presence of MPA. Their TG and DTG curves are shown in Figure 4.7.a and Figure 4.7.b, respectively. The addition of those combinations showed the same trend; they decreased the onset temperatures of the composite containing only APP (in the presence of MPA); however, they increased the T_{max}. The most reduction in onset temperature occurred when the combination of ZnB and CNT (AI13) was introduced to the PP/APP matrix. The combination of ZnB and ATH (AI11) resulted in a char residue of 7.223 % which is the highest residue obtained among all composites. Of binary combinations of inorganic FR additives, ZnB/ATH combination was found to be more promising for better thermal stability.

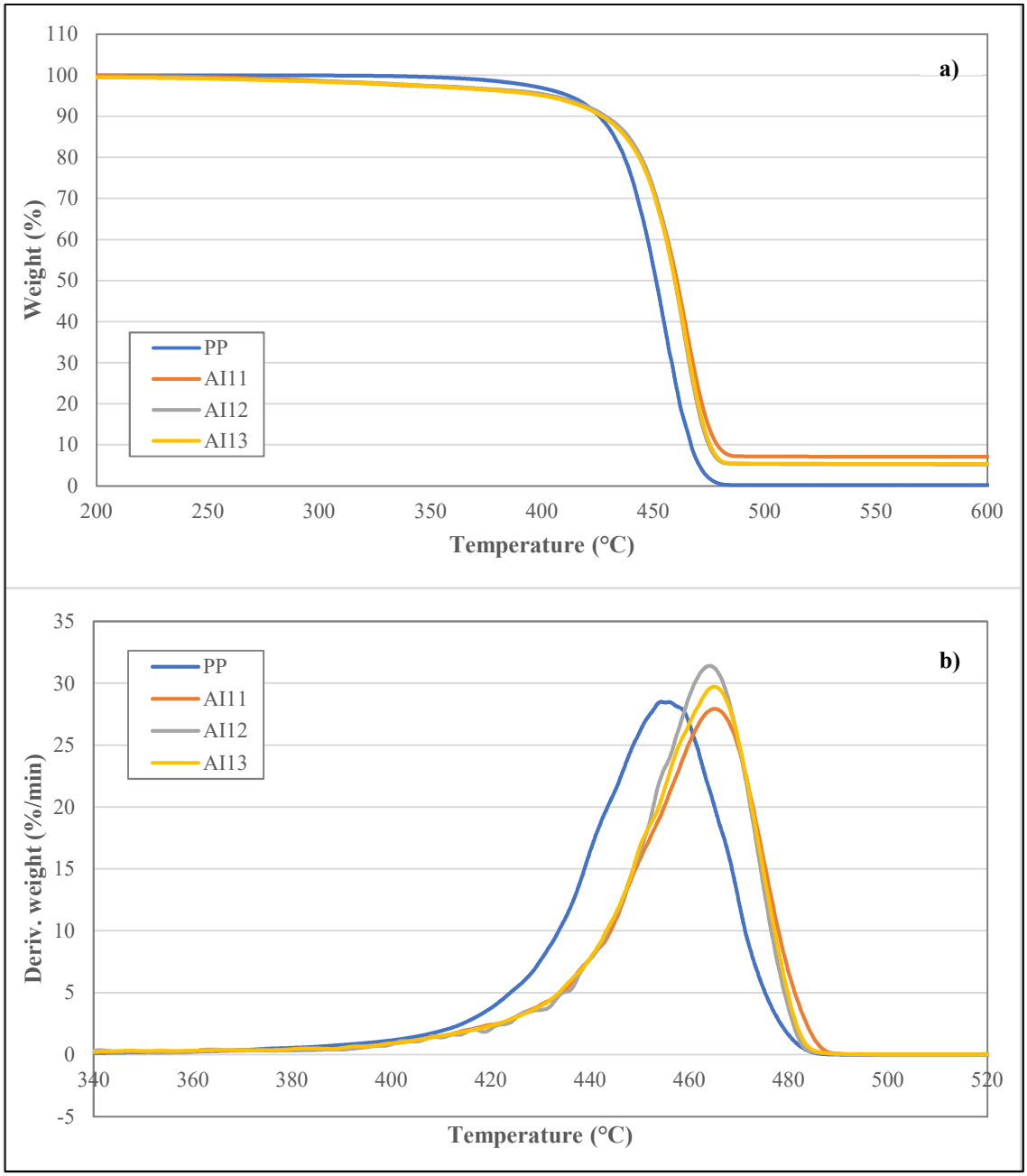

Figure 4.7. *a) TGA and b) DTG curves of PP/APP composites blended with the combinations of inorganic FR additives*

4.2.3. Cone calorimeter

Cone calorimeter is used to monitor heat release rate (HRR) which is the most important parameter in characterizing combustion behaviours, evaluating and predicting fire hazards of flammable materials. PHRR refers to the highest rate of heat release that a flammable material can produce. The higher the PHRR is, the more destruction a flammable material will cause under fire scenario [84]. The HRR versus the time curves of the samples are depicted in Figure 4.8. and the cone calorimeter data of samples are listed in Table 4.5. All data were obtained at a heat flux of 35 kW/m^2.

Table 4.5. *Cone calorimeter data of the PP composites blended with 5 wt% and 10 wt% APP*

Parameter	Sample ID		
	PP	A1	A2
TTI (s)	52	32	36
pHRR (kW/m²)	1566.40	988.16	494.63
avMLR (g/s)	0.143	0.139	0.070
THR (MJ/m²)	114.6	104.4	99.6
THR/TML (MJ/m^2g)	4.771	4.351	4.056
FPI (m²s/kW)	0.033	0.032	0.073
avCO (kg/kg)	0.047	0.069	0.074
avCO_2 (kg/kg)	2.624	2.492	2.269
CO/CO_2 ratio (kg/kg)	0.018	0.028	0.033
Char yield (%)	0.0	2.8	3.3

As seen in Figure 4.8, PP burned very fiercely after ignited at 52 s and one sharp HRR peak appeared with a heat release peak 1566 kW/m^2. The addition of 5 wt% APP reduced the maximum HRR by 36.91 % with a broadened the HRR curve. The total heat release (THR) and average mass loss rate (avMLR) were decreased slightly as well. When %10 APP was incorporated into PP Matrix, the peak heat release rate of neat PP was further reduced by 68.42 % whilst the burning time was prolonged significantly. It also gave rise to a relatively constant HRR curve decreasing slowly towards the end of combustion which is in conformity with the characteristic curve of an intumescent flame-retardant system. Moreover, THR and avMLR of PP were decreased by 13.09 % and 51.05 %, respectively, increasing the thermal stability of polypropylene in a more pronounced manner. Both loadings caused a reduction in TTI of PP whereas 10 wt % APP containing sample started to ignite a bit later than that contains 5 wt % APP. The

shorter ignition time may be due to the formation of a char layer that causes a rapid increase in the surface temperature of the samples [85].

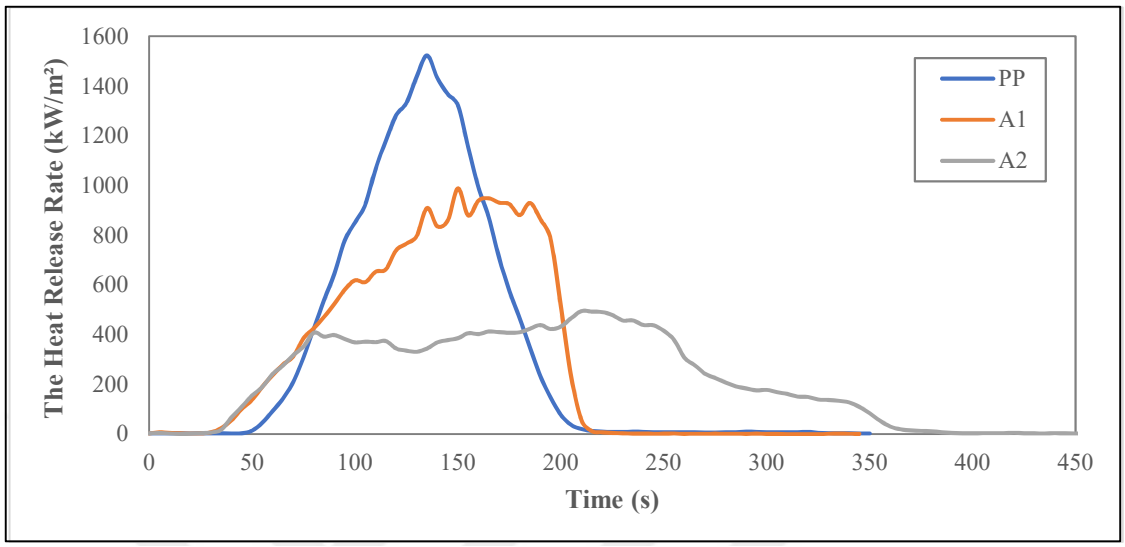

Figure 4.8. *HRR curves of the PP composites blended with 5 wt% and 10 wt% APP*

The total heat evolved per total mass loss (THE/TML) is a measure that used to define gas phase activity of a flame retardant [86]. The more APP was present, the more increase in char yield and the more decrease in THR/TML values were concluded. This result corresponded with the flame-retardant mechanism of APP mainly in the condensed phase.

The fire performance index (FPI) represents the ratio between the time to ignition (TTI) and the peak of rate heat release (PHRR) and expresses the propensity of a material to flashover [87,88]. Therefore, the higher the FPI value is, the better the fire safety is. The addition 5 wt% APP did not alter the fire performance index of PP. However, in the presence of 10 wt% APP, the FPI increased by 121.21% indicating that APP could inhibit the flashover of PP but dependently of its content.

The toxicity of the materials may be assessed by using CO/CO_2 ratios which is an important indicator to determine CO generation during combustion [89]. The CO is a product of incomplete combustion and an increase in that may be correlated to the relatively inefficient combustion but the efficient flame inhibition in the presence of a flame-retardant material [86]. Apparently, an increasing amount of APP was added to PP, it leads to more toxic gaseous mixture with an increased CO/CO_2 ratio by increasing the

CO yield while decreasing the CO_2 yield.

As a non-charring polymer, PP burns out leaving hardly any or no residue [90]. Char photos of the samples after cone calorimeter tests are shown in Figure 4.9. As it is clearly seen in Figure, the sample containing 5 wt% APP left a thin char. When 10 wt% APP were present, it resulted in a higher fluffy char formation. By the addition of an increased amount of APP, the intumescent layer became more pronounced.

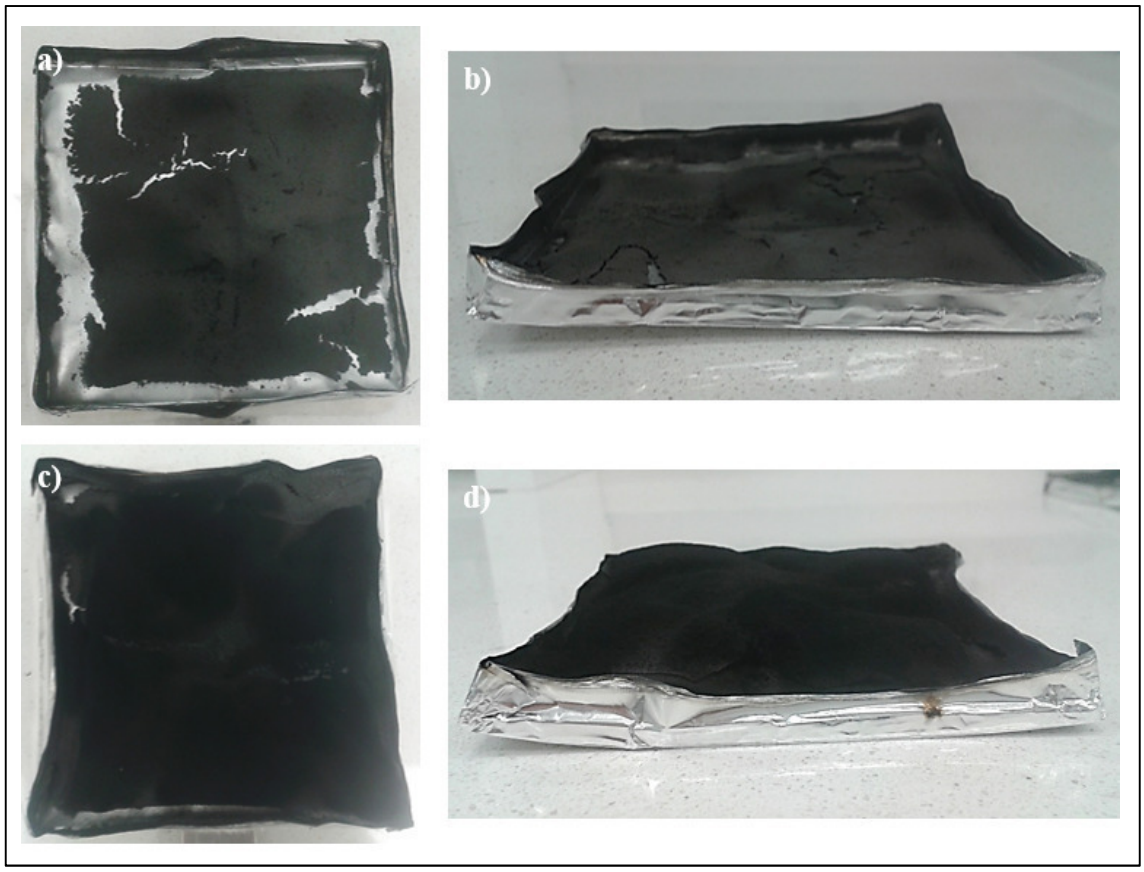

Figure 4.9. *a) Top view and b) cross sectional view char photos of the sample containing 5 wt% APP and c) Top view and d) cross sectional char photos of the sample containing 10 wt% APP*

4.3. Characterization of Cyclic Phosphonate-Based Flame Retardant PP Composites

4.3.1. LOI

The LOI value of reference PP (19 %) increased to 21.5 % by the addition of 3.5 wt% CPP. Incorporating 5 wt % CPP further increased the LOI to 22 %. As seen from Figure 4.10.a), the more CPP were blended in PP, the higher LOI values were obtained.

Compared to APP containing samples, CPP containing samples yielded higher LOI values at the same level of FR loading. Due to these promising results of CPP, it has been further examined for the production of melt-spun PP fibers.

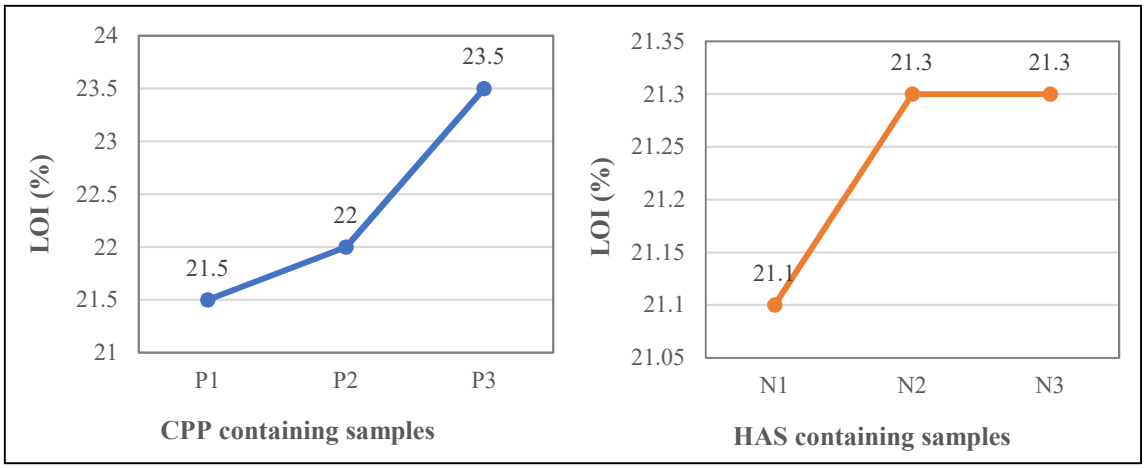

Figure 4.10. *LOI values of a) PP/CPP and b) PP/HAS composites*

Addition of 1 wt% HAS increased the LOI value of reference PP to 21.1 %. When 1.5 wt% of HAS was introduced in the PP matrix, LOI value increased to 21.3 %. However, incorporating more HAS did not alter the LOI value; it remained constant (21.3 %) when 5 wt% HAS was blended in PP. This trend is illustrated in Figure 4.10.b.

The synergetic effect between CPP and HAS was studied for further examinations. Total content of these additives was fixed at 5 wt% and their content was varied in proportion to each other. All combinations showed a synergetic effect even in the presence of small amounts of these additives in FR composition. The LOI values versus CPP/HAS combinations are shown in Figure 4.11.

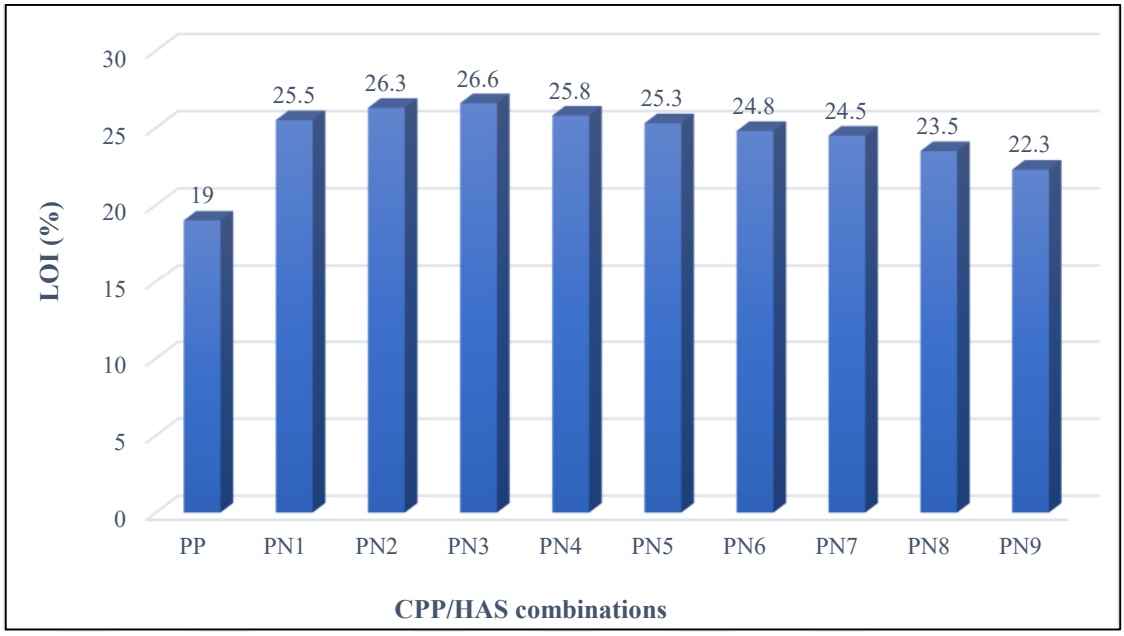

Figure 4.11. *LOI values of flame retardant PP with the addition of CPP/HAS combinations in different ratios (Total content of FRs is 5 wt%)*

The most significant synergistic effect was achieved by a combination of 3.5 wt% CPP and 1.5 wt% HAS with an LOI of 26.6 %. From this point on, the LOI values started to decrease when the content of HAS was increased (while CPP was decreased) in FR composition. The higher amount of HAS were present in FR composition the more reduction of LOI was concluded. Incorporation of 0.5 wt% CPP and 4.5 wt% HAS decreased the LOI value to 22.3 %, however, it is still higher than the LOI value of the samples containing 5 wt% these FR additives individually. Considering these results, the combination of 3.5 wt% CPP and 1.5 wt% HAS was chosen for a detailed examination in the following sections. The effect of inorganic additives on the flammability of this combination was also studied. The LOI values versus composites containing CPP/HAS (3.5:1.5) and inorganic additives are shown in Figure 4.12.

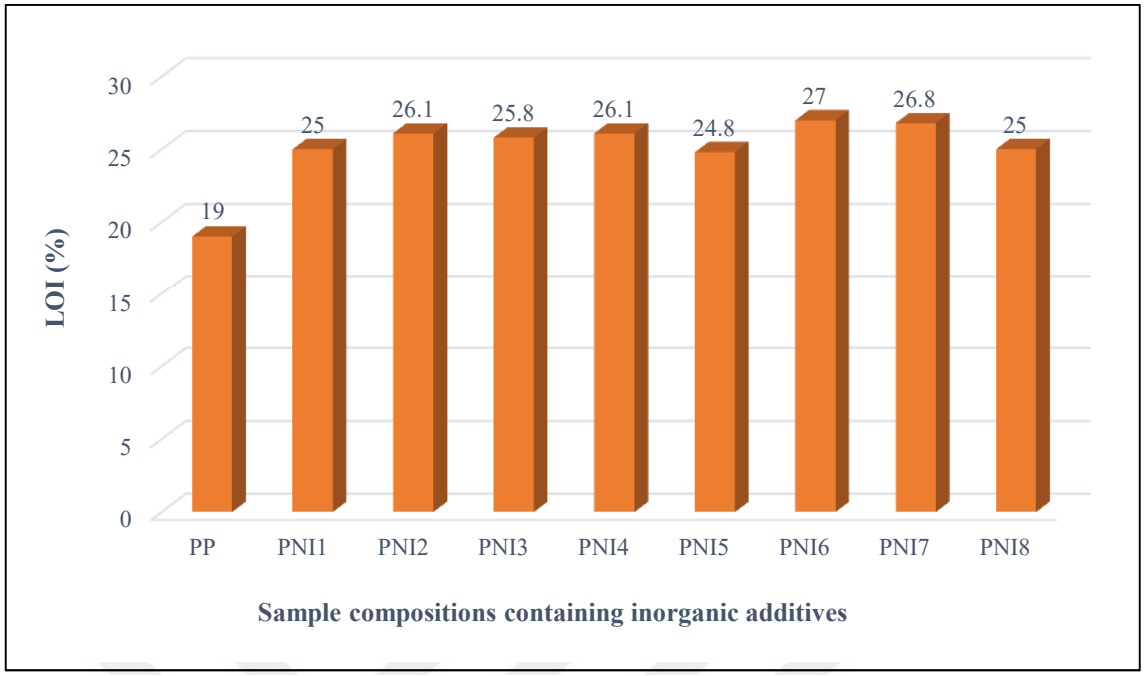

Figure 4.12. *LOI values of PP/CPP/HAS composites blended with inorganic additives*

Several inorganic additives were blended in PP/CPP/HAS system: zinc borate, aluminum trihydroxide, silica, carbon nanotubes, zinc oxide and cupric oxide. The addition of 0.25 wt% and 0.5 wt% nano-CuO increased the LOI values to 27 % and 26.8 %, respectively. As it is also an antibacterial additive in addition to its synergetic effect with PP/CPP/HAS system, nano-CuO was presumed to be the most promising candidate for the production of desired flame retardant and antibacterial fibers.

All other additives showed the antagonistic effect which results in a decrease of LOI values. The addition of 0.5 wt% ATH or 0.5 wt% CNT to PP/CPP/HAS system resulted in a relatively slight decrease of LOI value compared to other FR additives. The most reduction of LOI was concluded by the addition of 0.5 wt% ZnO by 2.5 %.

4.3.2. TGA

TGA was utilized to determine the thermal stability of the samples. TG and DTG curves of all samples containing CPP are shown in Figure 4.13.a and Figure 4.13.b, respectively. The detailed thermal decomposition temperatures are shown in Table 4.6.

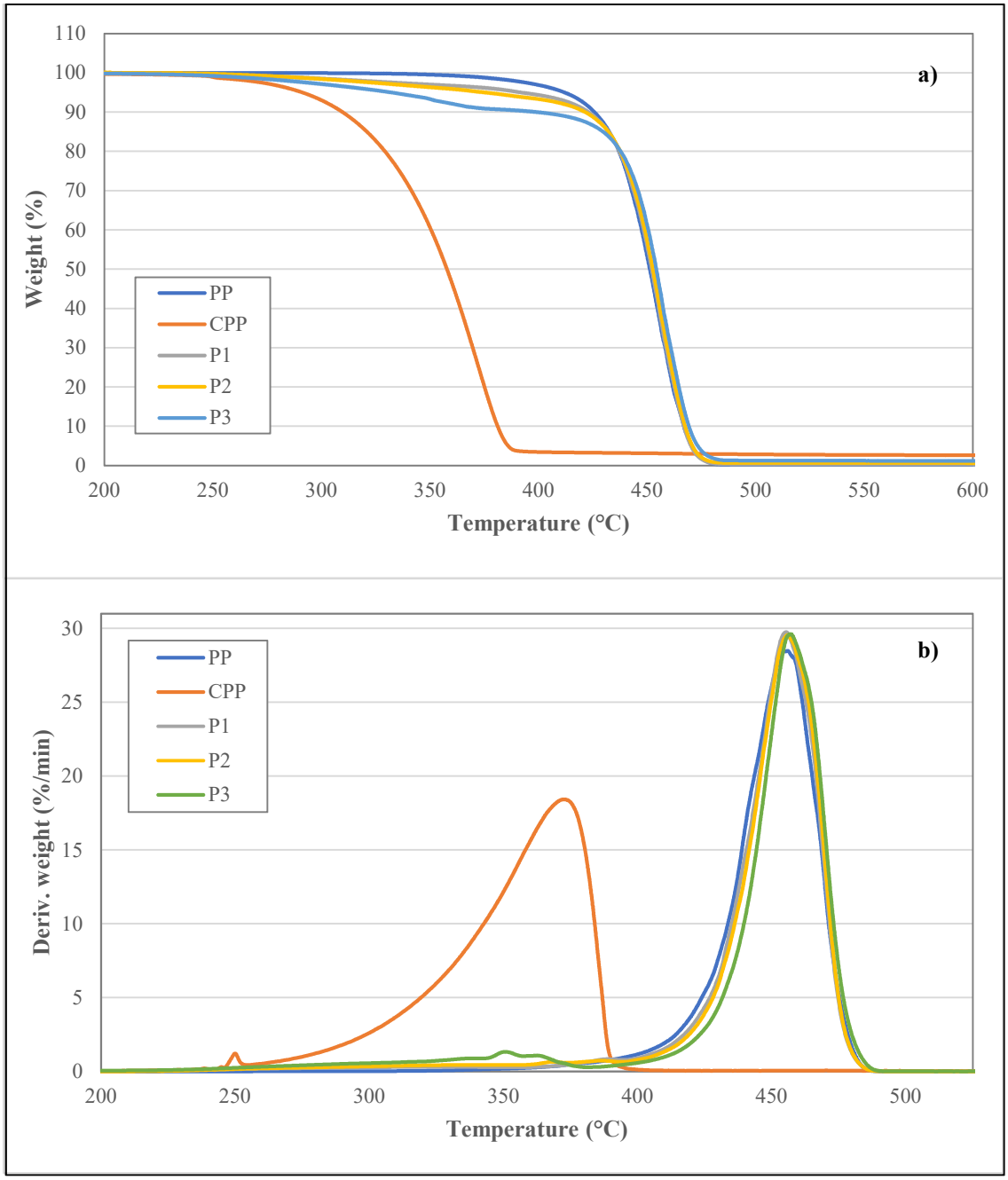

Figure 4.13. *a) TGA and b) DTG curves of PP/CPP composites*

Thermal decomposition of reference PP and pure CPP were first studied individually without any blending. As seen in Figure 4.13.b, a single step decomposition was observed for reference PP starting at 425.75 °C without leaving any char residue. Although its initial step was not easily distinguishable, two-step decomposition was occurred for pure CPP starting at 246.71 °C and at 309.76 °C for the first step and the second step, respectively. Reference PP decomposed with maximum weight loss rate

(T_{max}) at 454.40 °C without leaving any char residue at 700 °C. Compared to reference PP, pure CPP reached its both maximum weight losses at lower temperatures (at 249.92 °C for the first step and at 372.59 °C for the second step), however, it decomposed by leaving 2.623 % char residue at 700 °C.

In the presence of CPP, all samples showed a two-step decomposition process that the first step corresponded to the decomposition of CPP in the PP matrix. This step became more pronounced within the curve by the addition of 10 wt% CPP. Incorporation of CPP to PP shifted the onset decomposition temperatures, $T_{10\%}$ (the temperature at 10% weight loss), towards lower temperatures when the amount of CPP in the PP matrix was increased from 3.5 wt% to 10.0 wt%). However, $T_{50\%}$ (the temperature at 50% weight loss) and T_{max} values were both increased gradually by the incorporation of an increased amount of CPP. The residual masses at 500 °C and 700 °C were increased with the addition of CPP to PP as well. The more CPP was present, the more char residues were observed, as given in Table 4.6.

Table 4.6. *TGA data of PP/CPP composites*

Sample ID	$T_{10\%}$ (°C)	$T_{50\%}$ (°C)	T_{max} (°C)	Residue at 500 °C (%)	Residue at 700 °C (%)
PP	425.75	451.24	454.40	0.2632	0.2234
CPP	309.76	357.80	249.92 372.59	2.870	2.623
P1	423.04	452.11	455.40	0.3683	0.3447
P2	421.50	452.67	455.84	0.7057	0.6180
P3	399.62	454.21	457.01	1.3060	1.1810

Thermal decomposition of pure HAS and HAS-loaded PP samples were examined by TGA. TG and DTG curves of all samples are presented in Figure 4.14.a and Figure 4.14.b, respectively. The detailed TGA data are listed in Table 4.7.

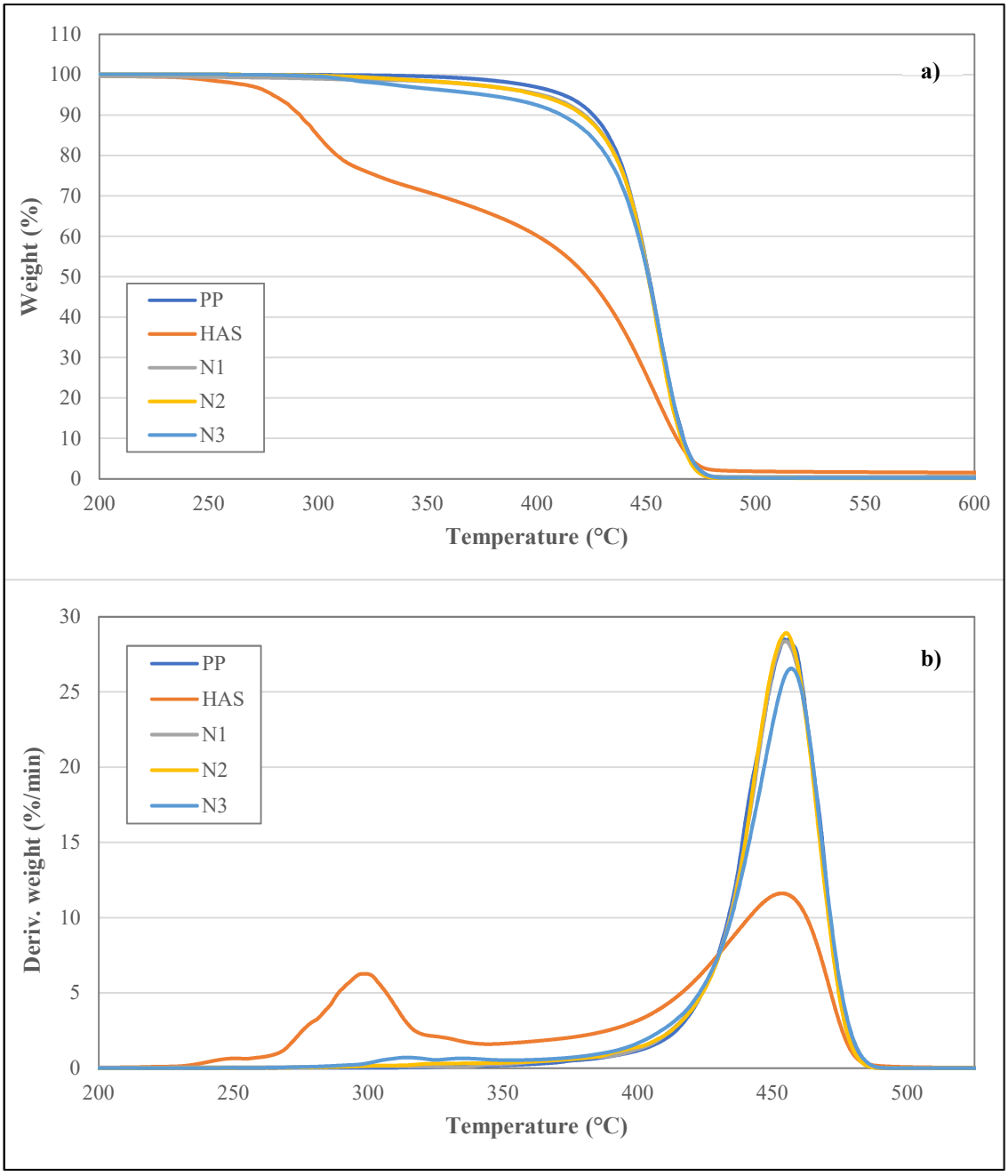

Figure 4.14. *a) TGA and b) DTG curves of PP/HAS composites*

Reference PP and pure HAS were first studied individually to determine their decomposition behaviour. As seen in Figure 4.14.b, a single step decomposition was observed for reference PP with the maximum mass loss rate at 454.40 °C without leaving any char residue. For HAS, two-step decomposition occurred with the maximum mass loss rates at 297.57 °C and at 453.53 °C for the first step and the second step, respectively. Pure HAS started to decompose in lower temperatures (291.73 °C) compared to PP, however, it left 1.347 % char residue at 700 °C.

HAS-loaded PP samples showed a two-step decomposition process. The first decomposition step may correspond to the first decomposition step of HAS while the second decomposition step may represent the merging of the decomposition step of PP and the second decomposition step of HAS. When only a small amount of HAS (1 wt%) is added to PP (N1), onset temperature decreased from to 425.75 °C to 421.76 °C. The more HAS was present, the more reduction was observed. This reduction in onset temperatures of PP may be associated with the interaction between HAS and PP that lowers the apparent activation energy in the first step of decomposition, indicating the destabilization of PP in higher degrees. The addition of HAS up to 1.5 wt% was decreased $T_{50\%}$ temperature slightly, however, it didn't alter the T_{max}. In the presence of 5 wt% HAS, $T_{50\%}$ was almost identical with that of the sample containing 1.5 wt% HAS, however, T_{max} was increased then slightly by 2.52 °C. The residual masses at 500 °C and 700 °C were increased with the addition of HAS to PP as well. The more HAS was present, the slightly more char residues were observed, as given in Table 4.7. The addition of 5 wt% HAS resulted in a residue formation of 0.5525 % at 700 °C which is slightly lower than those samples containing either APP or CPP at the same extent. Overall, all those samples decomposed without leaving a considerable residue due to the low loading of FR additives (≤ 5 wt%).

Table 4.7. *TGA data of PP/HAS composites*

Sample ID	$T_{10\%}$ (°C)	$T_{50\%}$ (°C)	T_{max} (°C)	Residue at 500 °C (%)	Residue at 700 °C (%)
PP	425.75	451.24	454.40	0.2632	0.2234
HAS	291.73	422.93	297.57 453.53	1.886	1.347
N1	421.76	451.05	454.20	0.2150	0.1864
N2	420.93	450.79	454.42	0.2811	0.2472
N3	411.39	450.90	456.94	0.5604	0.5525

Thermal decomposition of binary combinations of CPP and HAS were examined by TGA. The total FR content was kept at 5 wt% and the content of CPP and HAS were varied in proportion to each other. TG and DTG curves of selected combinations are shown in Figure 4.15.a and Figure 4.15.b, respectively. The detailed thermal decomposition temperatures are shown in Table 4.8.

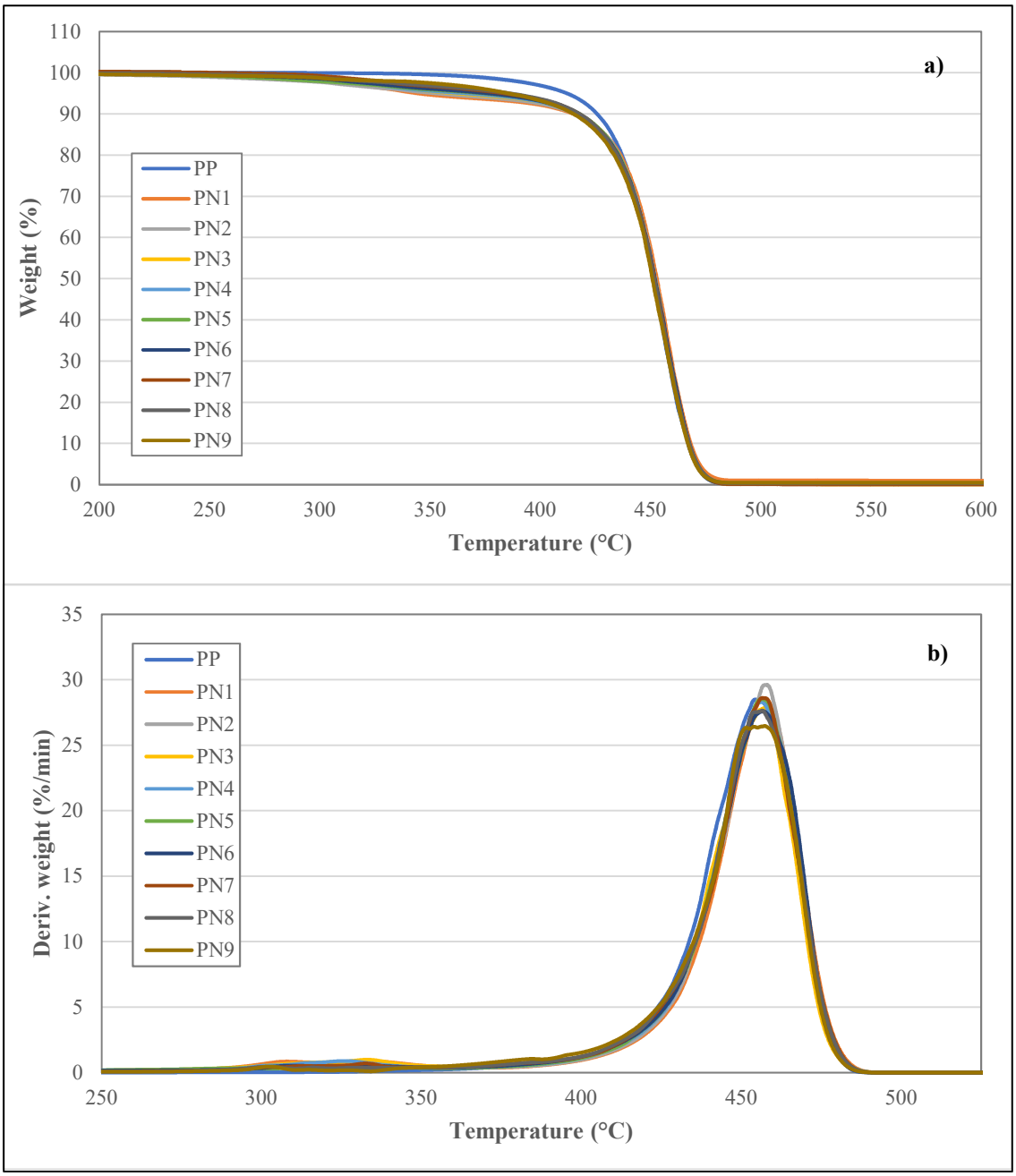

Figure 4.15. *a) TGA and b) DTG curves of PP/CPP/HAS composites*

As seen in Figure 4.15, a two-step decomposition was observed for all combinations. Regardless of the proportion of CPP and HAS, the addition of all combinations decreased the temperature at 10 % weight loss ($T_{10\%}$). In the presence of excess either CPP (PN1) or HAS (PN9), $T_{10\%}$ decreased from 425.75 °C to about 415.1 °C which is the greatest reduction occurred among all combinations. All combinations shifted the temperatures at 50 % weight loss ($T_{50\%}$) slightly to higher temperatures, however, only by the addition of excess HAS (PN9), T_{max} was reduced to 450.80 °C which is slightly lower than $T_{50\%}$ of reference PP. PN3, PN5, PN7 and PN8 samples lost 10 % of their weight at higher temperatures compared the other combinations, however, PN3 resulted in a higher T_{max} as well. Although the onset temperature of PN2 was relatively low compared to the other combinations, its T_{max} (459.64 °C) was the greatest temperature among all combinations, promising better thermal stability. Nevertheless, considering with LOI results that PN3 sample containing CPP/HAS (3.5:1.5) had a higher LOI value by 0.3 % than the PN2 sample, PN3 sample was chosen for further examinations on the thermal degradation of its ternary combinations with the inorganic additives.

As both pure CPP and pure HAS decomposed by leaving barely char residues, the addition of their binary combinations resulted in a residue less than 1 %. The highest residual mass at 700 °C was obtained for PN1 sample (0.9567 %) containing CPP/HAS (4.5:0.5) which may probably be due to the excess amount of CPP.

Table 4.8. *TGA data of PP/CPP/HAS composites*

Sample ID	$T_{10\%}$ (°C)	$T_{50\%}$ (°C)	T_{max} (°C)	Residue at 500 °C (%)	Residue at 700 °C (%)
PP	425.75	451.24	454.40	0.2632	0.2234
PN1	415.15	452.85	456.97	1.045	0.9567
PN2	415.90	452.06	459.64	0.1481	0.1265
PN3	417.01	451.63	458.36	0.1303	0.08806
PN4	416.65	451.97	456.65	0.3496	0.3239
PN5	417.80	451.81	456.01	0.3546	0.3340
PN6	416.63	451.89	456.84	0.2188	0.1852
PN7	417.62	451.75	456.54	0.1212	0.09303
PN8	417.78	451.54	456.74	0.3521	0.3284
PN9	415.08	450.80	457.67	0.4993	0.4884

The effect of inorganic additives on the thermal degradation of PP/CPP/HAS combination is examined by TGA. TG and DTG curves of the composites containing CPP/HAS (3.5:1.5) combination and inorganic additives are shown in Figure 4.16.a and Figure 4.16.b, respectively. The detailed thermal decomposition temperatures are shown in Table 4.9. CPP/HAS content was kept at 5 wt% in all composites and all inorganic additives were incorporated into PP/CPP/HAS formulation individually. The content of flame retardant additives (ZnB, ATH, nano-SiO_2, and CNT) was 0.5 wt% while the content of antibacterial additives (nano-CuO and ZnO) were both 0.25 %wt and 0.5 wt%.

The effect of CPP/HAS (3.5:1.5) combination on the thermal degradation of pure polypropylene was discussed in the previous section. It is found that in the presence of this combination (PN3), the onset temperature of the pure PP was reduced from 425.75 °C to 417.01 °C; however, Tmax was increased from 454.40 °C to 458.36 °C. It decomposed by leaving almost no residue (0.1303 % at 500 °C).

By the inclusion of ATH, the onset temperature of PN3 composite is slightly decreased and it did not change in the presence of nano-SiO_2; however, apart from these additives, all inorganic additives increased the onset temperature. When ZnB (PNI1), CNT (PNI4) and nano-CuO (PNI5 and PNI6) was present in PP/CPP/HAS matrix (PN3), $T_{50\%}$ value of PN3 composite was increased; however, the addition of nano-SiO_2 (PNI3) and ZnO (PNI7 and PNI8) did not result in a considerable change in $T_{50\%}$. Only in the presence of ATH, $T_{50\%}$ was slightly decreased. The same tendency was observed when these values were evaluated regarding those of pure polypropylene. All loadings of inorganic additives caused a decrease in T_{max} value of PN3 composite; however, in the presence of only ZnB, T_{max} value remained almost intact. Since $T_{10\%}$ and $T_{50\%}$ values were increased by 7.09 °C and 3.84 °C in company with an almost constant T_{max} of PN3 composite, the addition of ZnB increased thermal stability at high temperatures even at low loadings (0.5 wt). The addition of both 0.25 wt% ZnO and 0.50 wt% ZnO increased the onset temperature of PN3; however, it resulted in a higher decrease in T_{max} which indicates a thermal instability at high temperatures. Of all inorganic additives, the greatest reduction in T_{max} occurred was at 0.25 wt% loading of ZnO by 453.94 which is even smaller than T_{max} of the pure PP. The inclusion of 0.25 wt nano-CuO increased not only the onset temperature but also $T_{50\%}$ and T_{max} of the PN3 composite. When the content of nano-CuO was 0.5 wt%, those temperatures further increased indicating enhanced thermal stability of PN3 composite at high temperatures.

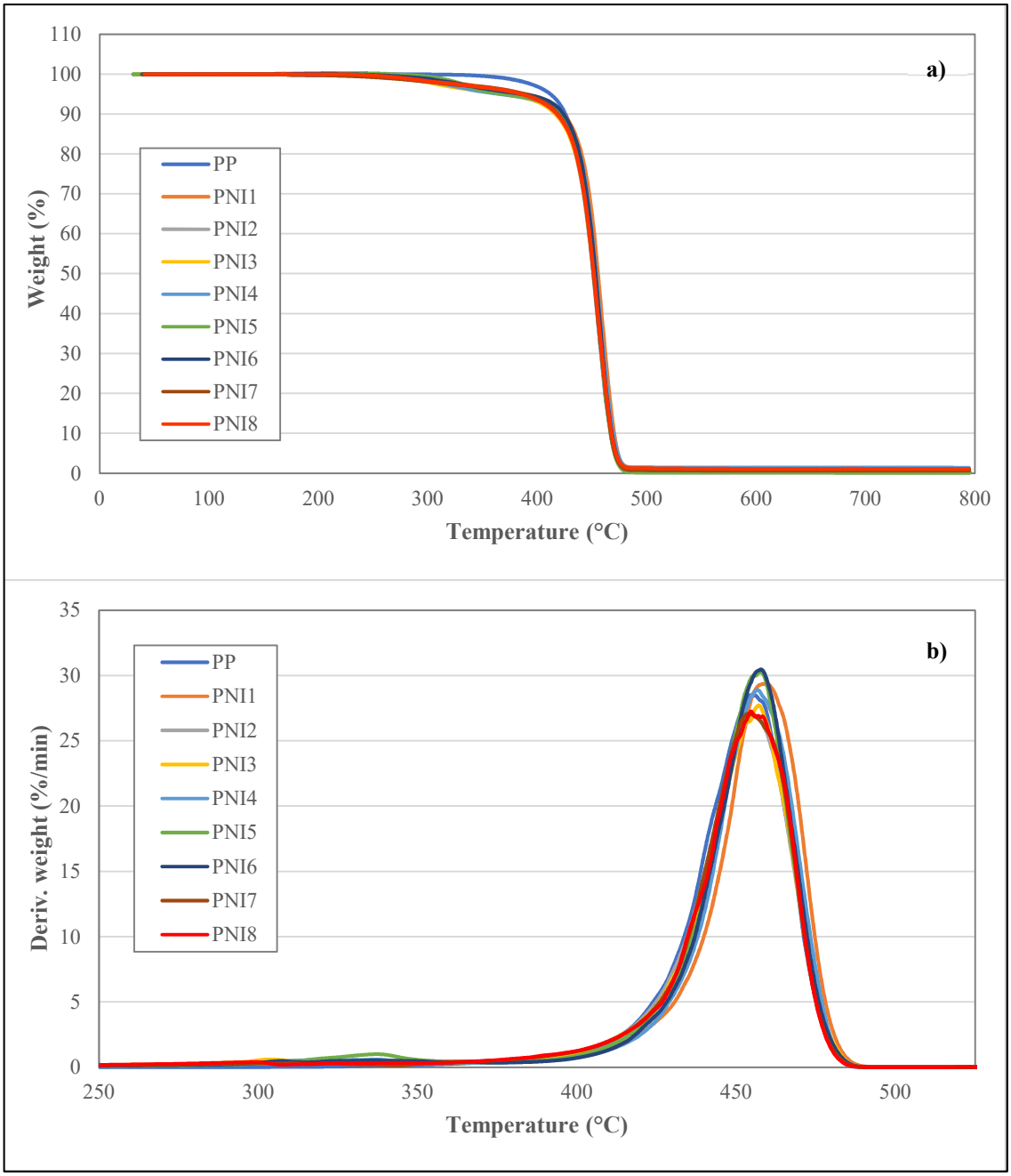

Figure 4.16. *a) TGA and b) DTG curves of PP/CPP/HAS composites blended with inorganic additives*

The addition of all inorganic additives increased the residue both the pure and PN3 composite. By the addition of nano-SiO_2, CNT, and ZnO at 0.5 wt% loading, this increase became more pronounced (>1%). The more either nano-CuO or ZnO was present, the more char residues were obtained. The greatest residue was obtained in the presence of CNT (1.22 % at 700 °C). Overall each combination of inorganic additives with CPP/HAS was started to decompose at a lower temperature than that of pure PP; nevertheless, their presence resulted in an increase of T_{max} of pure PP which also increases the thermal stability of it at higher temperatures even at small loadings (≤ 0.5 wt%).

Table 4.9. *TGA data of PP/CPP/HAS composites blended with inorganic additives*

Sample ID	$T_{10\%}$ (°C)	$T_{50\%}$ (°C)	T_{max} (°C)	Residue at 500 °C (%)	Residue at 700 °C (%)
PP	425.75	451.24	454.40	0.2632	0.2234
PNI1	424.10	455.47	458.23	0.5863	0.4450
PNI2	418.25	451.09	455.03	0.5103	0.4459
PNI3	416.55	451.64	457.19	1.300	1.196
PNI4	422.28	453.74	456.47	1.481	1.441
PNI5	419.81	452.17	457.56	0.1761	0.1044
PNI6	423.96	453.21	457.80	0.8988	0.8439
PNI7	418.87	451.37	453.94	0.7638	0.6656
PNI8	417.86	451.68	454.68	1.269	1.118

4.3.3. Cone calorimeter

The HRR versus the time curves of the samples containing either CPP or HAS, or CPP/HAS combination are depicted in Figure 4.17. The cone calorimeter data of samples are listed in Table 4.10. All data was obtained at a heat flux of 35 kW/m^2. Pure PP started to ignite after 52 s and burned very fast exhibiting a sharp peak with a peak heat release rate (PHRR) of 1134.7 W/g. The addition of only 3.5 wt% CPP reduced the maximum HRR to 1013.99 kW/m^2 with a broadened the HRR curve. The total heat release (THR) was also decreased by 13.87 % whilst the burning time was prolonged by approximately 30 s. When 1.5 wt% HAS was incorporated into PP Matrix, both PHRR and THR values of neat PP was reduced by 16.4 % and 4.36 % respectively with extended burning time. It resulted in a tapered HRR curve which has a shoulder observed towards the end of the curve. The addition of the CPP/HAS combination resulted in a decrease in PHRR of PP; however, the reduction was lower than those occurring in the presence of CPP and HAS

individually. On the other hand, the combination of CPP and HAS further decreased the THR, down to 98 MJ/m². avMLR of PP was also decreased to 0.10 g/s and it remained constant for all composites although the additives and their content differed in the PP formulation. Both loadings caused an increase in TTI of PP indicating that both CPP and HAS could delay the degradation of PP. However, HAS containing sample started to ignite 4.5 s later than that contains CPP which shows that HAS is more effective for a delayed degradation even at small loadings. When HAS was added into PP/CPP matrix, TTI was not further altered.

Table 4.10. *Cone calorimeter data of the composites blended with 3.5 wt% CPP and 1.5 wt% HAS individually and their combination*

Parameter	Sample ID			
	PP	**P1**	**N2**	**PN3**
TTI (s)	52	63.5	68	63
pHRR (kW/m²)	1566.40	1013.99	1309.46	1514.65
avMLR (g/s)	0.143	0.102	0.103	0.101
THR (MJ/m²)	114.6	98.7	109.6	98.0
THR/TML (MJ/m²g)	4.771	4.100	4.590	4.109
FPI (m²s/kW)	0.033	0.063	0.052	0.042
avCO (kg/kg)	0.047	0.082	0.042	0.081
$avCO_2$ (kg/kg)	2.624	2.642	3.028	2.688
CO/CO_2 ratio (kg/kg)	0.018	0.031	0.014	0.030
Char yield (%)	0.0	0.6	0.1	1.4

The FPI value of PN3 composite containing CPP/HAS combination was 0.042 m^2s/kW, which was lower than that for P1 (0.063 m^2s/kW) and that for N2 composite (0.052 m^2s/kW). Nevertheless, all samples resulted in a higher FPI value indicating that the fire safety of the PP upon addition of either CPP or HAS, or CPP/HAS combination was improved.

The THE/TML of the PP showed a reduction by 3.79 % in the presence of HAS (N2) indicating a flame inhibition effect arising from the gas phase mechanism of HAS dominantly. The more reduction in THE/TML (14.06 %) was observed in the case of CPP (P1) with a flame retardant mechanism in the gas phase. By the addition of HAS into PP/CPP matrix (PN3), no significant change in THR/TML was observed with respect to that of P1 sample. A possible reason for this is the counterbalancing effects of flame inhibition and increased char yield.

P1 and PN3 composites gave out more toxic gaseous mixture during combustion with an increased CO/CO_2 ratio (about 0.030) with regard to that of PP. However, the CO/CO_2 ratio of PP was decreased from 0.018 to 0.014 when only HAS was present in the FR formulation due to a decrease in CO yield and an increase in CO_2 yield. In other words, in the presence of only HAS, a less toxic gaseous mixture was emitted by N2 composite upon burning with respect to PP, P1, and PN3 composites.

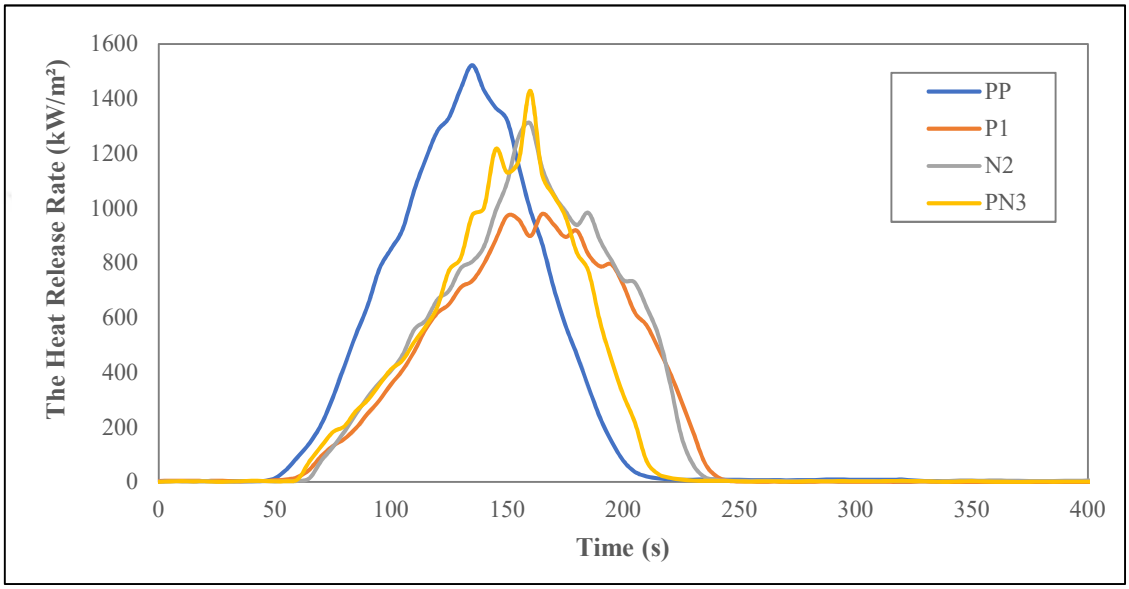

Figure 4.17. *HRR curves of the PP composites blended with 3.5 wt% CPP and 1.5 wt% HAS individually and their combination*

Char photos of the samples after cone calorimeter tests are shown in Figure 4.18. CPP containing sample (N1) resulted in more residue (0.6 %) with respect to HAS containing composite (0.1 %), however, it must be noted that the content of CPP was higher than that of HAS in PP matrix. In the presence of both CPP and HAS (PN3), the highest char residue was obtained (1.6 %). Although the residue of HAS was greyish when it is blended alone, it turned out a black residue in the presence of CPP. No matter which FR formulation (PP/CPP, PP/HAS or PP/CPP/HAS) was used, no intumescent char was observed.

Figure 4.18. *Char photos of the samples blended with a) 3.5 wt% CPP, b) 1.5 wt% HAS and c) their combination*

The HRR versus the time curves of the composites blended with inorganic additives (ZnB, ATH, nano-SiO_2, CNT and nano-CuO) individually in the presence of CPP/HAS are depicted in Figure 4.19. The cone calorimeter data of the composites are listed in Table 4.11. All data were obtained at a heat flux of 35 kW/m^2. Pure PP started to ignite after 52 s and burned very fast by showing a sharp peak which has a peak heat release rate (PHRR) of 1134.7 W/g. All inorganic additives decreased the PHRR of PN3 composite, however, only in the presence of CNT (PNI4), it increased slightly (1593.15 W/g). When 0.25 wt % nano-CuO was present in PP/CPP/HAS matrix (PNI5), the PHRR decreased to 1007.52 W/g which was lower than those of PNI1, PNI2, PNI3 and PNI6 containing 0.5 wt % ZnB, ATH, nano-SiO_2 and nano-CuO, respectively. Indeed, nano-CuO was very efficient at small loadings to decrease the fire risk by reducing the PHRR, however, it showed a reverse effect when the nano-CuO content was increased to 0.5 wt % that increased the PHRR to 1494.17 W/g. Nevertheless, it is still less than those of both PP and PN3 composites. The peak of HRR for all composites were ordered as: PNI5<PNI4<PNI2<PNI1<PNI6<PNI3. All composites exhibited HRR curve that is typical for intermediate thick non-charring samples [65].

As given in Table 4.11, the time to ignition (TTI) values were shortened for PNI1, PNI2 and PNI4 whereas no difference was observed for PNI3 and PNI6 composites. Of all the composites, the highest decrease in TTI was found in the presence of ZnB (PNI1) correlating to the fact that PNI1 composite also yielded the highest char yield (2.2 %). Only increase in TTI was observed for PNI5 composite.

Table 4.11. Cone calorimeter data of the PP/CPP/HAS composites blended with ZnB, ATH, nano SiO_2, CNT and nano-CuO

Parameter	Sample ID						
	PP	**PNI1**	**PNI2**	**PNI3**	**PNI4**	**PNI5**	**PNI6**
TTI (s)	52	38.5	51.5	63	42.5	73	62
pHRR (kW/m²)	1566.40	1354.60	1320.29	1593.15	1081.07	1007.52	1494.17
avMLR (g/s)	0.143	0.092	0.097	0.102	0.095	0.106	0.102
THR (MJ/m²)	114.6	102.5	102.0	103.7	99.8	93.4	94.1
THR/TML (MJ/m^2g)	4.771	4.295	4.265	4.308	4.118	3.889	3.919
FPI (m²s/kW)	0.033	0.028	0.039	0.040	0.039	0.072	0.041
avCO (kg/kg)	0.047	0.065	0.072	0.086	0.085	0.079	0.080
avCO_2 (kg/kg)	2.624	2.814	2.783	2.856	2.610	2.529	2.625
CO/CO_2 ratio (kg/kg)	0.018	0.023	0.026	0.030	0.033	0.031	0.030
Char yield (%)	0.0	2.2	1.6	1.6	1.1	1.4	1.5

All loadings increased the THR of PN3 composite; however, only nano-CuO containing composites resulted in a decrease in THR by 4.6 % and 4 % for PNI5 and PNI6, respectively. avMLR for PNI1, PNI2 and PNI4 showed a very slight reduction with respect to PN3, whereas no reduction was observed for PNI3 and PNI6. Only avMLR of PNI5 was slightly increased.

PNI1 and PNI2 composed decreased the toxicology hazard of PN3 composite by decreasing the CO/CO2 ratio; however, no clear effect was observed in case of PNI3, PNI4 and PNI5 and PNI6 composites. The CO/CO2 ratios for all the composites were ordered by increasing the toxicity hazard as: PNI4>PNI5>PNI6=PNI3>PNI2>PNI1.

The THR/TML value decreased with the addition of each additive indicating flame inhibition effect and therefore gas phase action. The highest reduction was occurred by PNI5 composite containing 0.25 wt % nano-CuO; in other words, majority of phosphorus-containing volatiles was released then. When the nano-CuO content was increased to 0.5 wt, THR/TML value slightly increased that the release of some phosphorus was suppressed. Still the THR/TML value of PNI6 composite was less than those of PNI1, PNI2, PNI3 and PNI4 indicating that nano-CuO allows the release of more phosphorus volatiles and hence acts in the gas phase more dominantly. Considering the decreased PHRR and TTI as well as the increased char yield and THR/TML value with respect to those of PN3 composite, the predominant mechanism for ZnB and ATH containing composites is the condensed phase mechanism. For all the composites, the flame inhibition was ordered as: PNI5>PNI6>PNI4>PNI2>PNI1>PNI3.

The results indicated that the addition of 0.25 wt% nano-CuO into PP/CPP/HAS matrix showed a truly synergistic effect resulting in the highest reduction in both PHRR and THR accompanied with an increase in TTI. Moreover, the only increase in FPI of PN3 occurred by 71.42 % in the presence of 0.25 wt% nano-CuO that the propensity of PN3 composite to flashover was significantly decreased. Thus, the flame retardant performance of PCO/HAS combination was strongly enhanced when nano-CuO was present in the polypropylene formulation, but dependently of its content.

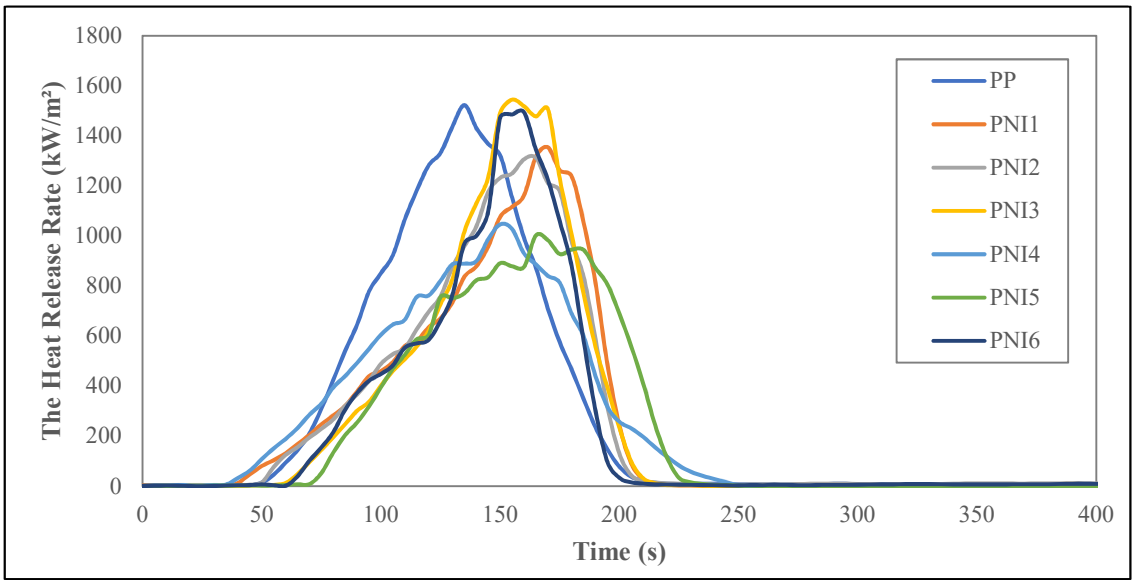

Figure 4.19. *HRR curves of PP/CPP/HAS composites blended with ZnB, ATH, nano SiO_2, CNT and nano-CuO*

The structure of residual char changes notably depending on the inorganic additive used. As seen in Figure 4.20, the residual char structures of both PNI1 and PNI2 are more compact than those of PNI3 and PNI4. This may due to condensed phase mechanism of ZnB and ATH. Char yield of the all composites was ordered as: PNI1>PNI2>PNI3>PNI6>PNI5>PNI4.

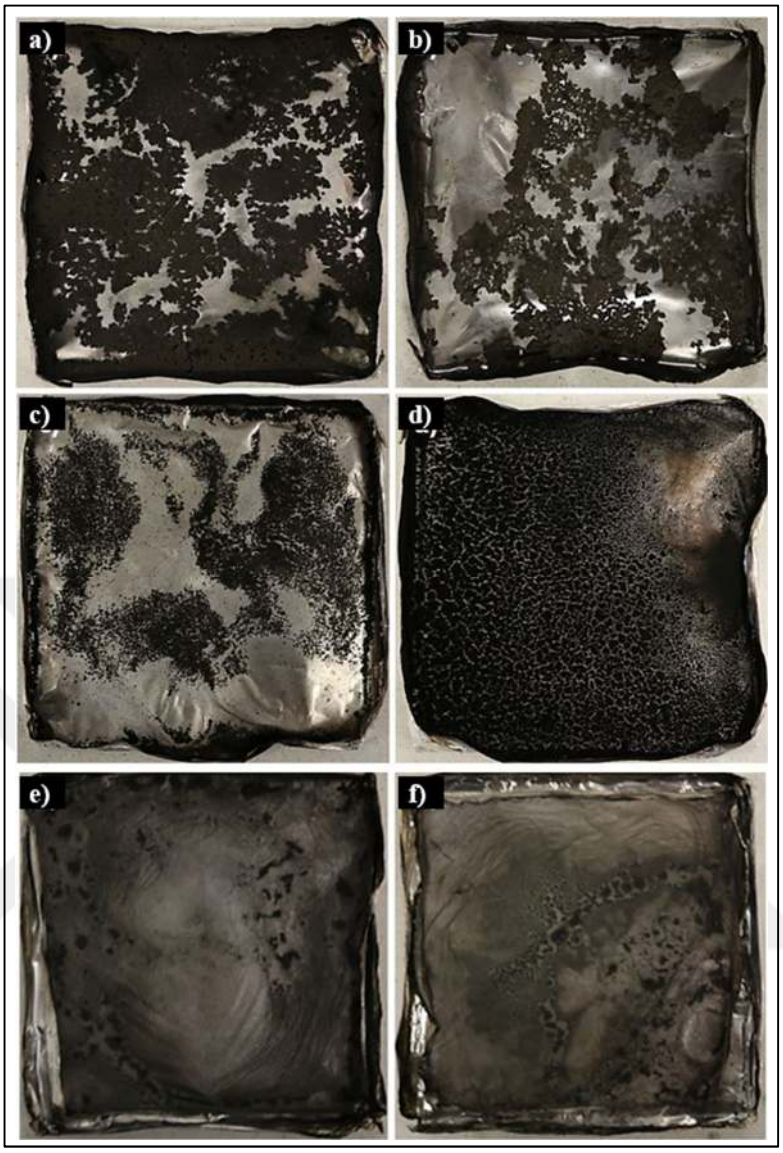

Figure 4.20. *Char photos of the PP/CPP/HAS composites blended with a) 0.5 wt% ZnB, b) 0.5 wt% ATH, c) 0.5 wt% nano-SiO_2, d) 0.5 wt% CNT, e) 0.5 wt% Nano-CuO and f) 0.25 wt% nano-CuO*

4.3.4. MCC

MCC was utilized to assess the flammability of reference PP and its composites. Firstly, the composites blended with CPP and HAS, individually and CPP/HAS combination were studied. The HRR versus temperature curves of those composites are depicted in Figure 4.21 and the corresponding heat release parameters are listed in Table 4.12.

Table 4.12. *MCC data of the composites blended with 3.5 wt% CPP and 1.5 wt% HAS individually and their combination*

Sample ID	HRC (J/(g K))	PHRR (W/g)	THR (kJ/g)	T_{PHRR} (°C)
PP	1164.0	1134.7	43.9	478.4
P1	1124.8	1105.5	43.4	479.4
N2	1056.7	1027.6	43.6	480.2
PN3	1033.0	1007.5	42.1	481.0

PP is a highly flammable material with a peak heat release rate (PHRR) of 1134.7 W/g, heat release capacity (HRC) of 1164.0 J/(gK), total heat release (THR) of 43.9 kJ/g and temperature at PHRR (T_{PHRR}) of 478.4 °C. With the addition of 3.5 wt% CPP in PP matrix, the PHRR decreased slightly from 1134.7 to 1105.5 W/g; and HRC decreased slightly from 1164.0 to 1124.8 J/(gK). In the presence of only 1.5 wt% HAS in PP matrix, the PHRR decreased significantly to 1027.6 W/g; and HRC decreased significantly to 1056.7 J/(gK). When CPP/HAS (3.5:1.5) combination was introduced to the PP matrix, both PHRR and HRC further decreased to 1007.5 W/g and 1033.0 J/(gK), respectively. With the incorporation of both CPP and HAS individually, THR values were decreased while the T_{PHRR} values were increased; however, the most reduction in THR (42.1 kJ/g) and the most increase in T_{PHRR} (481.0 °C) were obtained by the addition of CPP/HAS (3.5:1.5) combination.

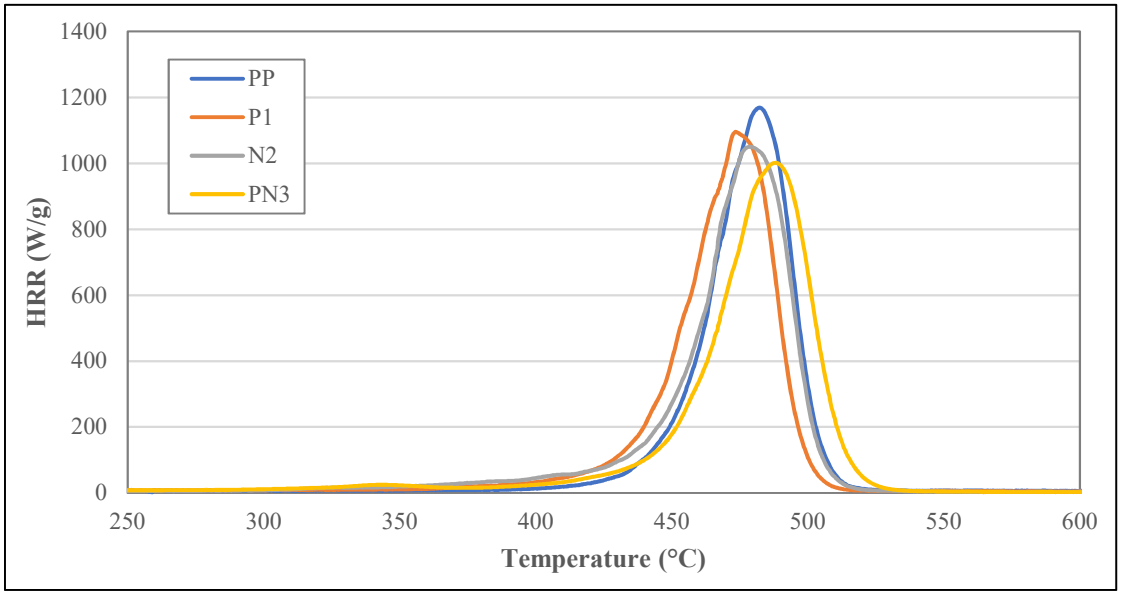

Figure 4.21. *HRR curves of the composites blended with 3.5 wt% CPP and 1.5 wt% HAS individually and their combination*

The effects of inorganic additives (flame retardant and antibacterial) on the flammability of the PP/CPP/HAS system were also determined by using MCC. The HRR versus temperature curves of the composites blended with CPP/HAS (3.5:1.5) in the presence of inorganic additives (0.5 wt%) are depicted in Figure 4.22 and the corresponding heat release parameters are listed in Table 4.13.

Table 4.13. *MCC data of PP/CPP/HAS composites blended with 0.5 wt% inorganic additives*

Sample ID	HRC (J/(g K))	PHRR (W/g)	THR (kJ/g)	T_{PHRR} (°C)
PP	1164.0	1134.7	43.9	478.4
PNI1	1039.2	1017.6	42.1	482.8
PNI2	1004.2	975.6	42.0	477.6
PNI3	1017.4	1000.5	41.4	482.3
PNI4	1068.8	1048.8	42.1	482.8
PNI6	1071.0	1042.2	42.0	480.3
PNI8	992.75	972.8	42.0	480.0

When introduced 0.5 wt% inorganic additives in PP/CPP/HAS system; PHRR, HRC and THR values of all composites decreased considerably, indicating a synergetic effect between the corresponding additive and PP/CPP/HAS system. The highest reduction in PHRR and HRC occurred in the presence of ZnO. The addition of nano-SiO_2 decreased the THR to 41.4 kJ/g which is the lowest THR value obtained. In the presence of all inorganic additives, T_{PHRR} values were shifted towards to higher temperatures; however, only by the addition of ATH, T_{PHRR} was reduced to 477.6 C which is slightly lower than T_{PHRR} of reference PP.

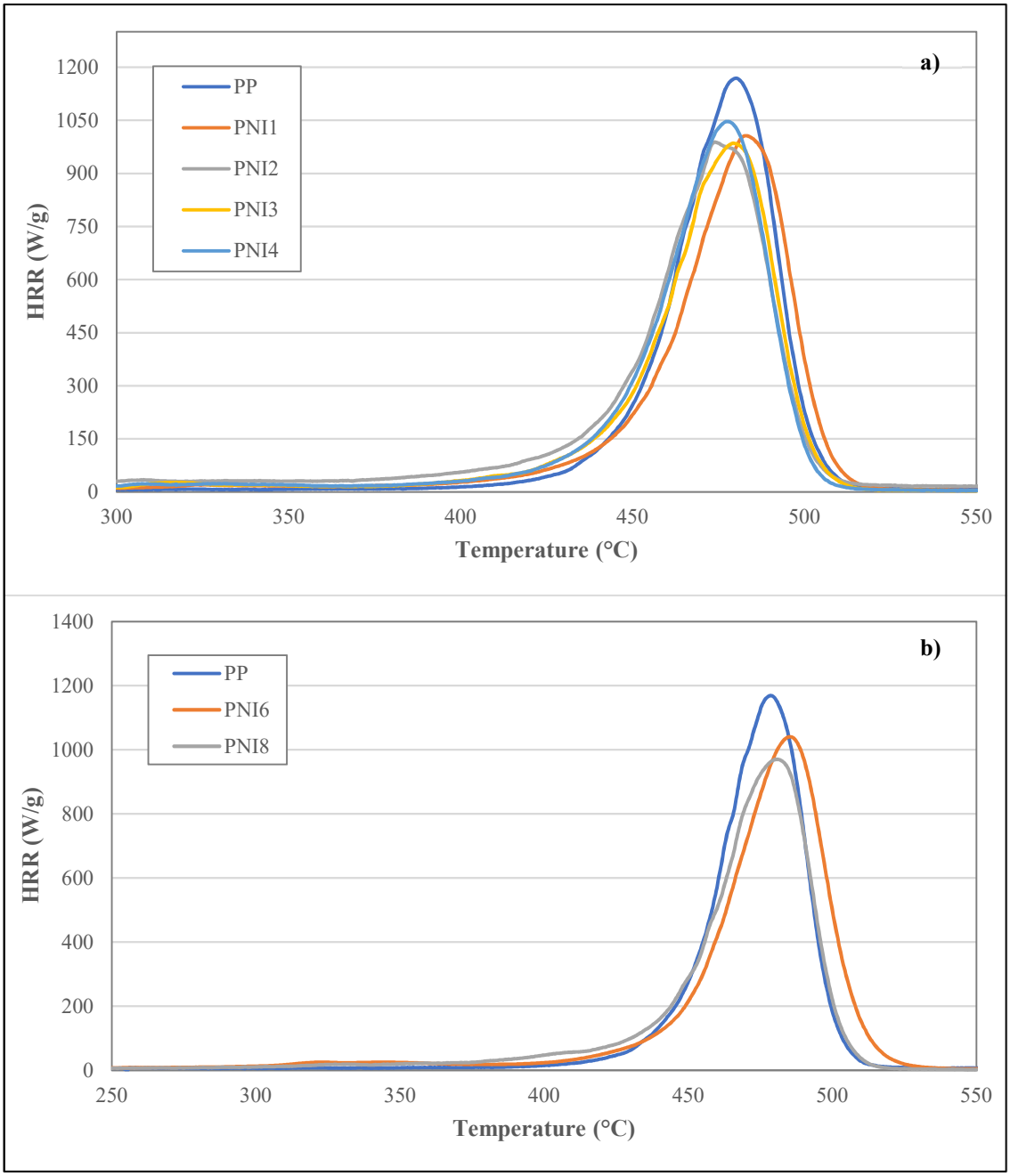

Figure 4.22. *HRR curves of the PP/CPP/HAS composites blended with 0.5 wt% a) ZnB, ATH, nano-SiO_2, and CNT and b) nano-CuO and ZnO*

4.3.5. SEM

SEM images of CPP, HAS and nano-CuO powders are given in Figure 4.23. All these powders were examined as received, without further purification. The images were taken in both 1500x and 5000x magnification. The SEM images clearly showed that every powder had remarkably different morphology. CPP powder particles had irregular shapes

in several micron sizes. HAS powder particles were smaller than those of CPP powder, however, they tended to be highly agglomerated. The particle size of Nano-CuO was less than 50 nm.

The dispersion of the flame retardants (CPP and HAS) in PP composites was investigated with SEM. No additive was observed in the PP sample as expected (Figure 4.24.a). CPP and HAS particles were easily visible in Figure 4.24.b and Figure 4.24.c, respectively. Clearly, the flame retardant additives were distributed well through extrusion, although aggregation of FR additives was still found in the PP matrix when CPP and HAS particles were blended together (Figure 4.24.d).

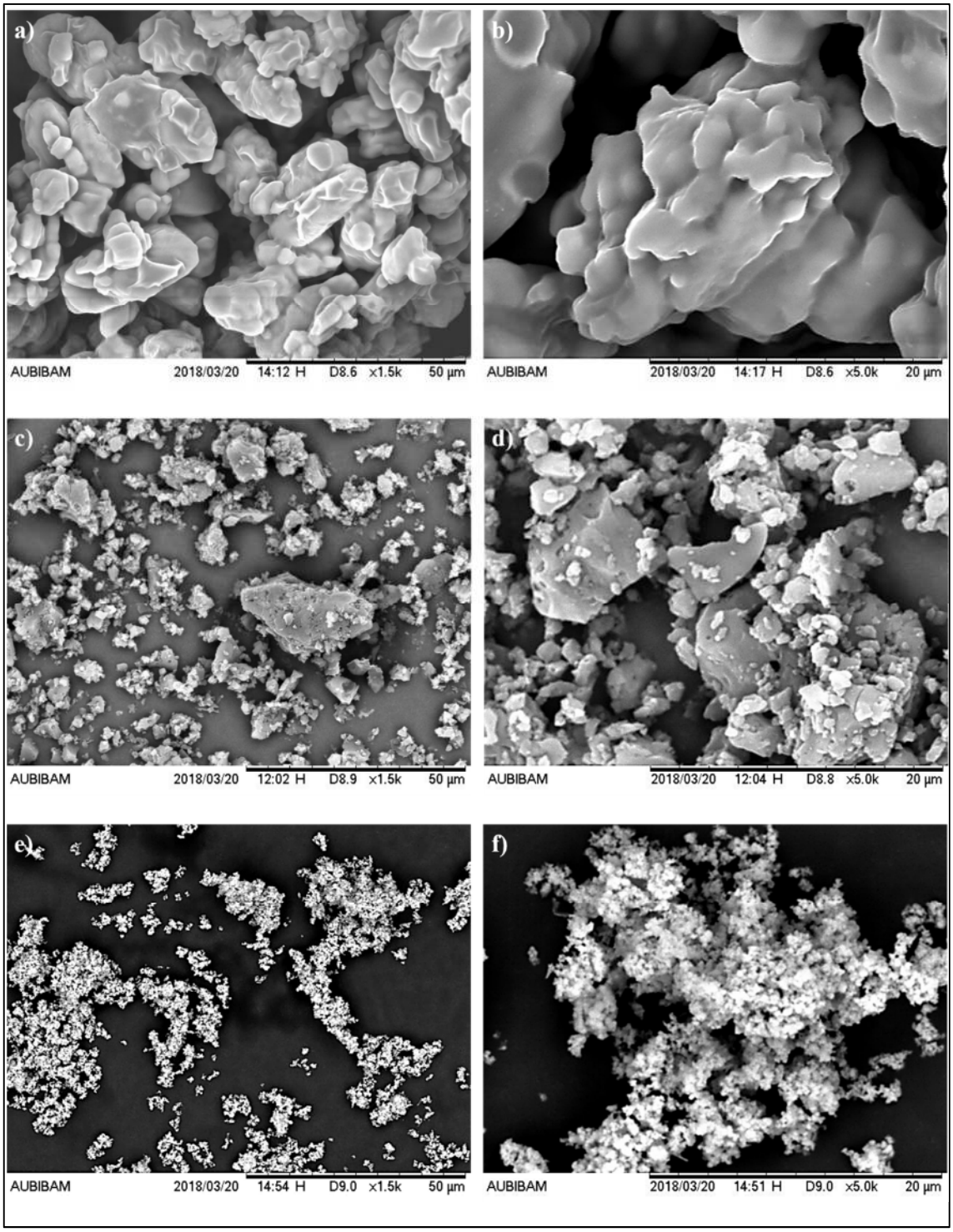

Figure 4.23. *SEM images of materials a) and b) CPP; c) and d) HAS; e) and f) nano-CuO at the magnifications of 1500X and 5000X, respectively.*

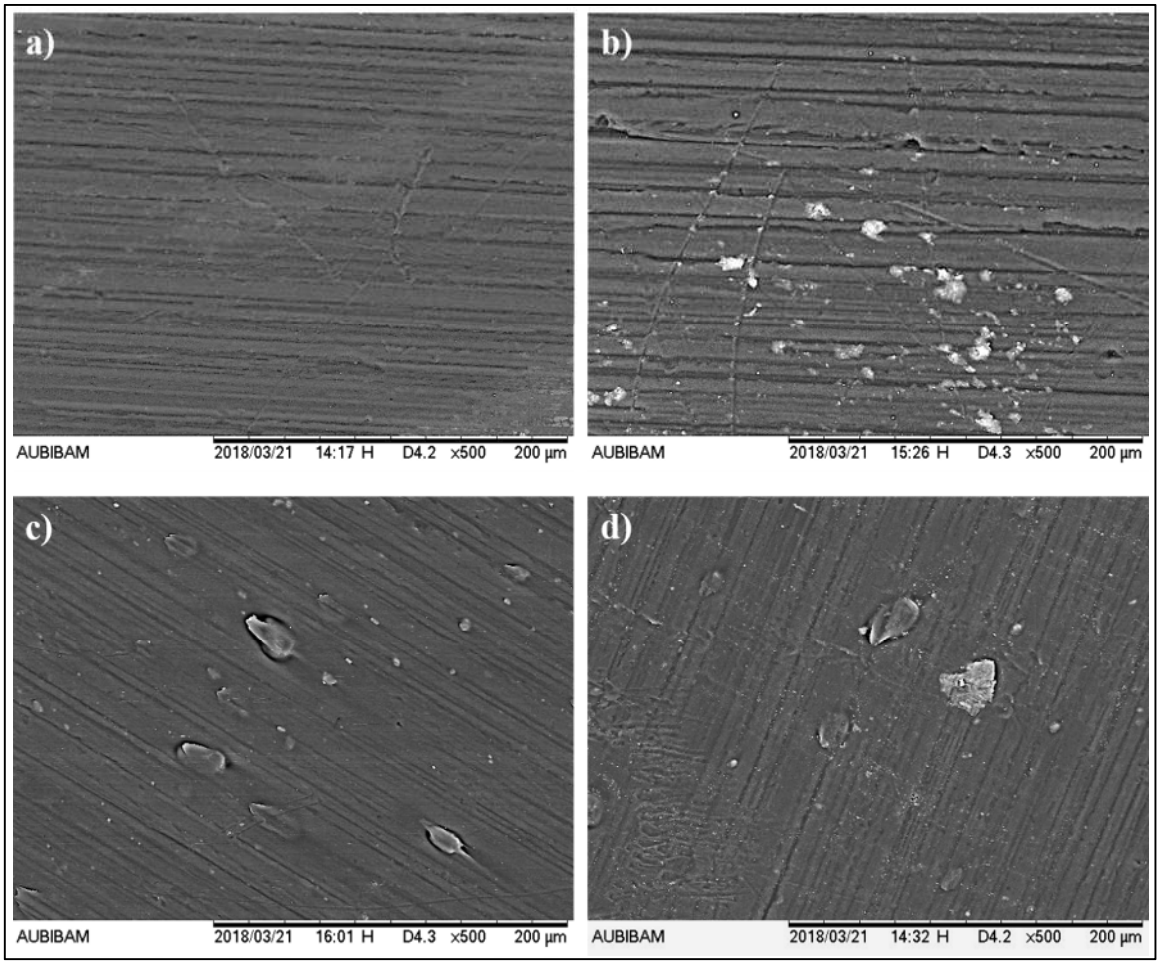

Figure 4.24. *SEM images of a) PP, b) N2, c) P1 and d) PN3 composites at a magnification of 500X*

SEM images of the composite containing 0.5 wt % Nano-CuO (PNI6) were presented in Figure 4.25. Nano-CuO particles were not only distributed homogeneously in the PP/CPP/HAS matrix but also contributed to the distribution of the CPP and HAS particles.

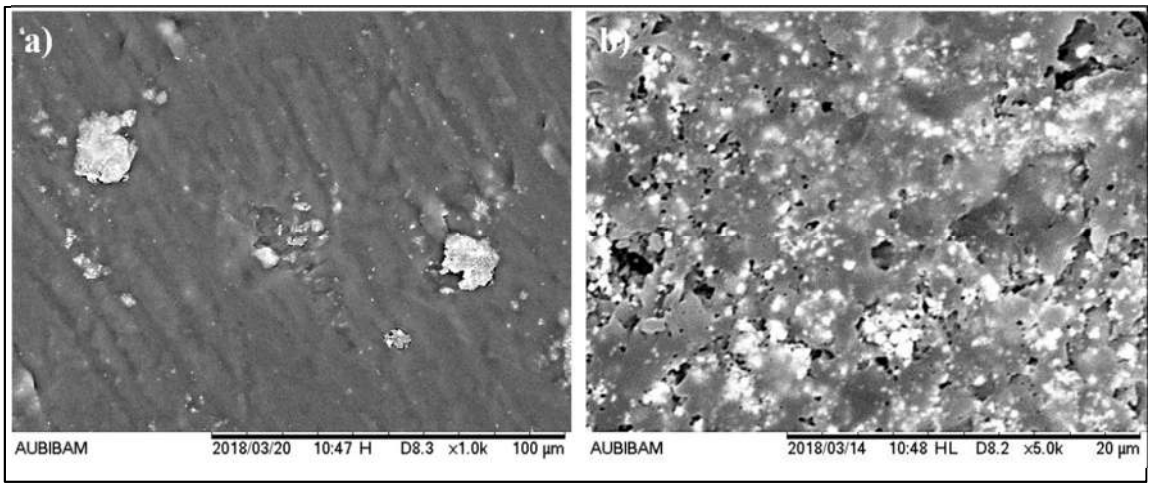

Figure 4.25. *SEM image of PNI6 composite containing 0.5 wt % nano-CuO at the magnifications of a) 1000X and b) 5000X, respectively.*

4.4. Characterization of Flame Retardant and Antibacterial PP Fibers

4.4.1. Optical microscope

Cross-sectional and longitudinal images of the melt spun PP fibers are given in Figure 4.26 and Figure 4.27, respectively. As seen from Figure 4.26, all PP fibers were spun successfully with the circular cross-sectional shape.

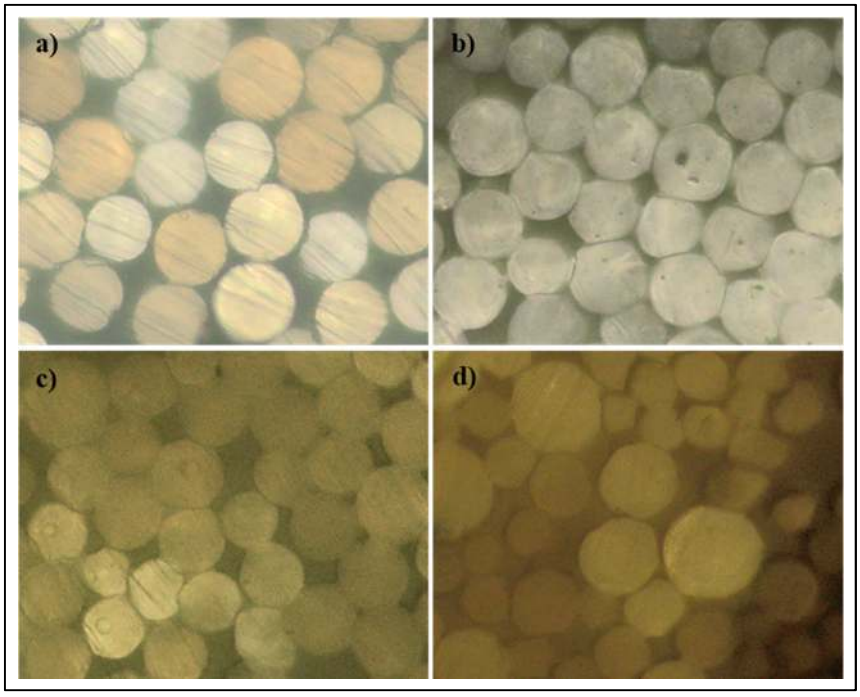

Figure 4.26. *Cross sectional images of the melt-spun multifilament fibres a) neat PP, b) PP/CPP/HAS, c) and d) PP/CPP/HAS blended with 0.25 wt% and 0.5 wt% nano-CuO, respectively (magnification:40X).*

As seen in Figure 4.27, neat PP fiber has smoother surfaces compared to other fibers. Small cavities appeared only on the surface of PN3 fiber. Whereas the surface of PNI5 fiber was roughened, no aggregation of cupric oxide particles were observed in PNI5 fiber. This could be attributed to a highly homogeneous distribution of Nano-CuO particles thanks to their nanometer size. However, the Nano-CuO particles became clearly visible on the surface of PNI6 fiber. The change in the appearance of PNI6 filament may probably be occurred because of the decomposition of HAS due to the processing above 250 °C during extrusion. At this point, it has to be taken into account that some Nano-CuO particles may have likely been agglomerated due to their content which is twice as high as those in PNI5 fiber.

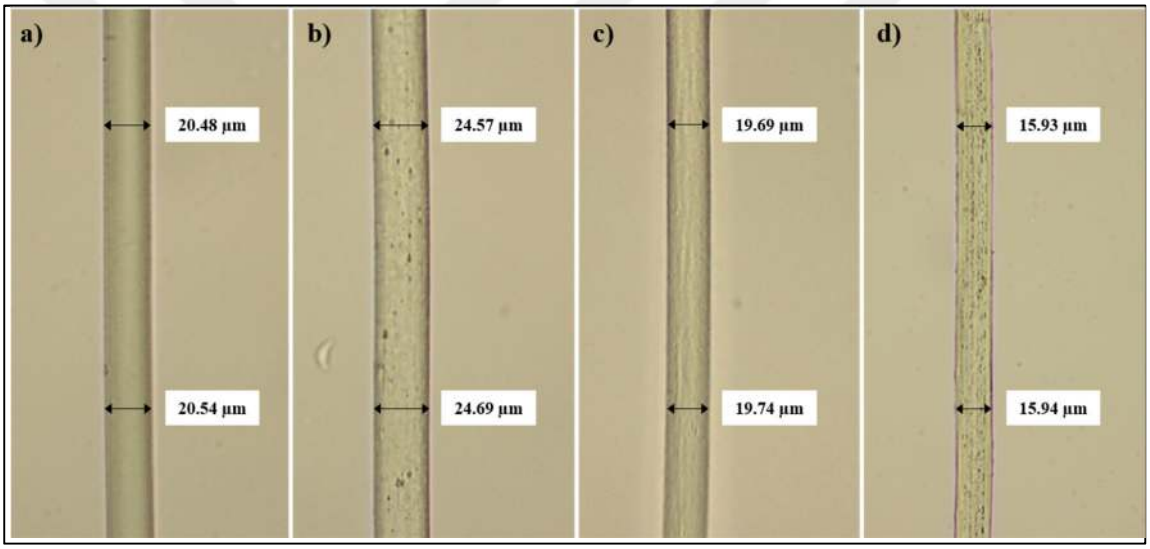

Figure 4.27. *Longitudinal images of the monofilaments of the melt-spun PP fibres a) neat PP, b) PP/CPP/HAS, c) and d) PP/CPP/HAS blended with 0.25 wt% and 0.5 wt% nano-CuO, respectively (magnification:40X).*

The diameter variation of the melt spun multifilament fibers are shown in Figure 4.28. All the results represent an average diameter of at least 30 different filaments with standard deviations for each fiber. As seen in Figure 4.28, PN3 fiber has a larger diameter than other fibers. Of the fibers containing CPP/HAS in the presence/absence of nano-CuO, PNI5 exhibited a smaller standard deviation which indicates that its spinning process is more promising for a better diameter consistency. PNI6 fiber was found to have the smallest diameter. This could be attributed to its higher extrusion temperature and

higher draw ratio which may lead to a decreased diameter than other fibers. It also has a larger standard deviation than other fibers.

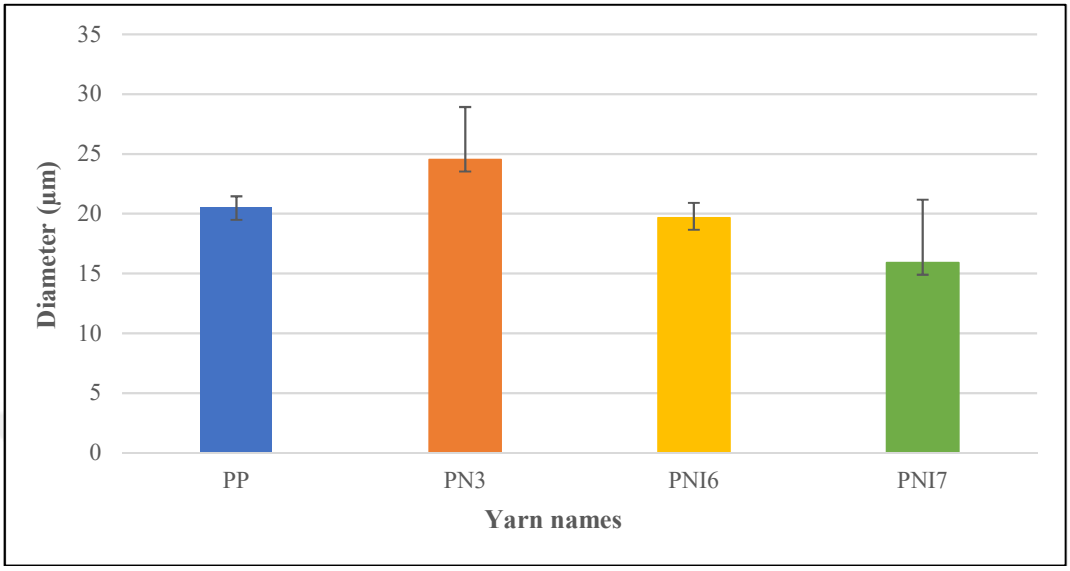

Figure 4.28. *Mean diameters of the monofilaments of the melt-spun PP fibres*

The distribution and homogeneity of FR and antibacterial additives were examined by performing fluorescence microscopy. Three filters in different colors (blue, green and red filters) were used to track the additives on the surface of polypropylene filaments, however; the fluorescence signal was detectable only with the blue filter. Fluorescence micrographs of PP filaments were shown in Figure 4.29. Neat PP filaments were observed with a bright dark blue color. CPP/HAS combination in the polypropylene (PN3) was detected in different color due to the intrinsic fluorescence characteristics of CPP and HAS. By the addition of this combination, the color of the neat PP filament turned into a lighter blue, as well. In the presence of nano-CuO (PNI5 and PNI6), CPP/HAS combination became seemingly invisible, possibly due to being veiled by a highly homogeneous distribution of nano-CuO nanoparticles.

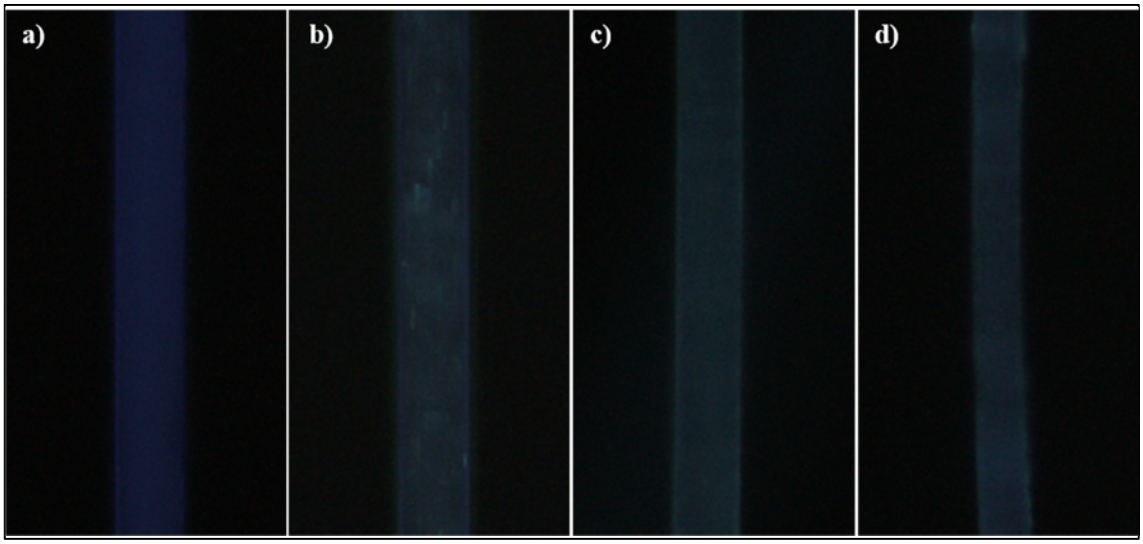

Figure 4.29. *The fluorescence micrographs of the melt-spun PP filaments a) neat PP, b) PP/CPP/HAS, c) and d) PP/CPP/HAS blended with 0.25 wt% and 0.5 wt% Nano-CuO, respectively (magnification:40X).*

4.4.2. SEM

SEM images of the multifilament fibers are presented in Figure 4.30. All images were taken at 1500x magnification. The surfaces of both PP and PN3 fibers were observed to be smooth. SEM images clearly showed that nano-CuO particles were distributed fairly along the fiber. However, the surface of the fibers (PNI5 and PNI6) was roughened in the presence of nano-CuO particles.

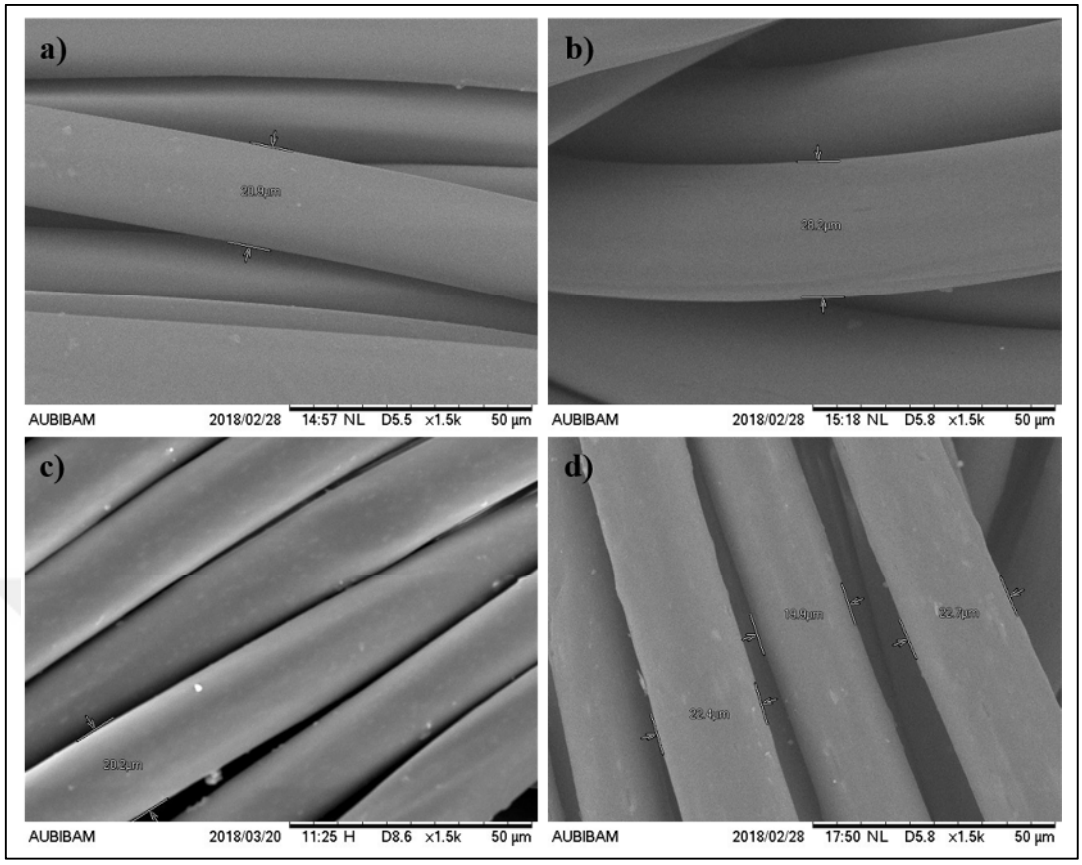

Figure 4.30. *SEM images of the multifilament fibres a) neat PP, b) PP/CPP/HAS, c) and d) PP/CPP/HAS blended with 0.25 wt% and 0.5 wt% Nano-CuO, respectively (magnification:1500X).*

4.4.3. Tensile test

The tenacity is one of the most important properties of a fiber which assess its application areas in textile industry. Tensile test results of the melt spun multifilament PP fibers were tabulated in Table 4.14. Neat PP fiber has a breaking strength of 2,81 N with a breaking extension of 160.63 %. PN3 fiber showed a higher tenacity by 5.70 % compared to neat PP. It also resulted in a higher breaking strength by 1.96 % and a higher breaking extension by 14% than those of neat PP. In the presence of 0.25 % nano-CuO (PNI5 fiber), both the breaking strength and the breaking extension of PN3 fiber were decreased, however, the tenacity was further increased. The reason for this increase in tenacity could be that the addition of nano-CuO particles may prevent the aggregation of CPP/HAS loading in the PP matrix, leading to a more homogenous distribution. The lowest breaking strength, tenacity and breaking extension values were found at PNI6 fiber. In general, the lower the linear density of the fiber was, the higher the tenacity was concluded. Only

PNI6 fiber exhibited the lowest tenacity whereas it has the lowest linear density. The inconsistency between these results may arise from the difference of parameters used in melt spinning process (such as temperature profile and extrusion speed) or failures during the texturing process. As all the fibers have the same number of filaments and cross-sectional shapes, the effects of these parameters on the mechanical properties of the fibers were not studied in the test.

Table 4.14. *Tensile test results of the melt-spun multifilament fibers*

Fiber ID	Breaking load (N)		Tenacity (cN/dtex)		Breaking extension (%)	
	Mean	**St. dev.***	**Mean**	**St. dev.***	**Mean**	**St. dev.***
PP	2.8076	0.2838	1.6515	0.1669	160.6308	23.9985
PN3	2.8626	0.2909	1.7455	0.1774	183.1339	93.4086
PNI5	2.3525	0.1018	2.3063	0.0998	67.6356	5.6578
PNI6	0.5374	0.0911	1.0748	0.1821	21.7713	4.4573

Figure 4.31 shows the stress-strain curves for the melt spun multifilament PP fibers. The load-tensile extension data were utilized to create the stress-strain curves. The stress data was calculated by dividing the corresponding load by the linear density of the fiber. The stress data was obtained by dividing the corresponding tensile extension by the gage length as well. In figure, the extension prior to failure reveals that the most ductile fiber is PN3. PN3 fiber is also the toughest while PNI5 fiber is the stiffest. Both nano-CuO containing fibers (PNI5 and PNI6) are brittler, however, PNI6 is the weakest fiber among all the fibers.

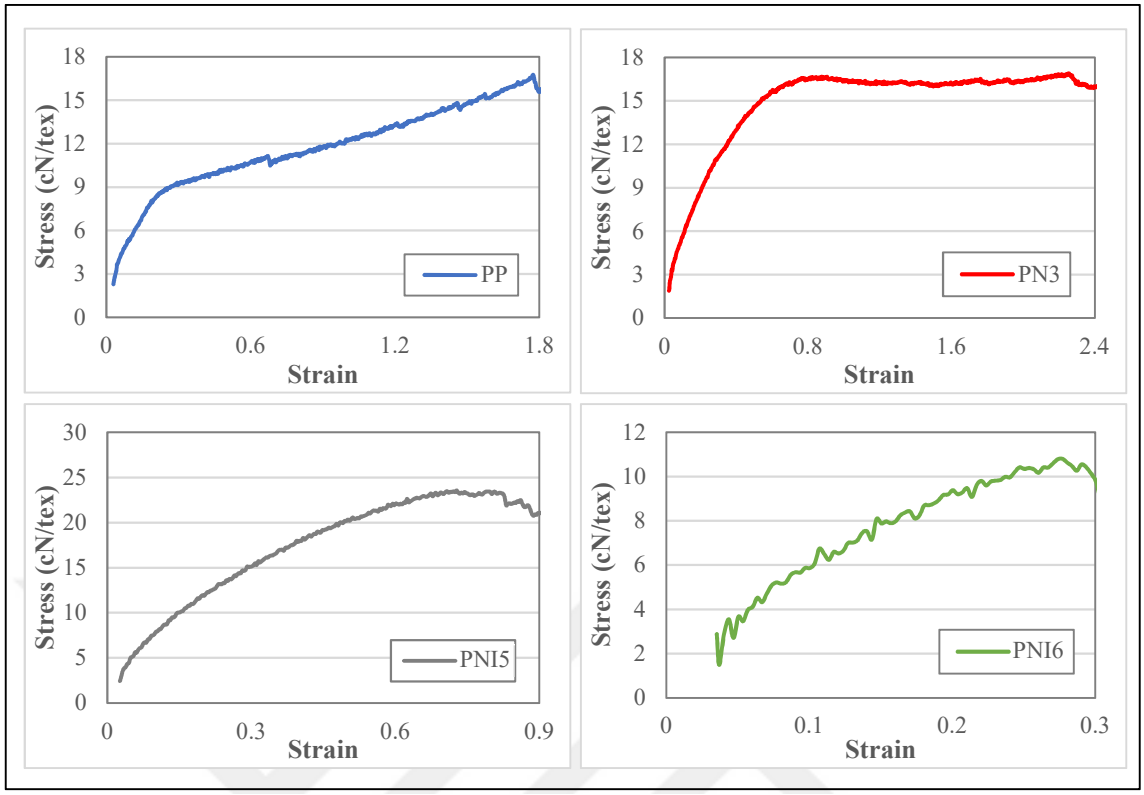

Figure 4.31. *Stress-strain curves of the melt spun multifilament fibres*

4.4.4. Antibacterial test

Antibacterial test was first examined on as-spun monofilament fibers. Antibacterial test results of the as-spun fibers are compiled in Table 4.15.

Table 4.15. *Antibacterial test results of as-spun monofilament fibers*

Fiber ID	Bacterial reduction	Antibacterial result	nano-CuO (%)	ZnO (%)
PP	~%20	No activity	-	
PN3	<2 (log10)	No activity	-	
PNI5	>2 (log10)	Antibacterial activity	0.25	
PNI6	>2 (log10)	Antibacterial activity	0.50	
PNI7	<2 (log10)	No activity		0.25
PNI8	<2 (log10)	No activity		0.50

Neat PP fibers resulted in about 20 % bacterial inactivation which points to no antibacterial activity. Fibers containing 0.25 wt% and 0.5 wt% ZnO revealed a reduction in activity at about 65-70 % (< log2) which indicates weak bactericidal activity. Since the used ZnO was in the bulk form and have a larger surface, these results are in agreement

with the previous studies describing that the antibacterial activity of the ZnO depends on the particle size [91,92].

Fibers blended with only CPP and HAS caused bacterial inactivation of about 90-95 % (< log2) with showing bactericidal activity, however, it is not enough for antibacterial activity. The reduction in activity in the fibers containing only CPP and HAS may stem from the presence of HAS which was not blended with the intention of utilizing as an antibacterial agent. The highest reduction in activity was found in the fibers blended with 0.25 wt% and 0.5 wt% nano-CuO at more than log2 (almost equivalent to 99 % reduction) which attest antibacterial activity. Due to the high specific surface area of nano-CuO arising from their small particle size, more interaction may occur between the nano-CuO particles and E. coli in addition to the more release of Cu^{+2} cations from the nano-CuO particle surface, and hence, an increased biocidal activity [69]. Regarding these results, composites containing CPP/HAS in the presence/absence of nano-CuO was determined for the melt spinning of the final fibers.

Antibacterial test results of PP fibers produced by melt spinning are given Table 4.16. All results agree with the results of as-spun monofilament fibers. Neat PP fibers showed neither bactericidal activity nor antibacterial activity. Containing only CPP and HAS fibers revealed only bactericidal activity again (< log2). According to the test results, only the fibers blended with nano-CuO brought out antibacterial activity with a reduction of more than log2 once again.

Table 4.16. *Antibacterial test results of melt-spun fibers*

Fiber ID	Bacterial reduction	Antibacterial result	nano-CuO (%)
PP	~%20	No activity	-
PN3	<2 (log10)	No activity	-
PNI5	>2 (log10)	Antibacterial activity	0.25
PNI6	>2 (log10)	Antibacterial activity	0.50

4.4.5. Color test

Melt spun fibers were evaluated according to the CIELAB color space. The relationship between a* and b* color values of the multifilament PP fibers is plotted in Figure 4.32.a). The a* value represents red (+a*) and green (-a*) while the b* value represents yellow (+b*) and blue (-b*). The L*values of the multifilament PP fibers is

illustrated in Figure 4.32.b). The L* value is an indicator to determine lightness of the samples and the higher the L* measuring, the lighter the color.

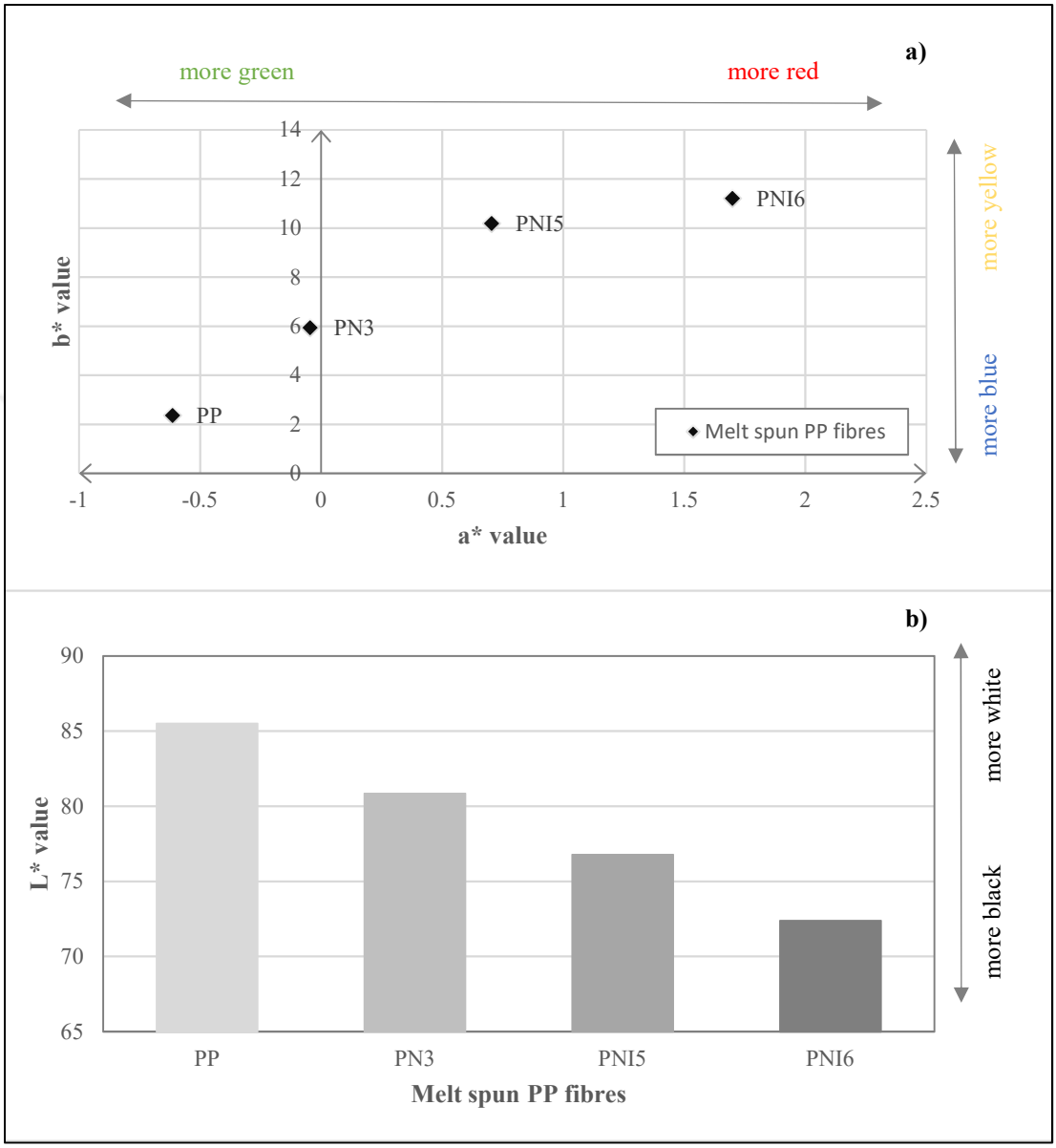

Figure 4.32. *Relationship between a) a* and b* and b) L* color values of the multifilament PP fibres*

The addition of CPP/HAS combination to PP increased both a and b values causing more red and more yellow in color than PP fiber. It decreased the L* values as well which turns out a darker fiber than PP. In the presence of 0.25 wt% nano-CuO, a* and b* values increased again and L* value decreased. When the 0.50 nano-CuO were blended in PP/CPP/HAS, it resulted in a further increase of a* and b* values and a further decrease

of L* value. Due to its dark brown color, the more nano-CuO were introduced, the darker fiber was obtained. Overall, all fibers containing flame retardant additives (CPP/HAS) in the presence/absence of nano-CuO had a more red, a more yellow and a darker color than the neat PP fibers.

Color differences (ΔE*) of melt spun multifilament fibers compared with the neat PP fibers (control sample) are listed in Table 4.17. The color difference between neat PP fiber and fiber containing CPP/HAS combination (PN3) was found to be 5.9 %. The addition of 0.25 wt% nano-CuO and 0.50 wt% nano-CuO resulted in an increase in this difference by 5.9 % and 10.1 %, respectively. Fibers containing flame retardant additives (CPP/HAS) in the presence/absence of nano-CuO were also compared to each other to define individual color differences between them. The color difference between PN3 and PNI5 was almost identical with that found between PP and PN3. From PNI5 to PNI6, the color underwent a change of 4.62 %, causing more darkening in color of PNI6.

Table 4.17. *Color differences (ΔE*) of the multifilament fibers*

ΔE*	**Fiber ID**			
	PP	**PN3**	**PNI5**	**PNI6**
PP	-	5.9	11.797	16.002
PN3	5.9	-	5.93	10.131
PNI6	11.797	5.93	-	4.623
PNI7	16.002	10.131	4.623	-

The color strength (K/S, where K and S indicate absorbance and scattering, respectively) and reflectance (R%) values of multifilament PP fibers are shown in Figure 4.33. The color strength of the neat PP fiber increased by 0.18 with the addition of CPP/HAS combination while its reflectance value decreased by 13.78 %. When 0.25 wt % nano-CuO was present, the color strength value further increased by 0.26 and reflectance value further decreased by 10.5 %. By the incorporation of an increased amount of nano-CuO, the tendency for an increased color strength and a decreased reflectance became more apparent.

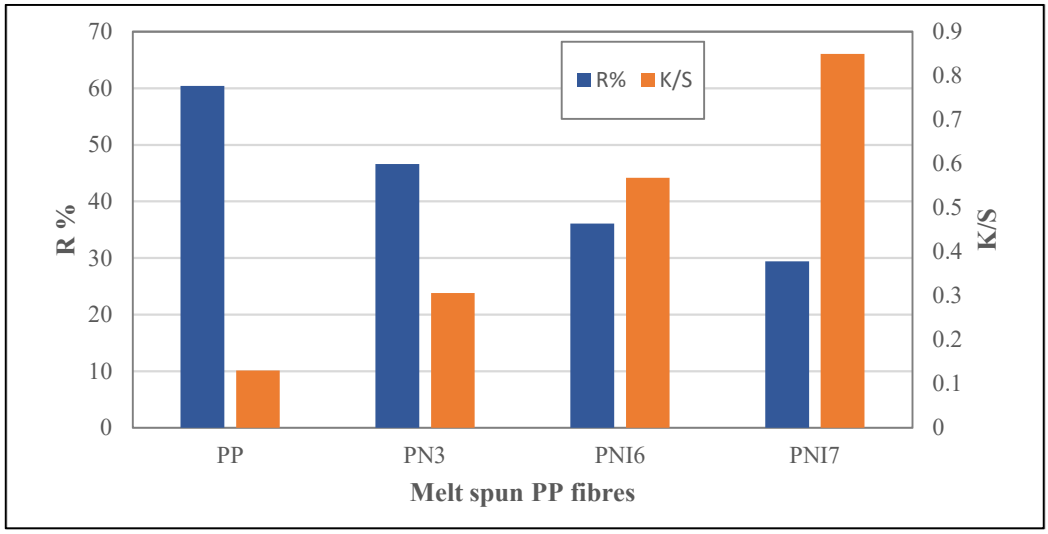

Figure 4.33. *Reflectance (R %) and color strength (K/S) values of multifilament fibres at 400 nm*

4.5. Characterization of Flame Retardant and Antibacterial Fabrics

4.5.1. Cone calorimeter

The cone calorimeter data of the fabrics are listed inTable 4.18. All data were obtained at a heat flux of 35 kW/m^2. Cone calorimeter characterization of fabrics showed that neat PP has a very sharp peak with a PHRR of 333.07 kW/m^2. PN3 fabric exhibited a higher peak of heat release rate by 3.58 % and THR by 33.85 %, however, a lower avMLR by 23.33 %. Both nano-CuO containing fabrics resulted in a decreased PHRR by 19.72 %. The lowest PHRR, avMLR and THR was observed at PNI6 fabric accompanied with the highest FPI. Compared to neat PP fabric, other fabrics were resulted in a decreased CO/CO_2 ratio, releasing relatively less toxic gaseous mixture, however, the most reduction was obtained with PN3 fabric.

Table 4.18. *Cone calorimeter data of the knitted fabrics*

Fabric ID	PP	PN3	PNI5	PNI6
TTI (s)	52	38	37	39
pHRR (kW/m²)	333.07	345.00	267.38	196.98
avMLR (g/s)	0.009	0.007	0.005	0.004
THR (MJ/m²)	6.5	8.7	5.7	4.8
FPI (m²s/kW)	0.156	0.110	0.138	0.198
avCO (kg/kg)	0.043	0.041	0.053	0.046
avCO_2 (kg/kg)	1.59	2.54	2.10	2.16
Initial thickness (mm)	0.34	0.34	0.34	0.34
Initial mass (g)	2.24	1.76	1.16	1.03

The HRR versus the time curves of the samples are depicted in Figure 4.34. All fabrics showed a sharp single peak in HRR which is typical for thermally thin materials. Compared to the samples with a thickness of 3 mm (given in Section 4.3.3), both the ignition time and the total burning time of the fabrics (except for the neat PP fabric) was shortened, which is typical for textiles [65].

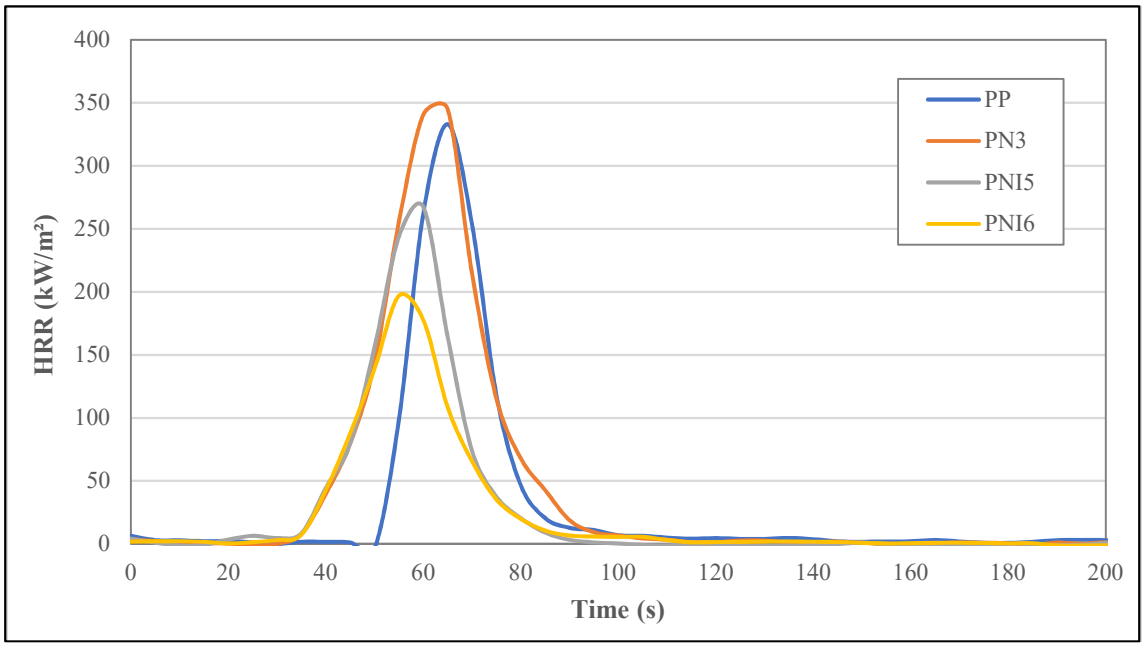

Figure 4.34. *HRR curves of the knitted fabrics*

It must be noted that the results of cone calorimeter are strongly dependent on the sample thickness and geometry. In case of fabrics, the burning behaviour was influenced by the fiber structure in a complex manner as well [48]. Although all the fabrics were prepared by single jersey knitting and had the same thickness, their area densities and air permeabilities were varied due to different linear densities and structures of the FR fibers. Thus, the effect of area density and air permeability must be taken into account for the evaluation of the test results.

4.5.2. Antibacterial test

Antibacterial test of the knitted fabrics resulted in a great match with the results of previous antibacterial tests. As it is clearly seen in Table 4.19., even small amount of loading of nano-CuO (0.25 wt%) revealed antibacterial activity in the PP/CPP/HAS blend.

Table 4.19. *Antibacterial test results of fabrics knitted from melt-spun multifilament fibers*

Fabric ID	Bacterial reduction	Antibacterial result
PP	~%20	No activity
PN3	<2 (log10)	No activity
PNI5	>2 (log10)	Antibacterial activity
PNI6	>2 (log10)	Antibacterial activity

4.5.3. Optical microscope

Optical microscope image of the knitted fabrics is given in Figure 4.35. As it is clearly seen, the flame retardant and antibacterial multifilament fibers were weft-knitted into single jersey structure successfully.

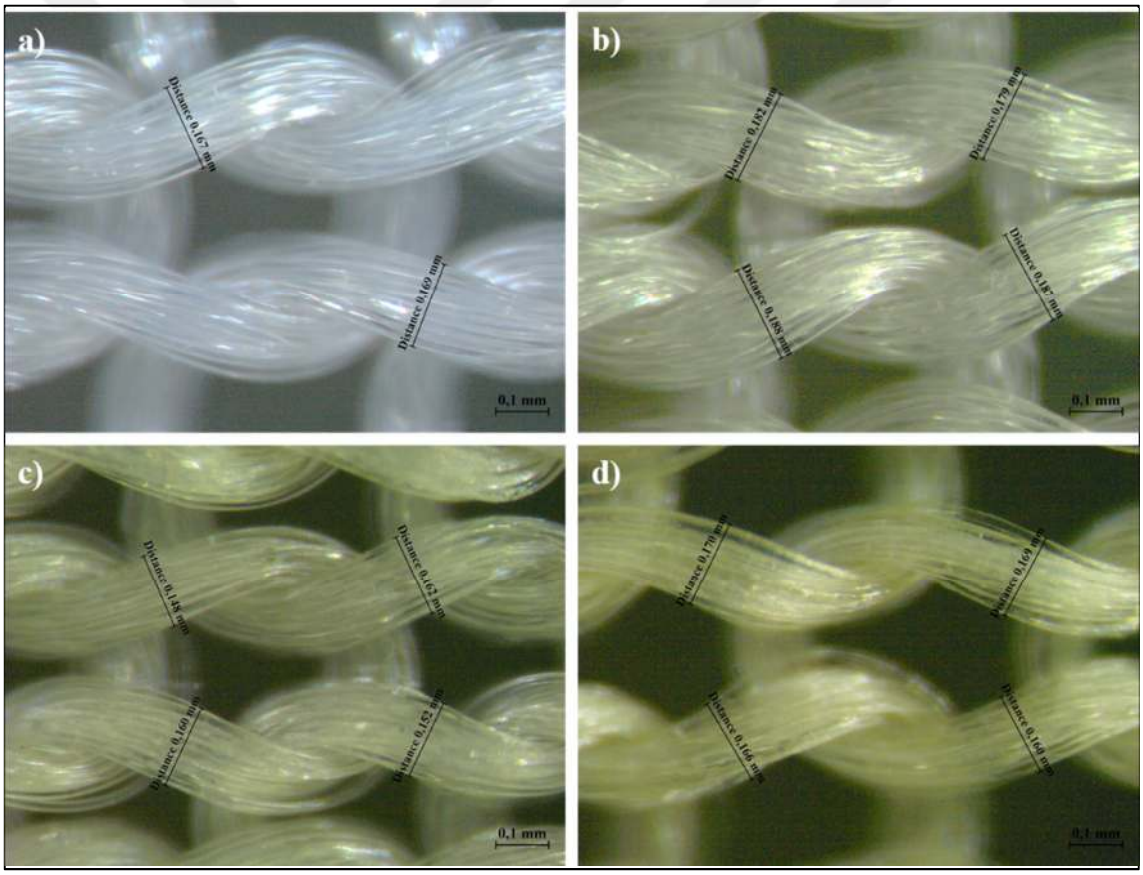

Figure 4.35. *Optical microscope image of the knitted fabrics a) neat PP, b) PP/CPP/HAS, c) and d) PP/CPP/HAS blended with 0.25 wt% and 0.5 wt% Nano-CuO, respectively (magnification:80X).*

5. CONCLUSIONS

Flame retardant polypropylene (PP) fiber is widely used in the textile industry and related fields such as transportation, electric wire and cable, and decorative materials, due to its good processing performance, excellent chemical and thermal resistance in addition to its low cost. However, PP is a highly flammable material that poses severe fire risks in public areas due to their low fire resistance. Due to the harmful nature of halogenated flame retardants on human health and environment, halogen-free flame retardants, especially phosphorus-based flame retardants, are proposed as an alternative to those. To achieve a reasonable flame retardancy in polypropylene, however, high levels of loading of flame retardant additives are generally needed which limits the spinnability of it with the risk of clogging the spinnerets. The upper limit for such flame-retardant loading for textile fibers is presumed to be 10 wt% in the literature [9].

This study focused on producing flame retardant and antibacterial polypropylene (PP) fibers containing PBFRs. With the reason given above, reducing the total amount of flame retardants were also aimed by investigating the synergistic effect between PBFRs and inorganic FR additives (Aluminum trihydroxide (ATH), zinc borate (ZnB), nano-silica (nano-SiO_2), and carbon nanotube (CNT)) on the flammability of PP. Ammonium polyphosphate-based (APP) and cyclic phosphonate-based (CPP) flame retardant additives were used as PBFRs. In addition to the antibacterial additives (Cupric oxide (nano-CuO) and zinc oxide (ZnO)), a coupling agent (MPA) and a hindered amine light stabilizer (HAS) were also used in the FR formulations. Moreover, ZnO and nano-CuO were utilized to impart antibacterial functionality to the fibers.

To increase the flame retardant effect of inorganic FR additives by dispersing them more homogeneously in the polymer matrix, in the first part of the study, the particle size of ZnB and ATH were reduced by wet-milling. Particle size measurements and XRD results showed that the particle size of those additives reduced from microscale to submicron scale successfully. Since silica and carbon nanotube are already nanoscale, were used directly without further processing.

Firstly, the effect of ammonium polyphosphate-based (APP) FR on the flammability of polypropylene is determined. LOI analysis showed that the LOI value of reference PP (19 %) increased to 21.5 % and 22.6 % by the addition of 5 wt% and 10 wt% APP, respectively. In the presence of APP, thermal decomposition temperatures of

pure PP was shifted to higher temperatures and more residue was observed according to TGA analysis. Cone calorimeters showed that the addition of 5 wt% APP reduced the maximum HRR by 36.91 % with a broadened the HRR curve. The more APP was present, the more reduction occurred in PHRR, THR, and avMLR whilst the burning time was prolonged significantly. The addition of APP resulted in an earlier ignition in pure PP that may be due to the formation of a char layer that causes a rapid increase in the surface temperature of the samples. The more APP was present, the more increase in char yield and the more decrease in THR/TML values were concluded. This result corresponded with the flame-retardant mechanism of APP mainly in the condensed phase. Cone calorimeter tests also showed that APP could inhibit the flashover of PP but dependently of its content. Unlike CPP, APP showed intumescence with an intumescent char formation. By the addition of an increased amount of APP, the intumescent layer became more pronounced.

The effects of inorganic FR additives (ZnB, ATH, nano-SiO_2 and CNT) on the flammability of polypropylene/APP composites were studied afterwards. Here total content of FR was kept at 10 wt% and 2 wt% of APP was replaced with inorganic FR additives. The addition of inorganic FR additives decreased the LOI values of PP/APP composite for all compositions. The most reduction in LOI was found for the composite blended CNT by 1.4 %. Nonetheless, they still yielded LOI values that above to that of neat PP. The addition of inorganic FR additives improved the flame retardancy of PP/APP composites by increasing the char formation, indicating their effects on the burning mechanism of PP/APP composition in the condensed phase. They also resulted in a delayed decomposition of those to high temperatures. CNT containing composite showed the highest thermal decomposition temperatures while the highest residue was formed in the presence of nano-SiO_2.

To disperse nanosized inorganic FR additives (especially multi-walled carbon nanotubes) into polymer matrix homogeneously, they were incorporated in the presence of a coupling agent (MPA) to have more homogeneous dispersion that could improve their effects. However, in the presence of MPA, LOI values of the composites were further decreased indicating an antagonistic effect. Only the composite containing CNT showed a synergetic effect with MPA and increased the LOI from 20.9 % to 21.2 % that could be attributed to a highly homogeneous distribution of CNT. In the light of this

result, CNT can be processed with some commercially available coupling agents for seeking of the synergy. Except for the composite containing APP alone, the decrease in residue formation of APP and nano-SiO_2 showed that the addition of MPA reduced the char forming ability of those additives and thus declines their condensed phase activity. On the other hand, a reverse effect was observed for the compositions containing either ZnB and ATH; more char was formed indicating an enhanced condensed phase activity of those. In the case of the CNT, no clear effect was observed on the char formation by the addition of MPA. The highest char formation occurred with ATH.

Binary combinations of inorganic FR additives (ZnB/ATH, ZnB/nano-SiO_2, ZnB/CNT) were blended into PP/APP matrix in the presence of MPA to determine the synergistic effect between them. ZnB/CNT combination improved the LOI value to 21.4 % which is higher than the LOI values they blended individually. The lowest LOI (21.0 %) was obtained with the ZnB/nano-SiO_2 combination. The combination of ZnB and ATH resulted in a char residue of 7.223 % higher than those of they introduced to PP/APP/MPA alone indicating that their combination enhanced condensed phase activity of those. In case of the combination of ZnB and nano-SiO_2, char formation was less than that of containing ZnB. This result correlates with the declined char formation of nano-SiO_2 in the presence of MPA that resulted in a decrease in the char formation of ZnB/nano-SiO_2 combination.

In the view of the results of flame retardancy tests, APP containing compositions in the presence/absence of inorganic FR additives and MPA were determined not to be suitable for fiber spinning and, thus, the following experiments were conducted with CPP.

First, the effect of CPP on the flammability of pure PP was investigated. Compared to the APP, the addition of CPP resulted in a more increase in LOI values at the same loadings. The addition of 5 wt% CPP increased the LOI value of pure PP to 22, however, this value was 21.5 in the presence of APP. The more CPP were blended in PP, the higher LOI values were obtained. TGA analysis showed that CPP decomposed at lower temperatures compared to those of pure PP and its decomposition products effected the thermal degradation reaction of PP in the gas phase. The addition of only 3.5 wt% CPP, resulted in a great decrease in PHRR and THR in addition to prolonged ignition. In addition to the formation of no char, decreased the THR/TML value in the presence of CPP revealed its gas phase mechanism. FPI value was increased showing less tendency to flashover.

The effect of HAS on the flammability of pure PP was also examined before examining its effect together with the CPP. HAS was found to be very effective to increase the LOI of pure PP when only small amounts of that were present in the PP matrix (up to 1.5 %). Similar to CPP, HAS decomposed at lower temperatures than pure PP and acted in the gas phase by quenching the free radicals. HAS containing PP composite also ignited later and decomposed with a reduced PHRR and THR values without leaving char. Again, the reduced THR/TML value in presence of HAS pointed out the gas phase mechanism of it. Although HAS was less than CPP in the PP matrix, it resulted in a more decrease in HRC and PHRR values according to the MCC results. FPI value again increased with promising an enhanced fire safety of the PP.

After considering the results from CPP and HAS that given above, the effect of their combinations on the flammability of pure PP was examined. A synergetic effect was found between HAS and CPP when their content was varied in proportion to each other (the total amount of FR at 5 wt%); however, the most significant synergistic effect was achieved by a combination of 3.5 wt% CPP and 1.5 wt% HAS with an LOI of 26.6 %. From this point on, the LOI values started to decrease when the content of HAS was increased (while CPP was decreased) in FR composition. The higher amount of HAS was present in FR composition the more reduction of LOI was concluded. This result is in agreement with the inverse concentration-effect reported before [93]. Up to 1.5 wt% loading, the nitroxyl radicals generated during the heating of HAS was able to quench the other free radicals (the aminyl and alkoxy radicals) improving the flame retardancy of PP/CPP/combinations. However, at higher loadings, the aminyl and alkoxy radicals could promote the chain scission reaction of PP which leads to the reduction of the respective LOI values [94]. During the combustion, HAS enhanced the gas phase mechanism of CPP by quenching the active free-radicals. According to the MCC results, both HRC, PHRR and THR values of CPP/HAS composition decreased below to that values of those when they introduced individually into the PP matrix.

CPP/HAS combination showed an antagonistic effect with ZnB that LOI was decreased from 26.6 % to 25 %. The addition of ZnB into PP/CPP/HAS promoted the formation of a glassy protective layer that acts as a physical barrier, reduced TTI, pHRR and delayed the decomposition of the PP/CPP/HAS combination to higher temperatures. The increase in char formation and THR/TML values indicate that an effective condensed

phase mechanism becomes predominant in the presence of ZnB, however, both condensed phase and gas phase mechanisms concurred together at the PP/CPP/HAS/ZnB composites. On the other hand, the FPI value reduced when ZnB was present that the tendency of PP/CPP/HAS composites to flashover is increased.

The introduction of ATH into PP/CPP/HAS composite reduced the LOI value to 26.1 %. According to cone calorimeter studies, the addition of IFR reduced the ignition time and pHRR. In the presence of ATH, char formation and THR/TML value increased indicating that the FR activity of ATH is in the condensed phase. The addition of ATH may lead to the formation of an insulation layer against oxygen in which the decomposition product A_2O_3 involves [95]. The FPI value remained almost intact. The addition of ATH did not change the tendency of PP/CPP/HAS composites to flashover.

When nano-SiO_2 was present, The LOI value of PP/CPP/HAS composite reduced to 25.8 %. The addition of nano-SiO_2 did not alter the TTI value PP/CPP/HAS composite. Of all the inorganic additives, the only increase in PHRR observed in the presence of nano-SiO_2 accompanied the highest THR value. However, the addition of nano-SiO_2 does not change the tendency of PP/CPP/HAS composites to flashover since FPI value remained almost the same. The increase in char formation and THR/TML values indicates consensed phase activity of nano-SiO_2 which was accompanied by the gas phase activity of CPP/HAS combinations in PP/CPP/HAS/nano-SiO_2 composites.

The addition of CNT reduced the LOI value of PP/CPP/HAS composite slightly. In the presence of CNT, the time to ignition (TTI) value were shortened because of the catalytic effect of CNT. Absorption of a large amount of radiation by CNT leads to a rapid increase in temperature around it. CNT acted at the condensed phase within the PP/CPP/HAS matrix, reducing the HRR and increasing the char formation and THR/TML value. CNT inclusion also delayed the decomposition of the PP/CPP/HAS combination. The reduction in PHRR is due to CNT-network layer emitting radiation from the composite surface which acts as an effective gas barrier [96]. Since CPP/HAS combinations act in the gas phase, both the condensed phase and gas phase mechanisms occurred together at the PP/CPP/HAS/CNT composites. On the other hand, the FPI value remained almost intact. The addition of CNT did not change the tendency of PP/CPP/HAS composites to flashover.

Although nano-CuO was utilized as an antibacterial additive, the addition of

0.25 wt% nano-CuO into PP/CPP/HAS matrix showed a truly synergistic effect resulting in a further increase in LOI to 27 %. Moreover, concerning other compositions, the highest reduction in both PHRR and THR that is accompanied by a prolonged ignition time was observed for that composition in the cone calorimeter test. THR/TML values were further decreased and no change was observed through char formation that the gas phase mechanism of CPP/HAS further enhanced. However, when the nano-CuO content was increased to 0.5 wt%, the PHRR value was increased greatly and TTI was shortened. This may be due to the inverse concentration effect.

The LOI value of the composite containing CPP/HAS composition again decreased by the addition of ZnO. According to the MCC results, HRC and PHRR values decreased for all inorganic additives, however, the highest reduction of those occurred in the presence of ZnO.

The antibacterial activity of compositions containing either nano-CuO or ZnO was first studied on as-spun monofilament PP fibers before the melt spinning process. It is found that ZnO containing fibers resulted in a bacterial reduction; however, it is not enough to postulate antibacterial activity. Since the ZnO was in the bulk form and have a larger surface area in our study, these results are in agreement with the previous studies describing that the antibacterial activity of the ZnO depends on the particle size [91,92]. In the case of nano-CuO containing melt-spun fibers, they showed a strong antibacterial even at small loadings (0.25 wt%) with an antibacterial reduction of >log 2. Due to the high specific surface area of nano-CuO arising from their small particle size, more interaction may occur between the nano-CuO particles and E. coli. In addition to this, the more release of Cu^{+2} cations from the nano-CuO particles may increase the biocidal activity [69,97].

In the light of the results of flame retardancy and antibacterial activity tests explained above, nano-CuO containing CPP/HAS formulation was determined for the melt spinning of the fibers and those compositions were melt-spun into multifilament PP fibers successfully. Antibacterial activity of the produced fibers was again tested and nano-CuO containing fibers showed a strong antibacterial activity in agreement with those of as-spun fibers.

Lastly, the flame retardant and antibacterial fabrics were produced by weft knitting of the melt-spun fibers to assess their flame retardancy and antibacterial activity. Cone

calorimeter results showed that nano-CuO containing fabrics reduced the PHRR and THR of the pure PP fabrics. However, both the ignition time and the total burning time of the fabrics shortened which is typical for thin textile fabrics. Since in this work, the main objective was to check the spinnability of the FR compositions for melt spinning, linear densities of the fibers are not primarily controlled. Thus, the differences in the area density and air permeability of the fabric arisen from linear densities of the fibers must be taken into account while determining the flame retardancy of those fabrics. Antibacterial activity of the fabrics was in agreement with the nano-CuO containing fibers.

In conclusion, it was found that at the loading of up to 5.5 wt%, formulations that containing CPP/HAS in the presence/absence of nano-CuO are spinnable with a continuous fiber spinning preserving the desired the fiber properties. Flame retardant and antibacterial fibers were produced successfully. For further studies, the release of nano-CuO from the produced fibers into human and water should be considered due to its nano size. The particle size of the phosphorus-based flame retardant can be reduced prior to use to improve their dispersibility in the PP matrix for fiber spinning. In addition to the other flammability tests, FTIR analysis of the char formed during burning can be utilized to identify the activity mechanism of flame retardant materials on polypropylene.

REFERENCES

[1] Du, B., Guo, Z., & Fang, Z. (2009). Effects of organo-clay and sodium dodecyl sulfonate intercalated layered double hydroxide on thermal and flame behaviour of intumescent flame retarded polypropylene. *Polymer Degradation and Stability,* 94(11), 1979-1985.

[2] Zhang, S., & Horrocks, A. R. (2003). A review of flame retardant polypropylene fibres. *Progress in Polymer Science,* 28(11), 1517-1538.

[3] Chen, X., Yu, J., & Guo, S. (2006). Structure and properties of polypropylene composites filled with magnesium hydroxide. *Journal of Applied Polymer Science,* 102(5), 4943-4951.

[4] Shehata, A. (2004). A new cobalt chelate as flame retardant for polypropylene filled with magnesium hydroxide. *Polymer Degradation and Stability,* 85(1), 577-582.

[5] Nelson, G. (1994). The future of fire retarded materials: applications and regulations. *FRCA fall*, 9-12.

[6] Alaee, M., Arias, P., Sjödin, A., & Bergman, Å. (2003). An overview of commercially used brominated flame retardants, their applications, their use patterns in different countries/regions and possible modes of release. *Environment international,* 29(6), 683-689.

[7] Ma, J., Addink, R., Yun, S., Cheng, J., Wang, W., & Kannan, K. (2009). Polybrominated dibenzo-p-dioxins/dibenzofurans and polybrominated diphenyl ethers in soil, vegetation, workshop-floor dust, and electronic shredder residue from an electronic waste recycling facility and in soils from a chemical industrial complex in eastern China. *Environmental science & technology,* 43(19), 7350-7356.

[8] Davis, J., & Huggard, M. (1996). The technology of halogen-free flame retardant phosphorus additives for polymeric systems. *Journal of Vinyl and Additive Technology,* 2(1), 69-75.

[9] Horrocks, A. R. (2011). Flame retardant challenges for textiles and fibres: new chemistry versus innovatory solutions. *Polymer Degradation and Stability,* 96(3), 377-392.

[10] Doğan, M., Yılmaz, A., & Bayramlı, E. (2010). Synergistic effect of boron containing substances on flame retardancy and thermal stability of intumescent

polypropylene composites. *Polymer Degradation and Stability,* 95(12), 2584-2588.

[11] Doğan, M., & Bayramlı, E. (2011). Synergistic effect of boron containing substances on flame retardancy and thermal stability of clay containing intumescent polypropylene nanoclay composites. *Polymers for advanced technologies,* 22(12), 1628-1632.

[12] Lewin, M., & Endo, M. (2003). Catalysis of intumescent flame retardancy of polypropylene by metallic compounds. *Polymers for advanced technologies,* 14(1), 3-11.

[13] Elbasuney, S. (2017). Novel multi-component flame retardant system based on nanoscopic aluminium-trihydroxide (ATH). *Powder Technology,* 305, 538-545.

[14] Qin, Z., Li, D., Li, Q., & Yang, R. (2016). Effect of nano-aluminum hydroxide on mechanical properties, flame retardancy and combustion behavior of intumescent flame retarded polypropylene. *Materials & Design,* 89, 988-995.

[15] Tang, W., Gu, X., Jiang, Y., Zhao, J., Ma, W., Jiang, P., & Zhang, S. (2015). Flammability and thermal behaviors of polypropylene composite containing modified kaolinite. *Journal of Applied Polymer Science,* 132(14).

[16] Gao, S., Li, B., Bai, P., & Zhang, S. (2011). Effect of polysiloxane and silane-modified SiO_2 on a novel intumescent flame retardant polypropylene system. *Polymers for advanced technologies,* 22(12), 2609-2616.

[17] Li, J., Wei, P., Li, L., Qian, Y., Wang, C., & Huang, N. H. (2011). Synergistic effect of mesoporous silica SBA-15 on intumescent flame-retardant polypropylene. *Fire and Materials,* 35(2), 83-91.

[18] Wei, P., Hao, J., Du, J., Han, Z., & Wang, J. (2003). An investigation on synergism of an intumescent flame retardant based on silica and alumina. *Journal of fire sciences,* 21(1), 17-28.

[19] Zhang, Z. X., Zhang, J., Lu, B.-X., Xin, Z. X., Kang, C. K., & Kim, J. K. (2012). Effect of flame retardants on mechanical properties, flammability and foamability of PP/wood–fiber composites. *Composites Part B: Engineering,* 43(2), 150-158.

[20] Huang, G., Wang, S., Song, P. a., Wu, C., Chen, S., & Wang, X. (2014). Combination effect of carbon nanotubes with graphene on intumescent flame-retardant polypropylene nanocomposites. *Composites Part A: Applied Science and Manufacturing,* 59, 18-25.

[21] Shahvazian, M., & Seyedmir, M. R. (2012). Effects of MWNTs on Flame Retardation and Thermal Stabilization Performance of Phosphorus-containing Flame Retardants in Polypropylene. *Orient. J. Chem.,* 28, 1631-1637.

[22] Zhang, Q., Zhan, J., Zhou, K., Lu, H., Zeng, W., Stec, A. A., Hull, T. R., Hu, Y., & Gui, Z. (2015). The influence of carbon nanotubes on the combustion toxicity of PP/intumescent flame retardant composites. *Polymer Degradation and Stability,* 115, 38-44.

[23] Wu, N., & Yang, R. (2011). Effects of metal oxides on intumescent flame-retardant polypropylene. *Polymers for advanced technologies,* 22(5), 495-501.

[24] Yi, J., Yin, H., & Cai, X. (2013). Effects of common synergistic agents on intumescent flame retardant polypropylene with a novel charring agent. *Journal of thermal analysis and calorimetry,* 111(1), 725-734.

[25] Laoutid, F., Bonnaud, L., Alexandre, M., Lopez-Cuesta, J.-M., & Dubois, P. (2009). New prospects in flame retardant polymer materials: from fundamentals to nanocomposites. *Materials Science and Engineering: R: Reports,* 63(3), 100-125.

[26] Kissel, W., Han, J. H., & Meyer, J. (2003). Polypropylene: Structure, Properties, Manufacturing Processes, and Applications. *Handbook of Polypropylene and Polypropylene Composites. New York, NY: Marcel Dekker, Inc, 2003.*, 11-34.

[27] Tripathi, D. (2002). *Practical guide to polypropylene*: iSmithers Rapra Publishing.

[28] Bajaj, P. (1992). Fire-retardant materials. *Bulletin of Materials Science,* 15(1), 67-76.

[29] Horrocks, A. R., & Anand, S. C. (2000). *Handbook of technical textiles*: Elsevier.

[30] Calamari Jr, T. A., & Harper Jr, R. J. (2000). Flame retardants for textiles. *Kirk-Othmer Encyclopedia of Chemical Technology*, 1-23.

[31] Grand, A. F., & Wilkie, C. A. (2000). *Fire retardancy of polymeric materials*: CRC Press.

[32] Birnbaum, L. S., Staskal, D. F., & Diliberto, J. J. (2003). Health effects of polybrominated dibenzo-p-dioxins (PBDDs) and dibenzofurans (PBDFs). *Environment international,* 29(6), 855-860.

[33] Meeker, J. D., & Stapleton, H. M. (2009). House dust concentrations of organophosphate flame retardants in relation to hormone levels and semen quality parameters. *Environmental health perspectives,* 118(3), 318-323.

[34] Turyk, M. E., Persky, V. W., Imm, P., Knobeloch, L., Chatterton Jr, R., & Anderson, H. A. (2008). Hormone disruption by PBDEs in adult male sport fish consumers. *Environmental health perspectives,* 116(12), 1635.

[35] Roze, E., Meijer, L., Bakker, A., Van Braeckel, K. N., Sauer, P. J., & Bos, A. F. (2009). Prenatal exposure to organohalogens, including brominated flame retardants, influences motor, cognitive, and behavioral performance at school age. *Environmental health perspectives,* 117(12), 1953.

[36] Herbstman, J. B., Sjödin, A., Apelberg, B. J., Witter, F. R., Halden, R. U., Patterson Jr, D. G., Panny, S. R., Needham, L. L., & Goldman, L. R. (2008). Birth delivery mode modifies the associations between prenatal polychlorinated biphenyl (PCB) and polybrominated diphenyl ether (PBDE) and neonatal thyroid hormone levels. *Environmental health perspectives,* 116(10), 1376-1382.

[37] Main, K. M., Kiviranta, H., Virtanen, H. E., Sundqvist, E., Tuomisto, J. T., Tuomisto, J., Vartiainen, T., Skakkebæk, N. E., & Toppari, J. (2007). Flame retardants in placenta and breast milk and cryptorchidism in newborn boys. *Environmental health perspectives,* 115(10), 1519-1526.

[38] Directive 2006/1907/EC on Registration, Evaluation and Authorization of Chemicals, 396 C.F.R. (2006).

[39] Substances restricted under REACH. Retrieved 17.11.2018, from https://echa.europa.eu/substances-restricted-under-reach

[40] Directive 2002/96/EC on Waste of Electric and Electronic Equipment, 37 C.F.R. (2003).

[41] Directive 2002/95/EC on Restriction of certain hazardous Substances in Electric and Electronic Equipment., 37 C.F.R. (2003).

[42] The Phosphorus, Inorganic and Nitrogen Flame Retardants Association (pinfa). Retrieved 17.11.2018, from https://www.pinfa.eu/

[43] Beard, A., & Leonards, P. (2010). Life cycle and risk assessment of environment-compatible flame retardants: ENFIRO, a prototypical case study. *Proceedings of Going Green–CARE INNOVATION*.

[44] Troitzsch, J. (1983). *International plastics flammability handbook: principles-regulations-testing and approval*: Hanser.

[45] Stepek, J., & Daoust, H. (2012). *Additives for plastics* (Vol. 5): Springer Science & Business Media.

[46] Wilkie, C. A., & Morgan, A. B. (2009). *Fire retardancy of polymeric materials*: CRC press.

[47] Vandersall, H. (1971). Intumescent coating system, their development and chemistry. *J Fire Flamm,* 2, 97-140.

[48] Horrocks, A. R., Price, D., & Price, D. (2001). *Fire retardant materials*: woodhead Publishing.

[49] Bourbigot, S. (2008). Flame retardancy of textiles: new approaches *Advances in fire retardant materials* (pp. 9-40): Elsevier.

[50] Tsafack, M. J., & Levalois-Grützmacher, J. (2006). Plasma-induced graft-polymerization of flame retardant monomers onto PAN fabrics. *Surface and Coatings Technology,* 200(11), 3503-3510.

[51] Muskatell, M., Utevski, L., Shenker, M., Daren, S., Peled, M., & Charit, Y. (1997). Flame retardant polypropylene fibers with good dyeability. *Journal of Applied Polymer Science,* 64(3), 601-606.

[52] Kaprinidis, N., Shields, P., & Leslie, G. (2002). *Antimony free flame retardant systems containing Flamestab NOR 116 for polypropylene molding.* Paper presented at the Flame retardants.

[53] Weil, E. D., & Levchik, S. V. (2008). Flame retardants in commercial use or development for textiles. *Journal of Fire Sciences,* 26(3), 243-281.

[54] Weil, E. D., & Levchik, S. V. (2015). *Flame retardants for plastics and textiles: practical applications*: Carl Hanser Verlag GmbH Co KG.

[55] Erdem, N., Cireli, A. A., & Erdogan, U. H. (2009). Flame retardancy behaviors and structural properties of polypropylene/nano-SiO_2 composite textile filaments. *Journal of Applied Polymer Science,* 111(4), 2085-2091.

[56] Horrocks, A. R., & Price, D. (2008). *Advances in fire retardant materials*: Elsevier.

[57] Fenimore, C. P., & Martin, F. J. (1966). Flammability of polymers. *Combustion and Flame,* 10(2), 135-139.

[58] NF. (1985). NF T 50-071. 11.

[59] ASTM. (2013). Standard Test Method for Measuring the Minimum Oxygen Concentration to Support Candle-Like Combustion of Plastics (Oxygen Index). (ASTM D2863-13).

[60] ISO. (1996). Determination of burning behaviour by oxygen index. (ISO 4589).

[61] Kiliaris, P., & Papaspyrides, C. (2010). Polymer/layered silicate (clay) nanocomposites: an overview of flame retardancy. *Progress in Polymer Science,* 35(7), 902-958.

[62] Horrocks, A. R., Tune, M., & Cegielka, L. (1988). The burning behaviour of textiles and its assessment by oxygen-index methods. *Textile Progress,* 18(1-3), 1-186.

[63] Schartel, B., Bartholmai, M., & Knoll, U. (2005). Some comments on the use of cone calorimeter data. *Polymer Degradation and Stability,* 88(3), 540-547.

[64] Mouritz, A. P., & Gibson, A. G. (2007). *Fire properties of polymer composite materials* (Vol. 143): Springer Science & Business Media.

[65] Schartel, B., & Hull, T. R. (2007). Development of fire-retarded materials—interpretation of cone calorimeter data. *Fire and Materials: An International Journal,* 31(5), 327-354.

[66] Lyon, R., Walters, R., Stoliarov, S., & Safronava, N. (2013). Principles and practice of microscale combustion calorimetry: DOT/FAA/TC-12/53, Federal Aviation Administration William J. Hughes Technical Center Atlantic City International Airport, NJ 08405.

[67] Uddin, A. J. (2010). Novel technical textile yarns *Technical textile yarns* (pp. 259-297): Elsevier.

[68] Gao, Y., & Cranston, R. (2008). Recent advances in antimicrobial treatments of textiles. *Textile research journal,* 78(1), 60-72.

[69] Simoncic, B., & Tomsic, B. (2010). Structures of novel antimicrobial agents for textiles-a review. *Textile research journal,* 80(16), 1721-1737.

[70] Fernández, A., Soriano, E., Hernández-Muñoz, P., & Gavara, R. (2010). Migration of antimicrobial silver from composites of polylactide with silver zeolites. *Journal of food science,* 75(3), E186-E193.

[71] Heine, E., Knops, H., Schaefer, K., Vangeyte, P., & Moeller, M. (2007). Antimicrobial functionalisation of textile materials *Multifunctional Barriers for Flexible Structure* (pp. 23-38): Springer.

[72] Kara, S., Ureyen, M., & Erdogan, U. (2016). Structural and Antibacterial Properties of PP/Nano-CuO Composite Filaments Having Different Cross Sectional Shapes. *International Polymer Processing,* 31(4), 398-409.

[73] Fiedot, M., Karbownik, I., Maliszewska, I., Rac, O., Suchorska-Woźniak, P., & Teterycz, H. (2015). Deposition of one-dimensional zinc oxide structures on polypropylene fabrics and their antibacterial properties. *Textile research journal,* 85(13), 1340-1354.

[74] Erem, A. D., Ozcan, G., & Skrifvars, M. (2013). In vitro assessment of antimicrobial polypropylene/zinc oxide nanocomposite fibers. *Textile research journal,* 83(20), 2152-2163.

[75] Sjollema, J., Zaat, S. A., Fontaine, V., Ramstedt, M., Luginbuehl, R., Thevissen, K., Li, J., Van der Mei, H. C., & Busscher, H. J. (2018). In vitro methods for the evaluation of antimicrobial surface designs. *Acta biomaterialia,* 70, 12-24.

[76] Hipler, U. C., & Elsner, P. (2006). *Biofunctional textiles and the skin* (Vol. 33): Karger Medical and Scientific Publishers.

[77] Farrar, D. (2011). *Advanced wound repair therapies*: Elsevier.

[78] Mark, H. F., Atlas, S. M., & Cernia, E. (1967). Man-made fibers; science and technology.

[79] Mishra, S. (2000). *A text book of fibre science and technology*: New Age International.

[80] Zhang, D. (2014). *Advances in filament yarn spinning of textiles and polymers*: Elsevier.

[81] Ugbolue, S. C. (2017). *Polyolefin Fibres: Structure, Properties and Industrial Applications*: Woodhead Publishing.

[82] Eichhorn, S., Hearle, J., Jaffe, M., & Kikutani, T. (2009). *Handbook of Textile Fibre Structure: Volume 1: Fundamentals and Manufactured Polymer Fibres*: Elsevier.

[83] Lawrence, C. A. (2003). *Fundamentals of spun yarn technology*: Crc Press.

[84] Babrauskas, V., & Peacock, R. D. (1992). Heat release rate: the single most important variable in fire hazard. *Fire safety journal,* 18(3), 255-272.

[85] Huang, N., Chen, Z., Wang, J., & Wei, P. (2010). Synergistic effects of sepiolite on intumescent flame retardant polypropylene. *Express Polymer Letters,* 4(12).

[86] Schartel, B. (2010). Phosphorus-based flame retardancy mechanisms—old hat or a starting point for future development? *Materials,* 3(10), 4710-4745.

[87] Hirschler, M. M., & Poletti, R. A. (1989). Latex backcoatings on polypropylene carpets: fire performance testing. *Journal of Coated Fabrics,* 19(2), 94-111.

[88] Wickström, U., & Göransson, U. (1987). Prediction of heat release rates of surface materials in large-scale fire tests based on cone calorimeter results. *Journal of testing and evaluation,* 15(6), 364-370.

[89] Tsuchiya, Y. (1994). CO/CO2 ratios in fire. *Fire Safety Science,* 4, 515-526.

[90] Kaynak, E., Ureyen, M. E., & Koparal, A. S. (2017). Thermal characterization and flammability of polypropylene containing sepiolite-APP combinations. *e-Polymers,* 17(4), 341-348.

[91] Stanković, A., Dimitrijević, S., & Uskoković, D. (2013). Influence of size scale and morphology on antibacterial properties of ZnO powders hydrothemally synthesized using different surface stabilizing agents. *Colloids and surfaces B: Biointerfaces,* 102, 21-28.

[92] Ohira, T., Yamamoto, O., Iida, Y., & Nakagawa, Z.-e. (2008). Antibacterial activity of ZnO powder with crystallographic orientation. *Journal of Materials Science: Materials in Medicine,* 19(3), 1407-1412.

[93] Cao, K., Wu, S.-l., Qiu, S.-l., Li, Y., & Yao, Z. (2012). Synthesis of N-alkoxy hindered amine containing silane as a multifunctional flame retardant synergist and its application in intumescent flame retardant polypropylene. *Industrial & Engineering Chemistry Research,* 52(1), 309-317.

[94] Aubert, M., Tirri, T., Wilén, C.-E., François-Heude, A., Pfaendner, R., Hoppe, H., & Roth, M. (2012). Versatile bis (1-alkoxy-2, 2, 6, 6-tetramethylpiperidin-4-yl)-diazenes (AZONORs) and related structures and their utilization as flame retardants in polypropylene, low density polyethylene and high-impact polystyrene. *Polymer Degradation and Stability,* 97(8), 1438-1446.

[95] Plentz, R. S., Miotto, M., Schneider, E. E., Forte, M. M. C., Mauler, R. S., & Nachtigall, S. M. (2006). Effect of a macromolecular coupling agent on the properties of aluminum hydroxide/PP composites. *Journal of Applied Polymer Science,* 101(3), 1799-1805.

[96] Arao, Y. (2015). *Flame retardancy of polymer nanocomposite.* Paper presented at the Flame Retardants.

[97] Morones, J. R., Elechiguerra, J. L., Camacho, A., Holt, K., Kouri, J. B., Ramírez, J. T., & Yacaman, M. J. (2005). The bactericidal effect of silver nanoparticles. *Nanotechnology,* 16(10), 2346.

CURRICULUM VITAE

Name & Surname : Ayfer İrem KOCA
Foreign Languages : English, German
Place and Date of Birth : Bornova, 23.05.1988
E-mail : airemkoca@gmail.com

Education

- 2019, Eskisehir Technical University, Institute of Graduate Programs, Department of Advanced Technologies/Nanotechnology Program
- 2013, Anadolu University, The Faculty of Business Administration, Business Administration
- 2010, Eskisehir Osmangazi University, Faculty of Engineering and Architecture, Chemical Engineering

Projects

- Eskisehir Technical University, Scientific Research Projects (BAP), "Development of Flame Retardant and Antibacterial Nanoparticle Doped Polypropylene Fibers" (2014-2019)

Publications

- Koca, A. İ., Üreyen, M. E., Yüksel, G., & Karaer, F. (2019). Effects of Carbon Nanotube-Phosphorus Based Flame Retardant Combinations on Flammability of Polypropylene. *International Periodical of Recent Technologies in Applied Engineering*, 1(1), 37-43
- 2018, Poster presentation, Koca, A. İ., Üreyen, M. E., Yüksel, G., & Karaer, F. Effects of Carbon Nanotube-Phosphorus Based Flame Retardant Combinations on Flammability of Polypropylene. *8th International Istanbul Textile Conference*, ETT 2018, Istanbul
- 2018, Oral presentation, Koca, A. İ., Üreyen, M. E. & Yüksel, G. Effects of CNT and Nano-SiO2 on the flammability of ammonium polyphosphate-based flame retardant/polypropylene system. *3. International Fiber and Polymer Research Symposium,* BUTEKOM Bursa